NOVEL CARBON NANOTUBE THERMAL INTERFACES FOR MICROELECTRONICS

A Thesis
Presented to
The Academic Faculty

by

Premkumar Nagarathnam

In Partial Fulfillment
of the Requirements for the Degree
Masters of Science in the
School of Mechanical Engineering

Georgia Institute of Technology
December 2009

NOVEL CARBON NANOTUBE THERMAL INTERFACES FOR MICROELECTRONICS

Approved by:

Dr Sam Graham, Advisor
School of Mechanical Engineering
Georgia Institute of Technology

Dr. Yogendra Joshi
School of Mechanical Engineering
Georgia Institute of Technology

Dr. Kyriaki Kalaitzidou
School of Mechanical Engineering
Georgia Institute of Technology

Date Approved: 11-13-09

ACKNOWLEDGEMENTS

I would like to start off by thanking my thesis adviser, Dr. Graham, for his patience and support throughout the project. He was always there when I needed a hand, refining my raw ideas, suggesting fresh ones and teaching me how to attack research problems systematically. I could not have completed this work without his guidance. I also want to thank the following professors who assisted our work at various stages of the project: Dr. Weissburg and Dr. Yen from biology and Dr. Fedorov and Dr. Joshi from mechanical engineering. Dr. Joshi and Dr. Kalaitzidou also have my thanks for their support as committee members.

Next, I would like to thank my fellow group members for their support. Even when our research went in different directions, they were there to offer their support. I'd like to give particular thanks to Adam Christensen and Minseok Ha for putting up with my questions and helping me with countless programming and processing issues. I also want to thank Mark Gleva for all the help and work he put in during the joint phase of the project.

Finally, I'd like to give thanks to my family and friends: my parents for starting me down the path of science and engineering, and my friends and my sister for letting me lean on them when I needed a break from science and engineering.

TABLE OF CONTENTS

LIST OF TABLES

Page

LIST OF FIGURES

LIST OF SYMBOLS AND ABBREVIATIONS

CNT	Carbon Nanotube
TIM	Thermal Interface Material
PCM	Phase Change Material
BLT	Bond Line Thickness
LED	Light Emitting Diode
IMC	Intermetallic Compound
SWNT	Single-Walled Nanotube
MWNT	Multi-Walled Nanotube
VLS	Vapor Liquid Solid
TCVD	Thermal Chemical Vapor Deposition
PECVD	Plasma Enhanced Chemical Vapor Deposition
PA	PhotoAcoustic
ITR	Interface Resistance

SUMMARY

The continued growth of the microelectronics industry has led to the creation of many new thermal management issues. To handle higher density microchips, multicore processors, wide bandgap power transistors and the advent of general solid state lighting, every component of the thermal management scheme needs to be evaluated and improved. Much work has gone into creating and optimizing better sinks, through novel heat spreader materials as well as new mechanisms of heat removal, such as liquid cooling, evaporation and ducted fans. Comparatively less effort has gone into the layer bridging the heat source to the sink. Improperly matched, this thermal interface layer can create a roadblock that prevents proper cooling of the source, raising temperature and limiting device load or lifetime. Just as important, yet less explored, is the range of use and mechanical strength of these layers.

Traditional thermal interface material (TIM) layers have employed solder, thermal greases, or thermal pads. Typical layers composed of these materials have resistances varying from 7 mm^2K/W for solders to 30-50 mm^2K/W for greases and pads [1, 2]. Despite this range, each type of TIM has proven useful for different products in the context of heat dissipation. However, as fluxes continue to increase, and products like LEDs promise extensive lifetimes, existing options fall short from issues such as thermal degradation, lattice mismatch and poor performance. In addition, with the continued development of power electronics based on SiC and GaN, TIMs which can withstand higher temperatures and minimize stresses induced in the die are a necessity. There is a pressing need for new interface materials with low resistivity and high ease of

manufacture. In the past few years, much work has examined using carbon nanotubes(CNTs) as interface materials, due to their high intrinsic thermal performance. Early attempts have focused on adding them to existing TIMs to form composites, but the best performance has come from using aligned arrays of CNTs. While extensive work has proven that CNT array based TIMs can match and exceed the performance of even solders thermally, the mechanical aspects and fabrication considerations for creating such interfaces have received comparatively less attention.

In this work, we improved on past techniques to create CNT array thermal interfaces which are more widely applicable in industry in terms of ease of application and mechanical stability. Building upon metal based transfer processes pioneered that proved effective in lowering thermal resistance in prior research, we grew CNT arrays of uniform thickness on a standard Si substrate and examined the transfer of these arrays to other substrates at low temperatures, using a thin intermediary metal layer. By controlling variables such as the thickness, deposition rate and composition of this layer, we were able to control the bonding temperatures necessary for this process. We characterized the resulting interfaces, with a focus on mechanical strength, particularly the tensile strength of the resulting bonds. We also attempt to find a way to incorporated a phase change material(PCM), which had proven effective in prior work, into the interfaces using various designs and schemes. Some of the interfaces created were characterized thermally to see the effects of our fabrication process on the interface performance.

CHAPTER 1

INTRODUCTION

1.1 Motivation of Research

Thermal interface materials (TIMs) can be a limiting element in the performance of microelectronic devices. Conventional solders, pastes and pads have limitations which make improvements in the efficient heat dissipation and thermomechanical responses at the die level a significant challenge. These materials can no longer provide sufficient performance to handle the ever higher heat fluxes when connecting newer devices to a heat spreader or a heat sink [2]. Carbon nanotubes(CNTs) have been proposed as a possible advanced thermal interface material, due to their thermal and mechanical properties, and prior research has established the effectiveness of vertically arranged CNT arrays to match the capabilities of the best conventional TIMs. However, to reach commercial applicability, many improvements need to be made. While almost all research in CNT TIMs has focused on lowering the thermal resistivity, the ease of manufacturing and the mechanical stability of the interface are equally important. This study seeks to supplement the thermal work of prior studies by exploring and expanding the range of application of these CNT thermal interfaces.

1.2 Thermal Management of Microelectronics

Every thermal management scheme involves removal of heat from the source to a sink where it can be dissipated. Both these elements in microelectronics have undergone dramatic shifts over the years. The heat sources have become more dense and varied. High end microprocessor chips utilizing multicore design and achieving high transistor density have created chip thermal powers in excess of 300W [3]. The switch to solid state lighting with LEDs presents a new challenge, not in terms of total heat loads, but in localized heat fluxes (>100W/cm^2) [4]. The associated challenges in dissipating these

large heat fluxes result in challenges in achieving longer lifetimes and light quality necessary to justify their utilization. New thermal dissipation schemes at the sink level have been developed to improve overall system level thermal management of LEDs. The traditional natural convection cooled fin designs have been replaced or coupled with ducts, piezoelectric and conventional fans, liquid cooling loops, evaporative heat pipes, thermoelectrics, and many other dissipative schemes [2, 5-7]. While these methods address the dissipation of heat to the environment, they do little to address the dissipation of heat from the die level where significant thermal resistances occur.

The performance of the source and sink can be constrained by the interface between the two regions. Commercial devices have many layers of separation between the two, including dielectrics and heat spreaders[7, 8]. At any interface, the problems to heat transfer are similar – with surface irregularities and defects can create insulating pockets of air or lattice mismatches. As Figure 1 depicts, this results in just 1-2% of the apparent surface area in contact with one another.

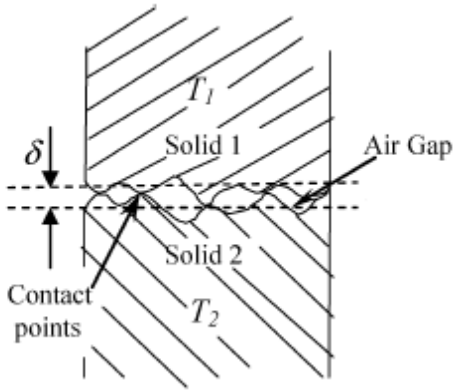

Figure 1. Model of contact region between a given interface between solid 1 and 2 with temperatures T_1 and T_2, with δ being the bond region – compare apparent line of contact with actual contact points [2].

A thermal interface material(TIM) is used to increase the area in contact and ensure proper transport of heat from source to sink. The ideal TIM has high internal thermal conductance and low contact resistance with the mating surfaces. It must also be conformable and thin, essentially filling in the contours and aligning the mismatched

crystal structures without creating much of a presence itself [1]. Most commercial TIMs fall into one of a few categories: solders, greases, phase-change-polymers, and solid pads and tape [9, 10]. Solders are currently the industry standard for high performance electronics. Indium based solders can be reflowed at temperatures of 157-200°C then cooled to form a conformal layer which is thin and has low bond line thickness(BLT) [11]. Indium's metallic nature imbues it with internal thermal conductivity ranging from 28-82W/m-K and thermal contact conductance as high as .2 W/mm^2-K [11, 12]. Such interfaces can range from 7 mm^{2}K/W - 28 mm^{2}K/W with decreasing purity of Indium, however suffer from issues such as oxidation and cracking under thermal stress [13]. Thermal greases, composed of silicone polymers are also used commonly but serve a different market niche, offering a tradeoff in thermal conductivity for ease of application. Their malleability also results in reduced thermally induced stress even at high temperatures. However, a nearly order of magnitude drop in thermal performance to internal conductivities of just .4-7 W/m-K precludes their use in high flux devices [14]. Thermal pads and tapes offer a thermal conductivity that falls in the middle of the range of greases, but at the cost of increased contact resistance due to poor conformality and increased bond line thickness [10]. However, it offers longer lifetimes than grease due to its solid nature. It is clear that much room is thus left for improvement in TIMs, especially for high power, long lifetime electronics.

1.3 Carbon Nanotube Thermal Interface Layers

Carbon nanotubes(CNTs) have been explored as a novel TIM due to their remarkable intrinsic properties. Individual multiwalled CNTs have been shown to have thermal conductivities of 3000 W/m-K [15]. Though the conductivity drops when such CNTs are grown in arrays, they still retain excellent mechanical properties that allow for tubes of various lengths to bend and conform to the various height spacings. While it would be expected that aligned arrays of such tubes would exhibit similar performance, conformal factors and poor adhesion to mating surfaces prevent transfer of the high

individual CNT performance. Still, overall thermal conductivities through as high as 141 W/m-K have been displayed in TIM CNT arrays and internal CNT conductivities as high as 500 W/m-K have been observed, making it clear that improving contact between array and mating layers would produce extremely conductive TIMs [16, 17].

While growth of CNT arrays directly on the sink and source would prove ideal for increasing contact resistance, it is non-ideal for several reasons. One, the process of growing CNTs on metallic substrates is not a trivial one, especially to achieve any control over growth height. The thermal CVD growth process commonly used for CNTs involves temperatures of 700°C or higher, well in excess of the critical values of electronic devices they'd be grown on, such as the 120°C industry standard for LEDs [18].

The more viable option is transferring CNTs to the surface. The bulk of research has focused on improving thermal performance by incorporating CNTs in a composite with other TIMs, or coating a CNT adhesive array with filler such as grease or liquids [2, 19-21]. Some have achieved very low resistance values of 12-16 mm^2 K/W, reaching even lower values with the sample under high pressure during tests [22, 23]. Almost none of these tests have addressed more pragmatic concerns such as processing and longevity.

Prior research has led to the development of a novel method of transferring CNT arrays to surfaces through the use of a thin layer of gold to form diffusion bonds at low temperatures [24]. By reducing the adhesion to the growth substrate through a post growth water vapor etch and by using a thermal press to apply heat and pressure between gold coated CNT arrays and another gold coated surface, the arrays were repeatably transferred to common materials in the microelectronics industry, such as copper, silicon and gold. Arrays bonded at 220°C demonstrated thermal resistances comparable to that of commercially available solders, with values of 10 mm^2 K/W under little applied pressure. Johnson et al. were able to use a very similar technique, using a dissolvable growth layer under the CNT arrays instead of a water vapor etch to transfer stable electrical contacts composed of CNT arrays [25].

While this technique is an important processing breakthrough, the minimum bonding temperature of 150°C is still not optimal for LED processing. Commercial lines do use solder at this temperature, but the processing leads to thermal stresses which hinder lifetime. The 500nm gold layer used for bonding in prior research can also add to the costs, with a $1cm^2$ square coming out to $.03, which can quickly add up in batch processing and material loss [26]. While the technique shows promise for matching and exceeding the performance of a solder thermally, more work also needs to be done to understand and improve the mechanical strength of the metal bond which currently has tensile strengths of just 38KPa [24].

1.4 Phase Change Thermal Interface

Phase change materials (PCMs) have also been used as a conventional TIM, however their operation is rather unique. They posses low internal conductivities of just .5-1 W/m-k in liquid form. However, the melting process allows for low viscosity to fill surface gaps thoroughly, store sudden bursts of heat, and increase lateral transport of heat and dissipation [27]. These properties can remedy issues that trouble CNT arrays such as irregular contact between tube and surface and almost nonexistent intertube-thermal conductivity [28].

The Fisher group at Purdue has demonstrated early proof of the PCMs ability to improve the performance of CNT TIMs, achieving record resistances of just $2mm^2$ K/W [29]. However, the issues of PCM containment and stable integration into even a basic manufacturable CNT TIM design still need to be explored.

1.5 Thesis Overview

The goal of this study was to gain a deeper understanding and improve the process of forming CNT interfaces by use of a metal bonding layer [24]. The primary targets were expanding the range of use for the manufacturing process and understanding the factors which affected the bond. This involved:

- Exploring the effects of altering the thickness and deposition rate of a gold bonding layer
- Reducing the temperature of the bonding process to enhance compatibility with microelectronic processing temperatures
- Testing the use of copper as an alternative for gold bond layer to reduce costs
- Characterizing the mechanical bond properties for the various interfaces, to determine their stability in usage
- Integrating phase change material within the CNT array in a manner that
- Testing the thermal performance of a range of interfaces to determine effects of bonding layer variables

Chapter 2 presents more detailed background on current TIMs: why they are needed, the types currently in use, and the state of the art of CNTs as TIMs. Chapter 3 explores the use of phase change material in TIMs, particularly in conjunction with CNTs. Chapter 4 presents the first part of the study, detailing our process for creating lower temperature, lower cost CNT TIMs and our work at fabricating various phase change interfaces. Chapter 5 describes the results of the mechanical characterization of these interfaces, as well presenting some thermal values for comparing the effects of our modifications with the existing body of thermal research. Chapter 6 presents a summary of the results obtained in the study and explores ways to expand upon it in future work.

CHAPTER 2

BACKGROUND OF CARBON NANOTUBE THERMAL INTERFACES

2.1 Microelectronics Cooling

Microelectronic devices are becoming more powerful and prominent in day to day life. From heavy duty servers to handheld portables, more processing power is being brought to bear in ever smaller packages. While there is now a large movement toward energy efficiency and lower power devices, the larger trend continues to be towards an increase in power and a decrease in size. Moreover, microelectronics markets have continued to expand from desktop and laptop origins to complex cell phones and LEDs. The combination of power and requirements of each device requires unique thermal management schemes.

On one end are computer processing chips. For many decades, the evolution of transistor density inside these chips has followed the well known Moore's law, doubling with each generation of chips or roughly every 18 months. The closer packing results in larger power densities passing through a smaller area of the chip, and with joule heating in the transistor, much of the energy is left to convert to waste heat. Without enhanced thermal management, temperatures can increase, and in LEDs, for example, just a 10-15°C, can decrease the lifespan of the device by half [6]. Higher temperatures also increase the gate delay on transistors leading to slower processor speeds. The switch from higher speed processing to multiple core technology was predicated on heat dissipation issues which arise as processors step past 4 GHz. Thermal fluxes on the order of 150 W/cm^2 are now common in chips with submillimeter hotspots such as those in Figure 3, developing as high as 1 kW/cm^2 [3]. Yet Moore's law, depicted in flux terms in Figure 2, shows no sign of abating.

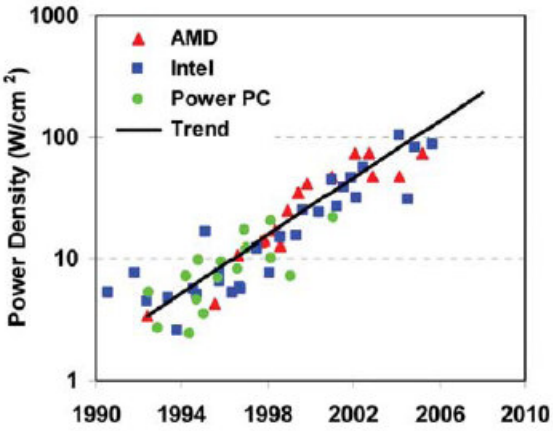

Figure 2. Increasing trend power and heat density with processor technology [30].

Future computer technologies are only expected to augment the problem. AlGaN-GaN MOSFET devices, used in high power devices, can create fluxes of 100 W/cm^2 or higher due to self-heating effects [31]. The same is true for nanometer scale transistor devices [30]. Another technology proposed for increasing transistor density are 3D chips, which add another geometric constraint on cooling schemes. Prototypes exhibit heat densities on the order of 3E3 W/mm^3 [32]. While thermal management is expected to be an increasing portion of the prices of computer hardware, accommodating the sheer magnitude of the thermal flows involved require new technologies altogether.

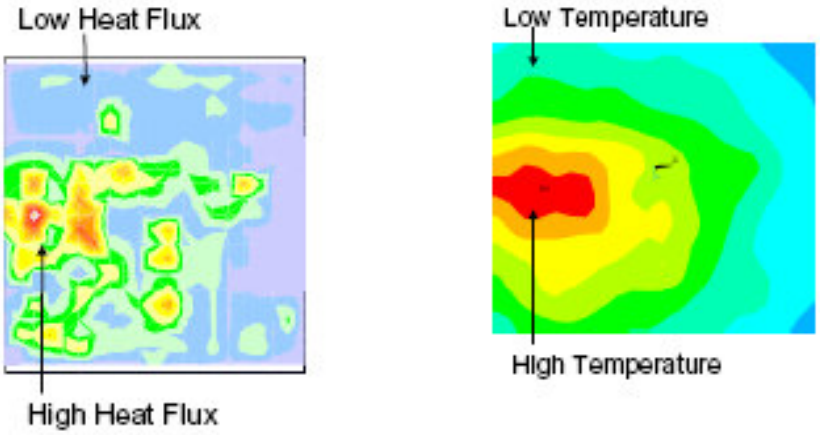

Figure 3. Uneven distribution of heat flux and temperature hot spots on chip surface [6].

Another important electronic device whose performance depends heavily on thermal management are light emitting diodes(LEDs). LEDS, or solid state lighting, can be viewed as the third revolution in lighting, after flame and resistive heating, producing

optical emissions efficiently through use of diodes. With lighting accounting for over 10% of world energy use, and the renewed focus on sustainable energy, a large scale shift now appears to be occurring towards LED lighting in all areas [4]. However, LED performance is highly susceptible to temperatures, whether driven in a pulsed or DC state[33]. Increases beyond the industry standard of 125°C at the junction can produce noticeable red shifts in the outcoming light, as well as reduce the light flux, the emission efficiency, the applicable injection current and the voltage bias, and the life time of the LEDs [34]. Ceramic materials commonly employed as an electrical insulating layer also crack under repeated thermal loads and can create significant increases in operating temperature due to the high thermal resistivity of their epoxy composition [18, 35]. Severe issues can lead to junction failure and thermal runaway from joule heating destroying the device altogether [36, 37]. Due to the high efficiency of the LED light generation, very high brightness LEDs can be created, which can produce thermal fluxes as high as 300 W/cm^2, comparable to processor heat fluxes. However, the vast majority of LED packages operate at lower power densities, where the key to cost efficiency is creating a thermal solution that can hold for 50,000+ hours. This requires extreme mechanical and thermal stability throughout the various elements of the packaging shown in Figure 4, while avoiding significant addition to manufacturing or unit costs.

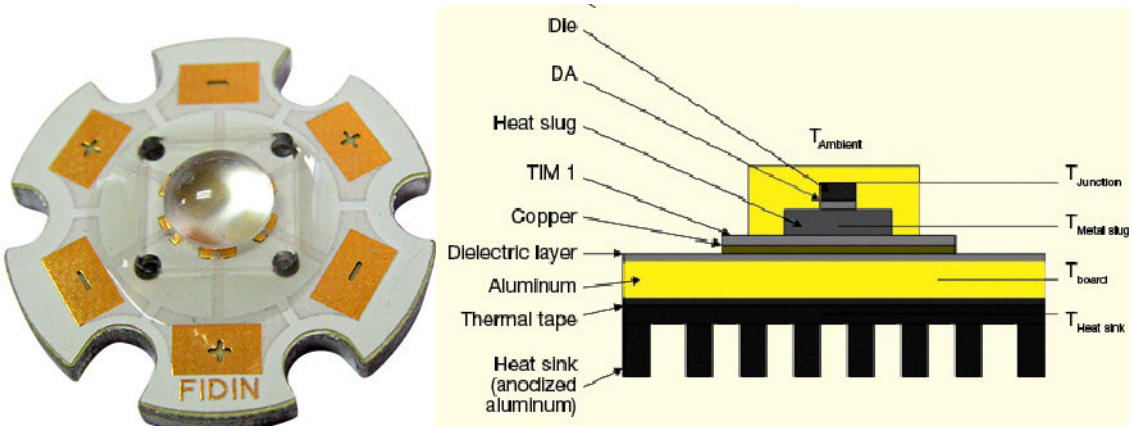

Figure 4. High brightness LED picture and crossection with numerous interface layers.

Both LEDs and processor chips share the common feature of relying on conduction as the main method of heat transfer. This is particularly noticeable in the LED industry where more than 90% of the heat is dissipated through conduction, whereas most commercial fixture have been and still are designed around the radiative heat dissipation of incandescent light bulbs [35]. Conduction involves passing energy directly through phononic and electronic interactions with adjacent atoms.

The goal is to dissipate the thermal energy generated without creating a large temperature at the source of heat. Temperature increases when internal thermal resistance is high and conductivity is low. As Figure 5 shows, common semiconducting materials exhibit only a moderate conductivity compared to the 400 W/m-k of metals like Cu.

Material	Thermal Conductivity ($Wm^{-1}K^{-1}$)
Si (bulk)	148
Ge (bulk)	60
Silicides	40
Si (10 nm)	13
$Si_{0.7}Ge_{0.3}$	8
SiO_2	1.4

Figure 5. Thermal conductivity of common semiconducting materials [30].

The usual strategy for thermal management involves exporting waste heat to a sink layer where it can be spread and carried off by the ambient, usually through some form of convection, maintaining a sub-critical temperature in the device. A vast amount of research and industrial expertise has targeted heat dissipation in the sink region, exploring schemes ranging from simple heat spreading fin design for natural convection, to forced convection fans, active and passive liquid cooling and solid state refrigeration, such as those depicted in Figure 6.

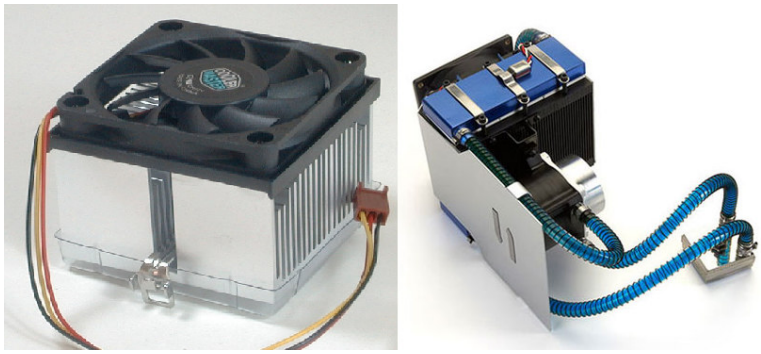

Figure 6. Common fan cooled fins and liquid cooling system.

However, due to the complexity of semiconductor manufacturing techniques and frequently, also, the sink, the two elements are built independently. The two must be bridged through a thermal interface layer.

2.2 Thermal Interface Materials

The chief objective of a thermal interface layer (TIM) is to lower the thermal contact resistance between materials and thus the overall resistance in the heat dissipation path for thermal management. When utilized as a die attach material as in Figure 4, its goal is to additionally provide mechanical stability for the contacting interfaces. If the metallic or ceramic interfaces were placed in direct contact, only 1-5% of the area would be in contact [38]. While these metallic microcontacts are often regions of high thermal conductivity, the air pockets between the remaining areas lead to a large overall contact resistance [10]. Polishing the surfaces can help, but ultimately a TIM is required to increase the contact area. Its resistance depends on the internal conductivity of the material and its conformity with surfaces [2]:

$$R_{material} = \frac{BLT}{k_{TIM}} + R_{c1} + R_{c2} \tag{1}$$

where BLT is the average thickness of the TIM layer, k is conductivity, and the R_cs are contact resistances at either side of the layer. The key is reducing R_c by eliminating gaps in contact while keeping BLT low using a material with high k. The contact resistance can be reduced by filling in the air pockets and increasing the real contact area as in

Figure 7, which depends on the conformability of the material chosen and the pressure applied in bonding.

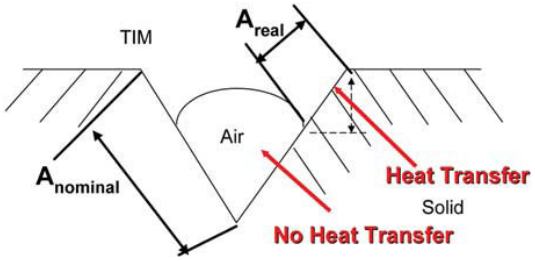

Figure 7. Schematic of heat transfer process at surface with the area of actual contact, A_{real}, lowered than the expect contact area, $A_{nominal}$ by air pockets [2].

Other properties that factor into contact resistance are the matches between the TIM and the surfaces in terms of phonon spectra and the coefficients of thermal expansion (CTE), which also affect the ability of the layer to withstand stress[7]. Mismatches that arise from lattice misalignment at interfaces can, over the long term, create resistances from phonon dispersion mismatch or heat carrier (electron–phonon) energy conversion [30].

The need for high internal conductivity within the TIM is evident, and the reason for keeping BLT small is to have a low temperature drop in the TIM, so that the "thermal budget" allows for a larger drop in the sink [39].

Good TIMs need to excel in many parameters. These include intrinsic ones such as thermal conductivity, electrical resistivity, and low viscosity and elastic modulus, the latter two affecting the ability of the TIM to conform to the surface roughness [12, 40]. They can also include application specific concerns such as wetability of the surfaces, appropriate CTE match, duration of operation, and the ambient environment's effects on TIM. Of course, manufacturing and economical concerns are critical for commercial usage – for example, conductive AlN fillers added to TIMs increase conductivity significantly, but boost the manufacturing cost of the step 100x [6]. Ultimately, a combination of factors determines which TIM is ideal for an application. Bridging rough surfaces with large air gaps, for example, will necessitate a higher BLT, which increases the importance of a high internal conductivity.

Four classes of TIMs are in commercial use: solders, greases, pads, and phase-change materials. The last will be examined in detail further on, but we now examine the advantages and drawbacks of the first three.

2.2.1 Solders

Solders are metallic compounds that can be melted and reflowed to form a conformal bond between surfaces. The solid state of the bond provides a high degree of mechanical stability, while its metallic nature endows it with high intrinsic thermal conductivity. Solders have long been employed commercially, usually in the form of a lead compound due to the melt temperature and durability of the bond [12]. However, current solder research is aimed at replacing lead with more environmentally friendly alternatives. New classes of low melt alloys (LMA) are composed of indium, bismuth, gallium, tin, copper and other safer and low cost elements. While these new LMAs exhibit a somewhat lower performance than prior solders, the $<150^{\circ}C$ reflow temperatures allow for integration into temperature sensitive microelectronic processes. They still exhibit thermal conductivities as high as 35 W/m-K, corresponding to resistances of 1.5 – 6 mm^2K/W [41, 42]. These values are roughly an order of magnitude higher than those of other TIM types.

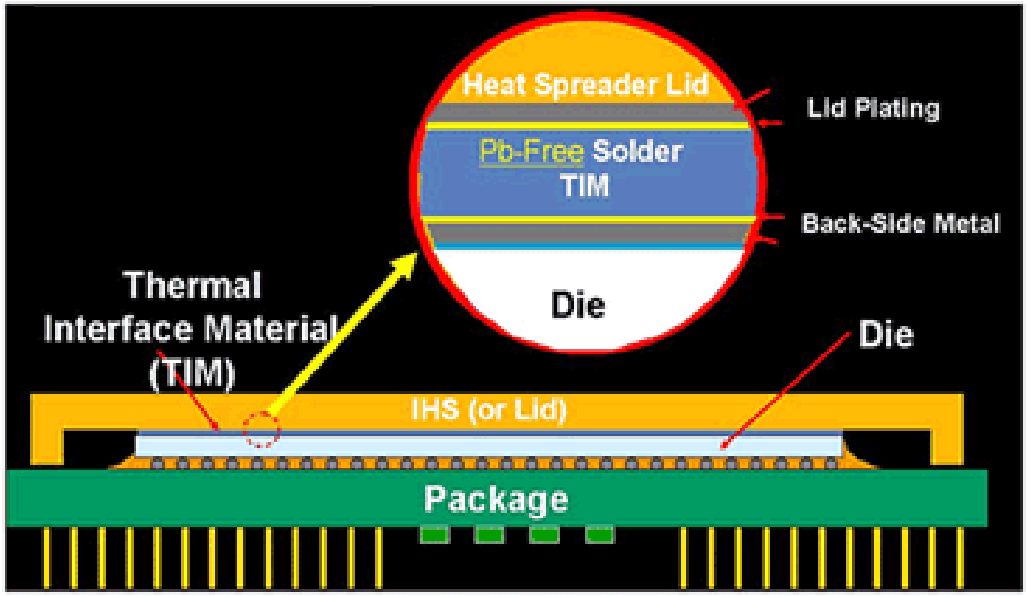

Figure 8. Schematic of 90nm node Intel chip featuring lead free solder.

Despite high initial performance, solders are very susceptible to environmental degradation, especially from cyclic stress. Repeated reflow may be necessary in manufacturing to avoid the formation of voids due to metal shrinkage from cooling [43]. Due to the rigid state of the final bond, it is important for the CTE of the solder to match that of the substrates to avoid shear stresses or slippage at the interface under heat load. LMA have the added issue of bond weakening with temperature and see up to a 75% loss in strength less than 50°C from their melting point [44]. Another issue arising from the fixed bond is obtaining low BLT. In surfaces with high roughness, it may prove difficult to apply a consistent pressure and solder amount [12]. This can lead to increased thickness and a large temperature gradient despite the intrinsic low conductivity.

Chemical issues pose another issue for solder. Oxidation of the compound can create its own thermal stresses, and is a particular issue for LMAs which will oxidize easier at lower ambient temperatures. Indium and non-lead solders compound this issue due to their increased surface tension in the melt state at gold or copper surfaces, leading to the formation of an increased oxide layer. Solders also have a proclivity of forming intermetallic compounds (IMCs) at boundaries significantly raising the contact resistance

terms [12]. The ease with which this happens for copper is an issue due to the high level of Cu use in heat sinks. Another study found that three distinct IMC compounds formed between indium compound solder and a nickel layer, another fairly common heat sink metal. The IMC layer thickened with increase cycling, eventually creating Kirkendall voids between the IMC and die and cracks between the pure solder and the IMC, ultimately causing the bond to fracture under minimal stress as in Figure 9 [41].

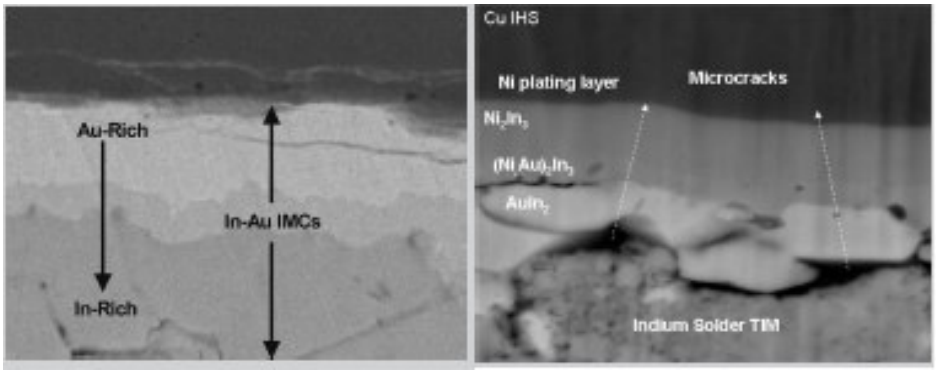

Figure 9. Appearance of IMCs at Au-In interface in solders(left), can lead to loss in thermal conductivity and cracking from lattice mismatch(picture width = 5um) [41].

In summation, while solder forms the most metallic bridge between sink and source and thus offers high thermal performance and mechanical stability, the solder must accommodate the environment and method of use. A longer lasting device or one exposed to higher thermal cycles is more vulnerable to decreases in thermal conductivity from crack formation. Studies have shown that utilizing thicker BLTs can inhibit this degradation, at the cost of some loss in performance [41]. Solder must thus be selected carefully to ensure compatibility at all phases of device lifetime.

2.2.2 Greases

Thermal greases and pastes are fluidic solids which can spread and conform to the surfaces in contact. Unlike solders, there is no thermal step in application – the grease is simply applied to the surfaces, and spread and bonded with pressure. Most TIMs of this type consist of a fluid silicone base, with filler particles of metal or metal oxide to raise conductivity [12]. The wetting ability, conformability, thermal properties and overall

classification of the TIM depends on the percentage and type of filler, with a larger % by weight leading to a thicker paste structure which has higher intrinsic conductivity but less malleability. Even with higher viscosity pastes, BLTs remain low, typically not exceeding 40um.

Relatively low viscosity pastes with internal thermal conductivity as high as 7.5 W/m-K have been reported in literature [38]. While this is considerably less than that of a solder, pastes can still outperform overall due to lower contact resistance. Pastes of carbon black filler in polyethylene glycol demonstrated a more than 50% increase in contact conductance over that of a tin-lead-antimony solder. Furthermore, the thin BLT enables more regions of high conductivity microcontact between the two bonding surfaces[10]. Paste selection is simpler than that of solder. Low surface roughness might prompt a switch to a thinner grease which can conform better – indeed, carbon black pastes have been shown to have a contact conductance 50% greater than that of even lead based solders at high thermal load situations [45].

The fluidity, however, can also produce disadvantages, particularly in the area of lifetime. Pump out, or grease migration, is one primary failure mechanism of grease TIMs, where the thermomechanical strains from expansion and contraction during heat cycling force the grease out of the bonding area, slowly discharging it altogether. Comparing Figure 10 to Figure 3 it is evident that a nonhomogenous interface leads to hotspots. Thermal bake is another failure mechanism wherein high temperature operation causes the filler particles and polymer base to segregate, drastically increasing contact resistances [6]. By nature, the mechanical strength of paste bonds is also quite low and a stiffer scaffold may be employed as a bonding structure in which to load the grease, decreasing available contact area. Alternatively, the polymer base can be designed chemically so that it crosslinks and cures at high heat into a more rigid gel structure, but this faces its own issues from thermomechanical stresses such as delamination [46].

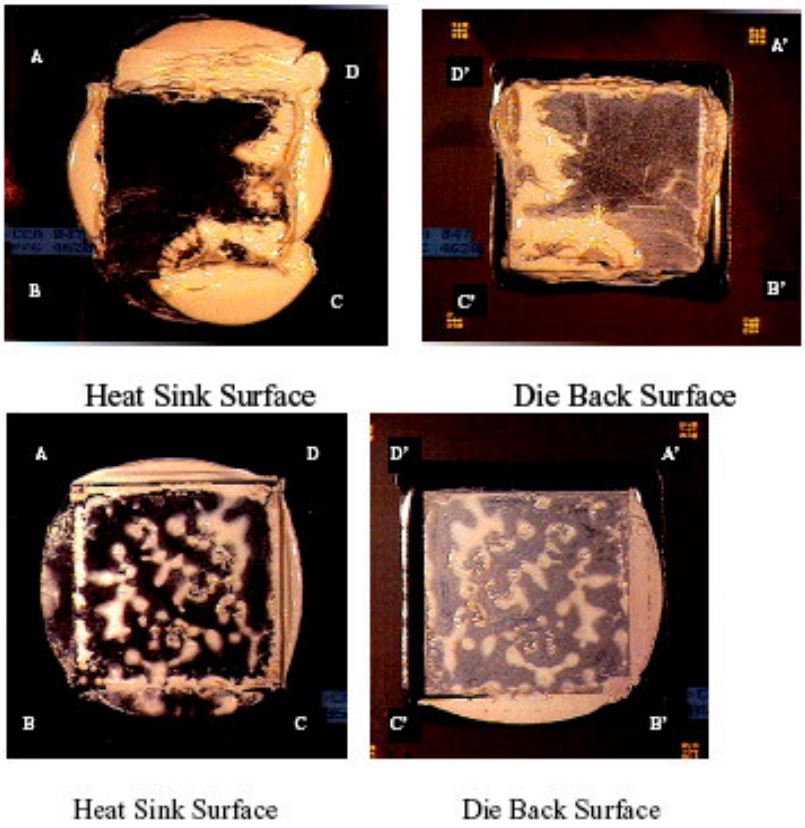

Figure 10. Typical examples of pumpout(top) and phase separation and dryout(bottom) in thermal grease [6].

Ultimately, greases are more suited for low power devices with lower cyclic stresses, or those with large surface areas, where the superior conformability outweighs the need for establishing a separate connector between source and sink.

2.2.3 Thermal Pads

Thermal pads, sometimes referred to as resilient thermal conductors, consist of a solid polymer pad which is sandwiched between the contact surfaces and held in place with pressure. As a TIM, it is sort of a compromise between rigid solders and fluid greases. Like greases, pads often rely upon a metallic filler to bolster thermal conductivity, such as ceramic or boron nitride. Due to the solid state of the elastomer matrix, even unfilled pads exhibit higher internal conductivity than most thermal grease with an average of .7 W/m-K, but this is still lower than that of solder [10]. However,

pads are typically thicker than grease layers, with a BLT from 200 microns and up. They also require high pressures to fill in gaps from surface roughness [6].

As expected, these create issues in performance. Pads must be capable of being compressed to ¼ their thickness, but suffer more than pastes in loss of elasticity with increased filler percentage. Very high pressures must be maintained, but even if present, it is hard to fully evacuate the air gaps at the interfaces. The high BLT prevents any high conductivity microcontacts between the two mating surfaces and compounds the rise in resistivity from the air gaps. Failure of the interface can occur with even a small drop in pressure, and cause loss of contact. Studies have shown that under intense heat load typical rubber and silicon based elastomers with high internal thermal conductivity were not able to outperform greases overall due to the presence of air gaps 25% that of the BLT layer. Polymers also degrade from oxidation under prolonged exposure to temperatures of 100°C, which is below the critical temperature for most devices [2].

The primary draw of pads is their convenience of application in specific instances, such as heat sinks weighted down on computer chips [6]. However they are not suited for high flux or high lifetime operation.

In short, the three TIMs commonly used address the issue of creating a thermal bond in different ways, trading off on some factors for others. Yet, it is possible to imagine a TIM with high internal thermal conductivity that can establish a strong conformal bond with the contact surfaces, and still be easy to manufacture and apply. CNTs may be able to create such an interface design.

2.3 Carbon Nanotubes and Composite Carbon Nanotube TIMs

Since the seminal paper published by Iijima et al in 1991, carbon nanotubes(CNTs) have been pursued for applications in many fields due to their excellent, structural, thermal and electrical properties. Yet, CNTs are simple naturally occurring allotropes of carbon. They can be viewed as rolled sheets of graphene, the

carbon atoms connected in a hexagonal pattern due to their sp^2 hybridization. The chirality of the tube depends on how these patterns are aligned as shown in Figure 11, resulting in CNTs with either metallic or semiconducting electronic properties [47].

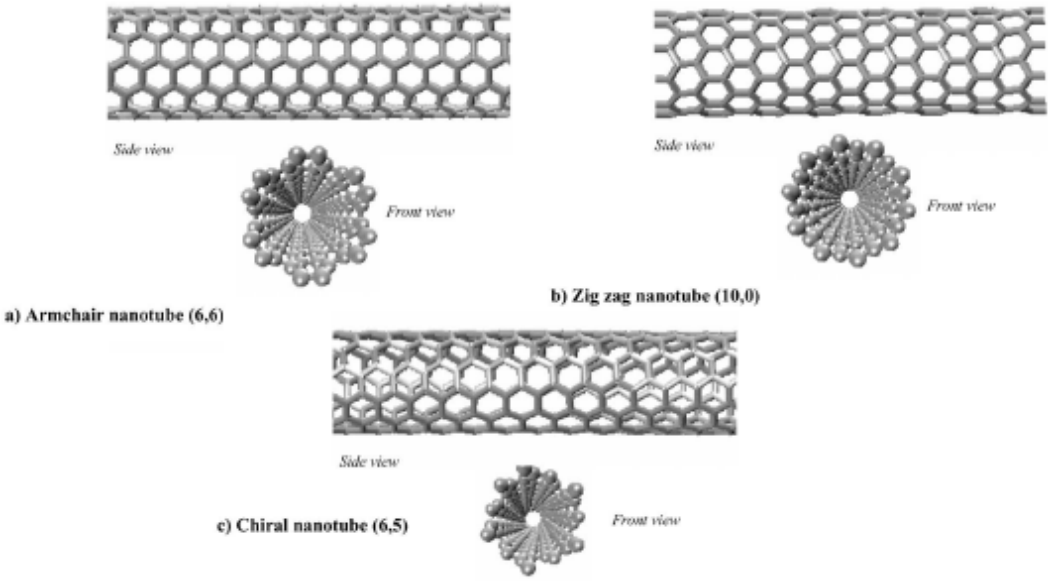

Figure 11. The three CNT classifications by carbon structure [48].

Many of the radical properties of the CNT stem from its anisotropic structure. A CNT's aspect ratio of length to width may reach as high as 28,000,000:1, unrivalled by any other material [49]. Singled walled carbon nanotubes(SWNTs) which consist of just a single hollow tube, can be less than a nanometer in diameter, while multi walled nanotubes(MWNTs) which consist of steadily widening SWNTs sheathed in one another, may be as wide as .1 micron. The difference in structure can be seen in Figure 12. However, they can be grown in bundles reaching more than 2 inches in length [47]. This disparity and overall small size means that SWNTs and most MWNTs can be viewed as 1D structures, where transport occurs along the length of the tube. In metallic CNTs, this leads to very low resistance ballistic transport, producing current densities of 10^{10} A/cm^2, 2 orders of magnitude greater than that of copper or aluminum. When semiconducting, low thickness SWCNTs may be used as very efficient transistors with high switching speeds.

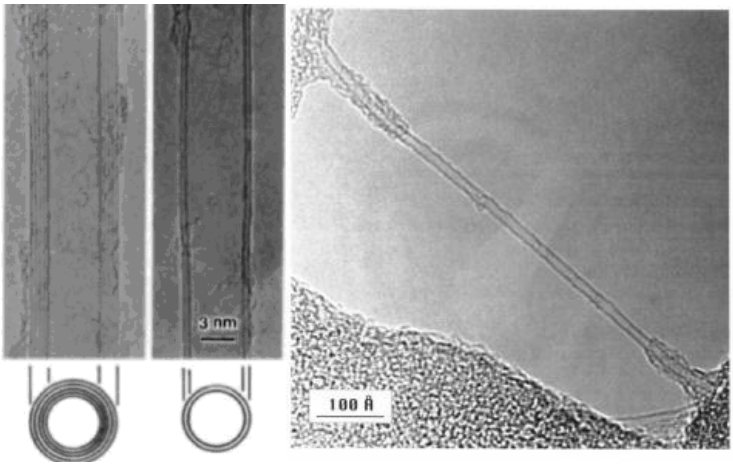

Figure 12. Transmission electron microscope images of MWNT, DWNT and SWNT(left to right) [47].

While these electrical properties are useful in their own right, it is the CNT's thermal and mechanical properties which make it attractive for use in TIMs, both individually and in aligned arrays.

2.3.1 Properties of Individual CNTs

Like with other nonmetals, the thermal conductivity of a CNT is based on phononic energy transfer through vibrations. Many ways have been used to measure the properties of individual nanotubes, including the four point measurement [50]. Similar to electron transport, the 1D structure of SWNTs due to the low defect density, allows for ballistic movement of phonons without dominated scattering effects from the lattice, except at the ends. Little heat is transferred laterally in SWNTs. Both carbon and other elements thus exhibit an exponential rise in conductivity with length:

$$k = \alpha L^{\beta} \tag{2}$$

Here, k is conductivity, L is length and the constants vary with the geometry and material used in the tube [17]. While CNTs have been reported structurally stable at up to 400°C, the conductivity of the tubes does vary with temperature, with sub 400K regimes restricted by a low mean free path and high temperatures leading to Umklapp scattering of the phonons. From 400K – 700K, in W/m-K, a SWNT's conductivity can be related to temperature with [30]:

$$k = 3600(\frac{300}{T}) \tag{3}$$

A quick estimate of conductivity of a SWNT based on both length and temperature for the range 100K< T< 800K is plotted in Figure 13 and can be given by [51]:

$$k(L,T) = \frac{1}{3.7e-7T + 9.7e-10T^2 + 9.3(1+\frac{.5}{L})T^{-2}} \tag{4}$$

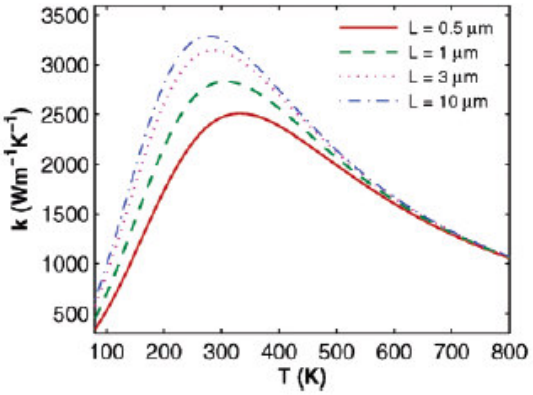

Figure 13. Variation of SWNT thermal conductivity with temperature and tube height[30]

The max axial conductivity actually measured in SWNTs was 6000 W/m-K, more than an order of magnitude higher than even copper.

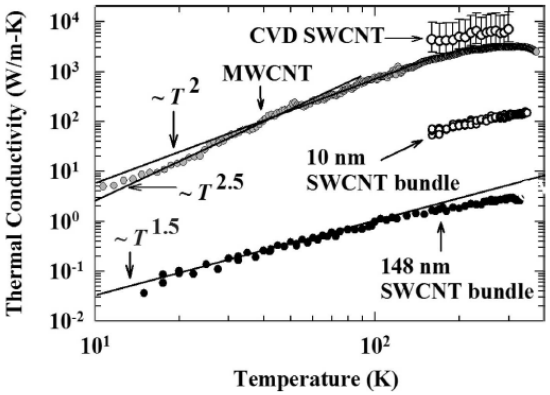

Figure 14. Thermal conductivity of various CNT forms with temperature [52].

MWNTs exhibit lower conductivities, with the highest reported value being 3000 W/m-K, and the average an order of magnitude lower, though this varies based on temperature and tube grouping as Figure 14 shows [19]. Measurements vary widely, as it

has been hard to establish a set procedure for creating MWNTs with a ring count greater than two. The Umklapp process is more prominent than in SWNTs, causing more intertubular scattering of phonons and anharmonic scattering at room temperature [50]. The 1D assumption may break down altogether, as MWNT conductivity exhibits a T^2 dependence at temperatures lower than 100K, as can be seen in Figure 14. This indicates diffusive rather than ballistic heat transport. IR observation of MWNTs supports this claim by demonstrating a gradient along the length of the tube [52]. As a result, MWNTs do not show an increase in conductivity with length.

In some ways, this loss of conductivity in MWNTs compared to SWNTs is a tradeoff for physical attributes, though both exhibit attributes well in excess of those for conventional solids. The Young's modulus of SWNTs, a measure of their elasticity, can be as high as 1TPa, as opposed to .2 TPa for steel [53]. This value is not dependent on the diameter of the SWNT. MWNTs have a lower modulus due to increasing rigidity and less buckling ability with increasing number of coaxial tubes, leading the value to drop from 1TPa to .1TPA when diameter increases from 8 to 40nm [54]. However, the increase in density endows MWNTs with a higher tensile strength – 150GPa, compared to 53 GPa for SWNTs and 1GPa for steel [55]. This strength makes CNTs resistant to strain, and stretching in excess of just 5% can cause nonelastic deformation. However, for most microelectronics, these sorts of forces would likely destroy the device before the CNTs incurred damage.

Both thermal and physical properties are affected by various defects, such as contamination, voids and boundary issues, which can occur in the growth process. Even in the same production batch, MWNTs were found with defects that varied widely enough to account for a 200% drop in tensile strength [54]. Similarly, thermal conductivity dropped an order of magnitude due to defect density in MWNTs [52]. Careful preparation in controlled environments can be used to avoid many of these issues.

Free standing CNTs are commonly created through the arc discharge synthesis process. An electric arc is created between two carbon electrodes under either DC or AC current. The process takes place in an inert atmosphere and the air is turned into plasma, through growth from a glow discharge or from slowly touching and separating the electrodes [47]. The continuous arc maintains a high current density and low internal voltage drop, generating very high temperatures capable of causing the carbon on the negative electrode to sublimate and reform as carbon soot containing CNTs on the cathode. Roughly 30% by weight of this is actually low height SWNTs and MWNTs. The anode and cathode can be replenished to maintain the process rate. The <1000°C temperatures of the process lead to tubes with low defect density.

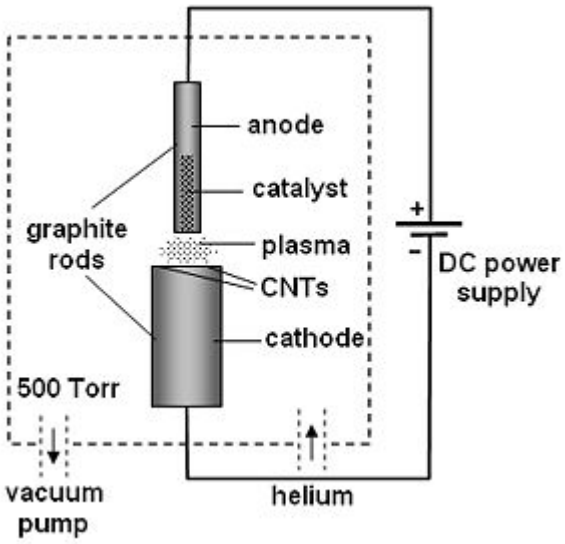

Figure 15. Electric arc discharge growth setup.

Another method of producing primarily SWNTs is ablation of graphite with a pulsed laser. Again, the vaporized carbon reforms as CNT, this time with a 70% by weight ratio.

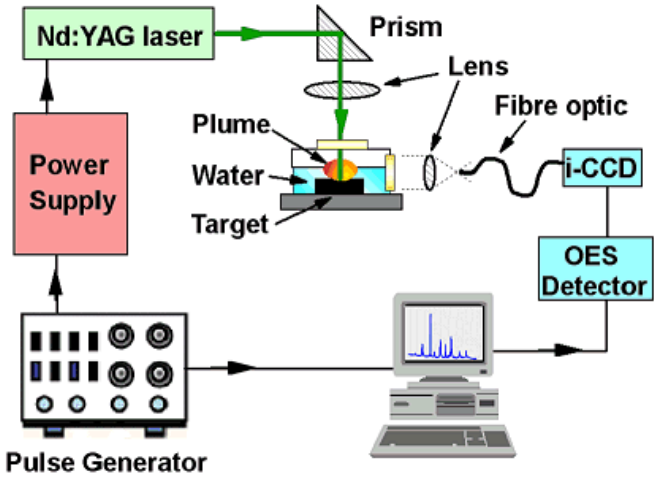

Figure 16. Liquid phase pulsed laser ablation setup.

2.3.2 CNTs composite TIMs

Many groups have tried to utilize the thermal and mechanical properties of CNTs by adding them to TIMs in suspension as filler. The process for doing so depends on the substrate. CNTs can be added to epoxies by simple mechanical mixing of randomly dispersed tubes [47].

Polymers can be loaded through the melt blending process. The polymer TIM is heated above its glass transition temperature and the CNTs are then mixed in and dispersed by rheological shear stress. These stresses can sometimes fracture the CNTs so the process must be carefully controlled [56]. However, some level of orientation control of CNTs can be achieved by stretching the polymer. Upon cooling, the CNTs will show some directionality towards the strained orientation [47]. CNTs do have a tendency to clump – very quickly, as Figure 17 shows - in a melted polymer matrix, though, so other mix methods have been tailored to enhance homogenous dispersion in polymers such as PS, PVA, PMMA, and PVC. In situ polymerization can be accomplished by mixing the monomer and CNTs and then conducting the polymerization [54].

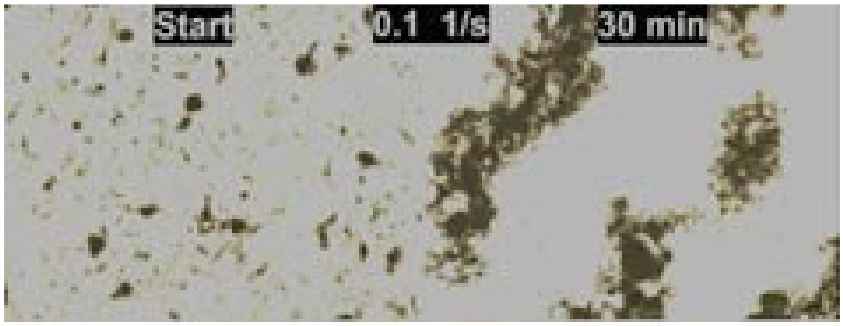

Figure 17. Phase segregation results in clumping of CNTs in epoxy under shear stress [47].

CNTs can also be loaded into solders in the melt state, but is difficult to accomplish with any level of ease due to wetability issues and material compatibility.

The nanotube/TIM composites typically improve thermal properties. CNT/epoxy composites have shown a steady increase in thermal conductivity up to 60% with 5% weight loading, however at least one study found an 125% improvement in the epoxy conductivity with just 1% weight loading, though the improvement varied with temperature [47, 56, 57]. CNT loading can also change properties such as the glass transition temperature – increasing that of DEGBA epoxy, for example, from 167^{o}C to 189^{o}C for just .5% weight loading [58]. This may be beneficial at maintaining mechanical stability, for example, but can also lead to issues like increased delamination from lowering the epoxy's CTE and increased BLT from deformation resistance.

Mechanical properties also experience a double edged effect from CNT loading. The Young's modulus of polymers increased with weight loading of randomly oriented tubes up to 1% load, but decreased with further increase, sometimes below that of even plain polymer [59]. Oriented CNT loading can drastically improve both tensile strength and elastic modulus, up to as much as 3.6 GPa and 80GPa respectively with a 60% weight loaded CNT/PVA mix [56]. Oxidation of CNTs also increases short term mechanical properties, but can lead to more rapid thermal degradation later [47].

While these improvements are impressive, they all fall short of properties predicted through the law of mixtures, which states that a property of a composite material will be the weighted sum of its components' properties [57]. That is:

$$X_{composite} = \sum_{n=1,2,3\ldots} X_n V_n \quad (5)$$

where V is volume fraction and X is any property. While this is only a crude approximation which falters when the materials are non isotropic like CNTs, the drop is still notable significant. Some of this is a result of the nonhomogenous distribution of CNTs in TIM composites. Another factor is the effect of the anisotropic conductivity of CNTs. Despite high k along the axis, the overall thermal conductance of CNTs is low due to their small overall diameter, which is particularly apparent when disperse [30]. While the length of the tube is exposed, the transverse conductivity is still not significant and the phonon and electron interaction with the TIM matrix material can disrupt the ballistic heat transport. The contact resistance thus takes precedence over internal resistance. This resistance poses the biggest limit on composite TIM performance, yet attempts at chemical functionalization of CNTs only lower overall conductivity. Finally, composite TIMs are prone to degradation with cycling as CNTs clump together and separate, disrupting the homogenous dispersion, and leading to hotspots.

Composites may still have some uses, but the most benefit seems to occur when the tubes are aligned. As seen in Figure 18, a .3% loading of SWNTs which were aligned by stretching enhanced thermal conductivity by .65 W/m-K, whereas even a 4.6% loading of disperse MWNTs barely boosted conductivity by .2 W/m-K.

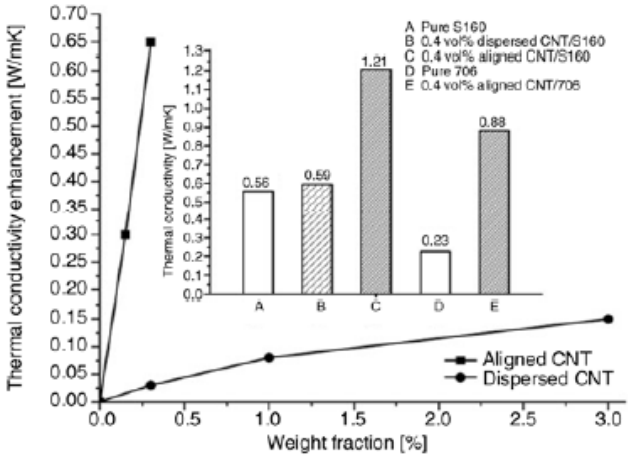

Figure 18. Thermal conductivity enhancement of polymer from aligned and nonaligned CNTs [30].

With 10% weight loading of polymer an aligned filmed should exceed the performance of any commercial TIMs by an order of magnitude [30]. However, the stretching alignment process can also increase the number of defects in the CNTs lowering their intrinsic conductivity. The better option is starting with aligned CNTs and transforming them into a TIM material.

2.4 CNT arrays and CNT array interfaces

CNT growth can be controlled precisely to create arrays with varying tube density, tube diameters and heights, internal alignment, adhesion to the substrate and defect concentration. Each stage of the growth process plays a role in the array properties starting with the selection of the substrate. While CNT arrays can be grown on even the copper or aluminum used in heat sinks, the best control occurs on Si or SiO_2 – the former typically coated with a thin oxide layer anyway to prevent substrate-seed interaction [46]. The seed layer is then deposited, usually on top of an underlayer of metals like Ti and Al which promote adhesion and separation of particles in the seed layer. The seed layer itself consists of transition metals with high absorption of carbon based gases such as Ni or Fe, and sometimes Co. The layer thickness is usually no more than 10nm, so as to promote

the formation of discrete nanoparticles rather than film. A typical layer might be 10nm Ti/20nm Al/10nm Fe or 6nm Fe [23].

MWNT arrays are easier to create than those composed of SWNTs. This is because catalyst size controls the number of tubes that form coaxially from a seed layer of a material like Fe, using Ti as an adhesion underlayer. Obtaining SWNTs requires patterning the metal layer using deep ultraviolet photolithography, which is somewhat costly to achieve on a large scale [60, 61].

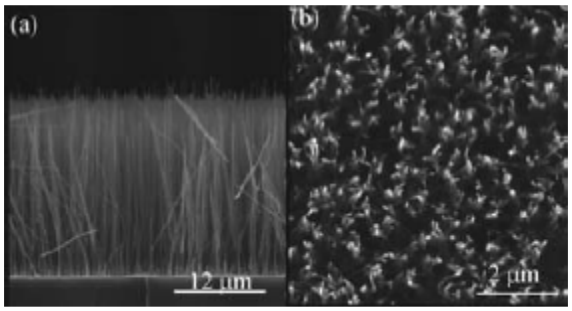

Figure 19. Side(a) and top(b) views of a MWNT array(white dots are CNT tips) [62].

Instead, physical vapor deposition methods such as sputtering or e-beam evaporation are the usual choice for applying the metals. Sintering can be utilized post deposition to promote the formation of discrete nanoparticles. Other possibilities for deposition include electro and electroless plating and coprecipitation of all the layers. This can create binary or trinary alloys that can promote better growth [6]. Another study used Fe_2O_3 as the seed layer, structuring the spacing through the use of a dendrimer template, and obtained very fine control over ensuing CNT diameter based on calcination temperature [63].

CNTs form from any seed metal through a process known as vapor-liquid-solid(VLS). The vapor is the carbon carrying gas, typically a hydrocarbon. The liquid is the seed metal after it has been heated to temperatures typically above $700^{\circ}C$. The hydrocarbon gas adsorbs into the liquid metal where it is decomposed. The carbon dissolves and diffuses through the metal particle, and precipitates in solid form, as Figure 20 shows, resulting in either growth at the base or tip, rarely in the middle.

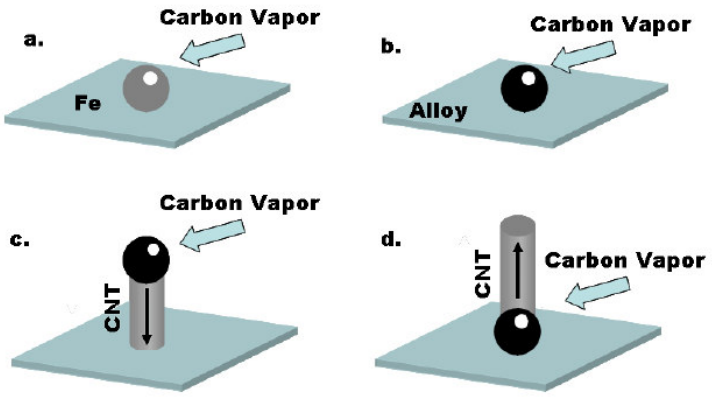

Figure 20. Growth of CNT from Fe particle via tip(c) or base(d)

The CNT continues to grow until gas flow is cut or reactant can no longer diffuse to the metal or to the top of the tube [53]. The resultant tubes are roughly the same diameter as the size of the original nanoparticle catalyst. While individual tubes do not have a preferred growth orientation, the sheer density of growing tubes ensures that each will come in contact with its neighbors and attain vertical alignment after a certain point. It is important to note that other carbon allotropes can form through VLS – with just a 100°C rise in temperature, and a slight shift in reactant gas, a process used to grow CNT arrays instead produced a layer of graphite with a minuscule layer of CNTs atop, growing at a 99.9% reduced rate [64]. Even a thin layer of graphite of amorphous carbon can have deleterious effects when producing arrays for a distinct purpose such as TIMs, so all growth recipes must be followed rigorously.

The chemical vapor deposition(CVD) tool used for growth can maintain strict parameters. Several different CVD methods exist, classified by their energy source. Thermal CVD(TCVD) is one of the more common ones and uses a resistive heater to raise the temperature to between 400-1000°C [53]. A typical TCVD system, shown in Figure 21 consists of a sealed quartz tube that passes through a furnace and connected to gas flow channels.

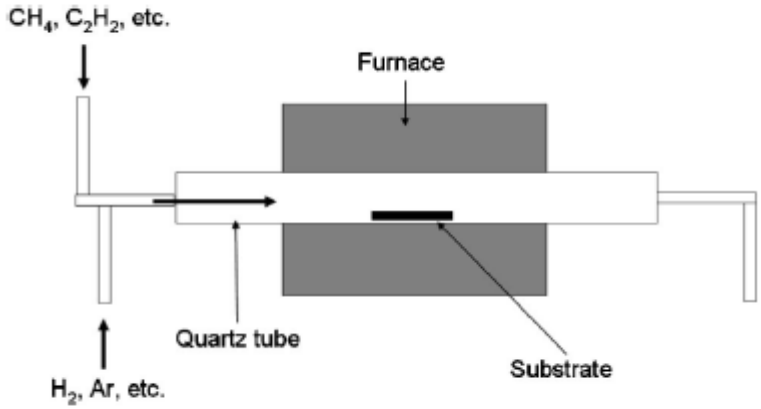

Figure 21. Schematic of Thermal CVD furnace [53].

The seeded sample is loaded into the tube then sealed inside the furnace and heated to the growth temperature. A passive gas, typically Ar, prevents oxidation at this stage. Once the temperature is reached, reactant gases such as acetylene, methane and hydrogen are released into the tube at proscribed rates for a short period of time. The chamber is then flooded with Ar again to prevent oxidation, while it is cooled to ambient. TVCD has been used to grow arrays as tall as 9.25mm. The type of CNT grown can also be controlled – with SWNTs being more common above 900°C and MWNTs at lower temperatures. The relative lack of complexity makes TCVD one of the more promising techniques for commercial scale manufacture of arrays.

Plasma-Enhanced CVD(PECVD) activates the catalyst using via electron impact from a plasma source. This allows the dissolution of the precursor gases to happen at much lower substrate temperatures, with good density films and high growth achieved as low as 450°C. The length of the process is shortened due to the lower temperatures. Vertical alignment can also be observed at much lower heights due to the field induced by the electric charge. However, as Figure 22 shows, the equipment for creating glow discharge is more complicated and expensive than TCVD tools, and most electronic devices that require TIMs would degrade in minutes if direct CVD growth were attempted even at 450°C [53].

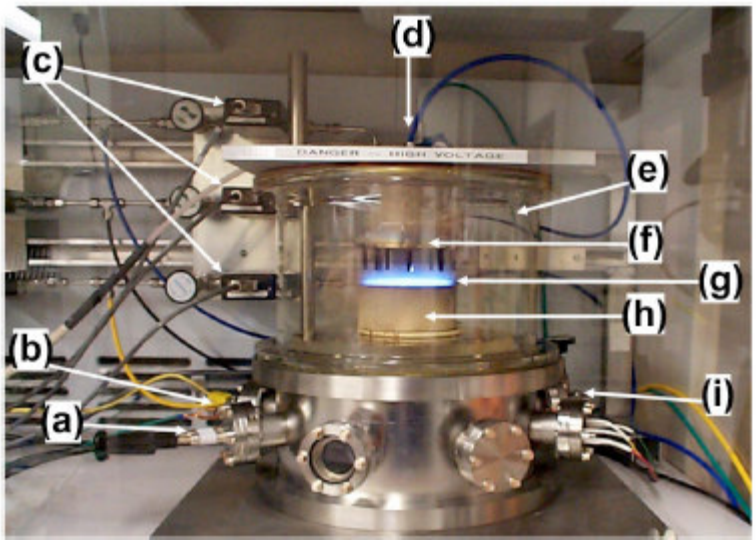

Figure 22. PECVD setup featuring (a) High current heater wiring (b) thermocouple wiring (c) mass flow controllers for C_2H_2, NH_3, H_2 (d) gas inlet (e) glass cylinder vacuum chamber (f) gas showerhead and anode (g) cathode glow of acetylene/ammonia plasma (h) substrate heater and cathode (i) pressure valve [53].

One growth mechanism that could resolve this issue is radio frequency assisted hot-filament chemical vapor deposition. By using the correct frequencies and positioning the RF waves, the catalyst could be heated selectively to 850°C with little heating of the substrate [65]. SWNTs of various diameters were grown through this process using Ni substrate, but other allotropes of carbon also form. If this could be prevented, direct growth on sink and source may be possible, though the cost may be prohibitive.

Figure 23. 3ft x 6ft sheet of CNT grown via large TCVD furnace.

2.4.1 Properties of CNT arrays

CNT arrays exhibit properties lower than either individual SWNTs or MWNTs. Defects are uncommon in a single tube, but given the millions of tubes in even a small array, lower average thermal and physical properties are expected. Allotrope formations can be minimized but some amorphous carbon will still likely be present. The contact resistances also play a more important role than the internal conductivity for short tubes.

The measurement of CNT array properties is itself a difficult task due to the small size and low thermal resistance. One way is using the photoacoustic(PA) technique as applied to CNT interfaces by Dr. Xianfan Xu at Purdue, which exploits the ability of photons to apply pressure. The sample is sealed in an acoustic cell and the surface is heated locally with a modulated energy source such as a laser. The laser cycles through a range of heating frequencies and a microphone records the amplitude and phase shift of the pressure response. The controller can translate the pressure values into a resistance measurement. The setup, pictured in Figure 24, shows the position of components, with the sapphire PA cell designed to transmit incident laser light with little loss [62]. The measurements need to be tuned to account for the metal or substrate being measured.

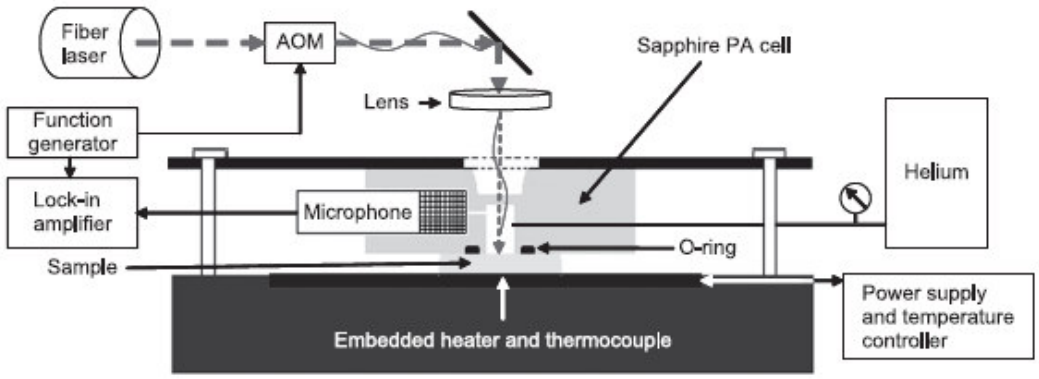

Figure 24. Schematic of photoacoustic test cell [62].

The PA offers the advantage of being noninvasive, adding little observer effect to results and allowing the sample to be used. Its transient nature allows it to measure the internal resistances of layered structures and those incorporating MWNTs, however long periods of heating(30min+) can be used to measure steady state conditions [66]. The

uncertainty for PA is acceptable, ranging from .5 – 1 mm^2 K/W based on the materials measured and the degree of calibration.

The substrate, catalyst and growth type all have major effects on the conductivity of the TIM. One study found that annealing the seed layer and substrate in oxygen prior to PECVD growth resulted in an 85% drop in resistance in resultant arrays. Another study found a large drop in resistance occurring when particle density corresponded to a critical point for attaining vertical alignment, a value that varies based on height. Arrays of MWNTs grown from Ni after this point were able to achieve a resistance of 80 mm^2K/W, comparable to that of thermal grease [67]. Those grown from nanostructured Fe_2O_3 templates matched that with low densities, with thicker samples at higher calcination temperatures reaching resistances as low as 10mm^2K/W [63]. Hu et al were able to find effective conductivity values of SWNT arrays at 74-83 W/m-K [62]. The discrepancy between conductance and conductivity from lower areas still plays an effect, and leads to over predictions of TIM performance, though attempts have been made to derive equations for the volume and area fraction of SWNTs from measuring array weight [48]. It took a 2.3 um diameter wide SWNT to actually obtain the thermal conductance predicted for a 1 nm SWNT [52].

The transverse conductivity between the tubes has also been examined. At 300K, MWNT arrays exhibited conductivity of just 1.52 W/m-K and SWNT arrays only 1.64 W/m-k along this direction, 200x less than copper conductivity, and 20x less than CNT arrays measured in the axial direction [28]. Simulations have verified the transport to occur through phonon scattering rather than ballistic transport. Heat spreading, in general, across the array is poor, as the temperature gradient from the center of an array to its edges varies by only .3% [20].

Physical properties are also lower. Even nanotubes bundled as wire show a 68% drop in Young's modulus [68]. Arrays have exhibited elastic modulus as low as 10-20 MPa, an order of magnitude below individual tubes [62].

2.4.2 CNT Array Thermal Interfaces

Using CNT arrays as a TIMs not only requires maximizing thermal performance, but doing so in a way which can be integrated into the manufacturing process. An array must maintain its strength and vertical alignment when transported, and must wet and conform to the bonding surfaces, all the while maintaining a low bond line thickness and cost. In CNT arrays, all these factors can be controlled, and different research has attacked the issue of improving such interfaces from different directions.

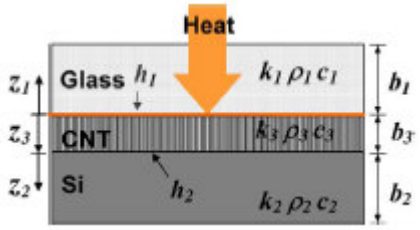

Figure 25. Heat conduction model for a very basic CNT TIM [16].

Improving the thermal properties of CNT arrays remains the primary avenue of improvement. TIM CNT arrays have been modeled to determine the flow of heat, and studies have found that the dominant source of resistance is at single CNT contacts with the interface. These regions could be modeled through ballistic thermal resistance, as opposed to constriction resistance. The internal thermal conductivity of the interface had negligible effect on resistance for arrays below 30um in height, and thus only tube density and contact mattered [69]. While the low height dependence allowed for a decreased BLT and the pliancy of the CNTs allowed for good contact with compression, a minimum height is needed to ensure CNTs are in full contact with the opposing bonding surface. This occurred only at 40-55um for a typical low density growth of 270 CNTs/um^2, but would drop with higher densities [67].

Retaining the growth substrate as part of TIM ensures good contact with most tubes. This does, though, allow for variation in properties based on the catalyst used. By simply varying the growth conditions for Ni and Fe seeds, Fisher et al created interfaces ranging from 20-32 mm^{2}K/W at 445KPa pressure , two to three times lower than

resistances achieved by CNT based composites [23]. Despite good contact, growth stresses can still break contact with the substrate. This may account for the two order of magnitude difference between predicted interface resistance and that measured at the growth interface. Even in a >100um sample, this value was found to account for 33% of the overall interface resistance(ITR), when there was no pressure applied beyond simple atmosphere.

Improved performance comes with higher pressures as Figure 27 highlights. At 241 KPa pressures on a Si-CNT-Ag interface, Fisher et al, found ITR at CNT-Si of 2 mm^2K/W and CNT-Ag of 14 mm^2K/W, the latter being due to the lack of bond between the CNT and silver foil. The overall resistance of the interface measured using PA testing methodology was 15 mm^2 K/W [62]. For PECVD grown MWNTs on Ni, with a Ni coated ZnSe window on top, the overall resistance including ITR, decreased from 15.5 mm^2K/W at a low 147KPa to 12 mm^2K/W at 550KPa. This range of results makes it comparable overall to a 5.2 W/m-K conductive thermal grease [21]. Naturally, the pressure dependence also depends on the contact surface and tube height. A 7um CNT array pressed to copper showed a 60% drop in resistance from a 169-445KPa pressure rise, whereas a slightly taller 10um maintained a lower resistance and showed only a 35% drop, as seen in Fig 27 [20]. Fisher et al again managed to lower the requisite pressure by using a 2^{nd} CNT layer, creating a Si-CNT-Cu foil-CNT-Ag foil interface shown in Figure 26, which not only allows CNTs to deform but also the Cu foil, increasing contact points. The foil achieved 7 mm^2K/W with just 100KPa pressure [56].

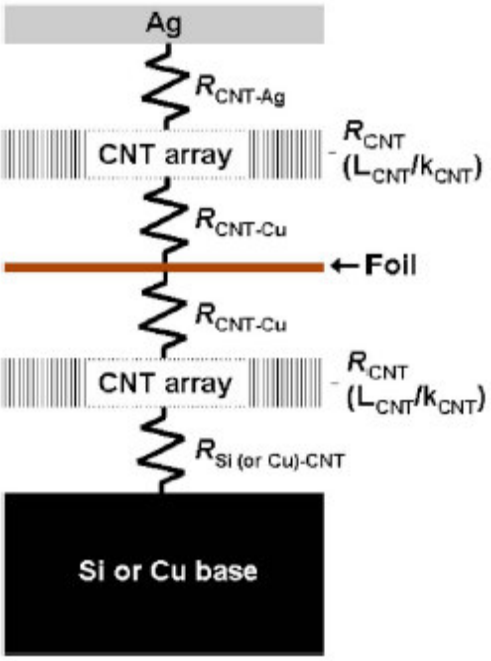

Figure 26. Double sided Si-CNT-Cu-SNT-AG interface created by Cola et al [22].

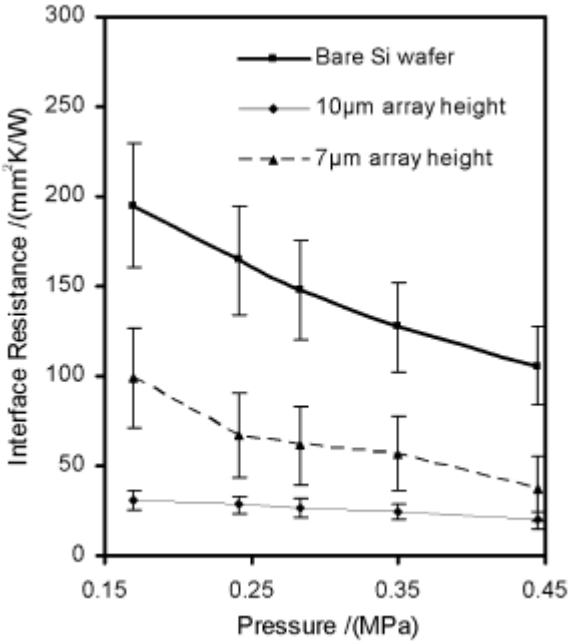

Figure 27. Pressure effect on ITR with array height [20].

Filler and bonding material has been used to lower ITR at lower pressures. “Wet interfaces” incorporate polymers to enhance thermal flow between tubes and at interfaces. Huang et al were able to create an aligned polymer-CNT composite by injecting S160 polymer into a CVD grown array, as displayed in Figure 28. A 50um film

of .4% by volume loading achieved a modest 100mm^{2}K/W, but still an improvement over pure polymer or unaligned tubes.

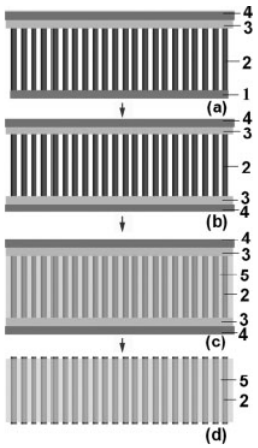

Figure 28. Formation of aligned CNT/polymer TIM with: (1) Silicon Substrate (2) CNT (3) Adhesive Layer (4) Polyester Film (5) Polymer Matrix (a) Coating a protective layer (b) Forming the mold (c) Injecting Polymers (d) Removing covers [57].

"Dry interfaces" incorporate no filler but may still use a metal bonding layer. Majumdar et al created a Si-MWNT-glass interface shown in Figure 25 using a 1um thick layer of indium to bond the CNTs and glass by a melt and reflow process at ~150°C. While the resistance in the Indium/glass interface was still an order of magnitude larger than the Si-CNT, the overall conductance of the interface showed an order of magnitude increase over the non welded version [16]. Goodson et al attempted a similar procedure, using a thin adhesion layer of Al/Pd to bond the exposed CNTs and achieving a resistance of 12mm^{2}K/W, comparable to the Ag foil results but without the need for excessive pressure [70]. Slightly higher values of 25 mm^{2}K/W were achieved at 413KPa in interfaces by Meyappan et al, who created arrays of carbon nanofibers and used electro deposition to fill in the trenches with copper. This value is fairly high considering the height of the layer was 500um and the copper composite layer did not form a bond with the top. A summary of all the CNT TIMs is presented in Table 1 below.

Table 1. Performance of various CNT array based TIMs

Group	Interface Layer	R_{int} (mm^2K/W)	CNT Thickness (μm)	Applied Pressure(KPa)	Filler/Bonding Material	Ref.
Huang et. al.	MWNT	110-400	50-525	-	S160 Polymer	[57]
Son et. al.	Si-MWNT	49	215	0	-	[71]
Liu et al.	Metal - MWNT-Ni/ZnSe	11-29	10-60	-	-	[67]
Cola et. al	Si-MWNT-Ag Si-MWNT-MWNT-Cu	16 4	15 35	241 172-379	- -	[22]
Cola et al.	SiC-MWNT-Ag	8	25	350	-	[66]
Cola et al.	SiC-MWNT-Cu-MWNT-Ag	4	100	80-150	-	[69]
Zhang et. al.	Si-Al-MWNT-LED	15	45	0	-	[72]
Tong et. al.	Si-CNF-Cu	25	500	413	Cu	[16]
Xu et. Al.	Si-MWNT-Ni/ZnSe	12-15.5	30	137-550	-	[21]
Panzer et. al.	Si-MWNT-Al/PD	12	28	-	Al/Pd	[70]
Cross	Cu-MWNT-Au-Si	10	35	60	Transferred	[24]
Majumdar et. al.	Si-MWNT-In-Glass	11	7	-	-	[16]

While the thermal performance of the CNT TIMs outlined can now match and exceed that of existing TIMs at 5-30 mm^2K/W resistance, their manufacturability and implementation poses an additional challenge. Research in this area has focused on TIM storage and transfer, package compatibility with processes, and economics [25]. Aligned CNT-polymer composites can be stored and applied simply [19]. Dry interfaces have the added advantage of being reusable. The SiC-MWNT-Ag foil and other preparations created by Fisher et all function similar to a thermal pad, relying on pressure to remain in contact, which can be released with the loss of adhesion from the foil of only a few CNTs [66]. If able to be created at lower cost, SWNT arrays can be used to form a strong bond with a surface from pressure, the fibers adhering through Van der Waals forces like hairs on a gecko's foot. An SWNT array actually achieved a dry adhesion strength of 29 N/cm^2

outperforming an actual gecko foot by a factor of 2 [73]. SWNT arrays also exhibit good thermal properties but are more challenging to grown the MWNT arrays.

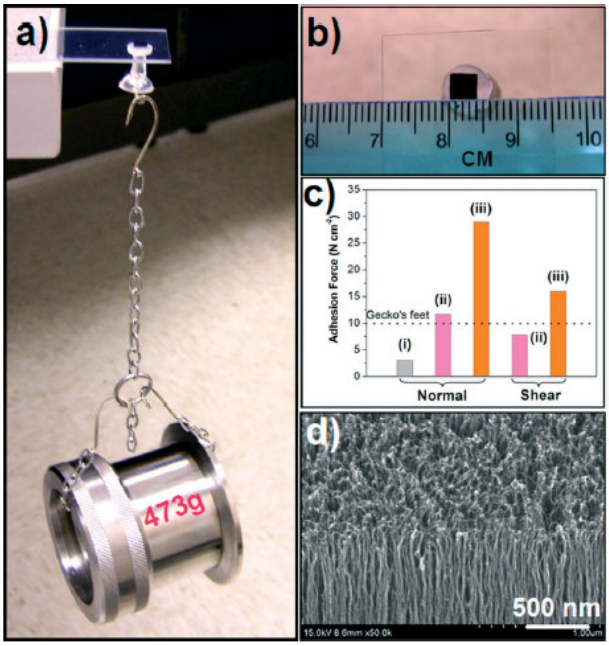

Figure 29. 4mm x 4mm SWNT adhesive holding .47kg weight [73].

Transfer of arrays remains a major issue for making CNT TIMs readily usable. Chan et al were able to bond a PECVD grown MWNT array to the back of an LED using a room temperature fast cure polymer. The light output of this LED maintained a linear relation with input current as high as 900mA, compared to a peak of 700mA for a commercial epoxy [72].

Diffusion bonds have also been used to connect arrays. This type of bond does not involve melting and resolidification of either side of the bond, but a slow reshaping of the contact surface under pressure and temperatures of .4 to .6 of the melting point. As the asperities and gaps at the interface yield under creep and the two surfaces come into atomic contact the surfaces fuse and bond obtains strengths near that of the bulk material itself [26]. Gold has been particularly successful as a bonding material at low temperatures shown in Figure 30, as it does not form an oxide at the bonding surface.

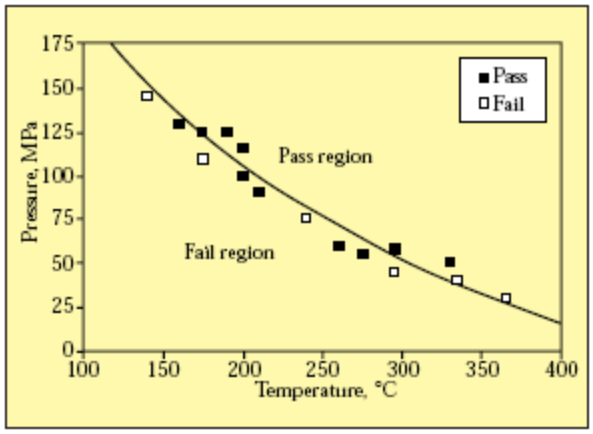

Figure 30. Thermocompressive forces needed to form diffusion bond of 3um thick gold [26].

Jiao et al exploited this to create a dry interface as Figure 31 depicts. A layer of 5nm TiW and 300nm of Au were deposited onto the surface of MWNTs grown via CVD on a sol-gel substrate. The thin film of gold was not uniform but formed nanoparticles. Their small size allowed them to form diffusion bonds with a similarly coated Si chip at 150°C. The solgel was then dissolved and with the sample cooled, the CNT array was effectively transferred to form a bond with an average tensile strength of .55 MPA [25].

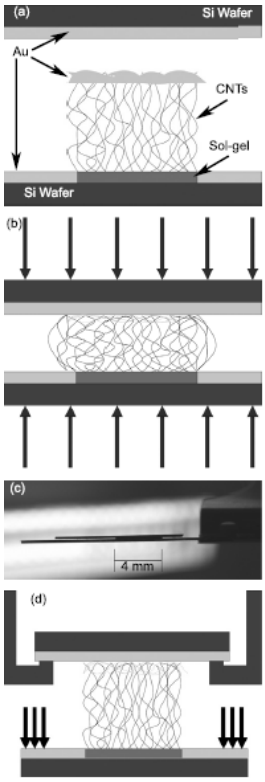

Figure 31. Thermocompression bonding and transfer of gold tipped CNT arrays [25].

Previous work has built upon both thermal and mechanical work, but has focused on manufacturability. Prior study has established our ability to transfer 35um tall MWNT arrays using a version of the diffusion bonding method above. These MWNTs were grown via simple TCVD and were water vapor etched to reduce their adhesion the growth substrate, allowing them to be transferred to polyimide tape prior to transfer. The transfer was achieved through the use of a 500nm Au layer at 200°C producing bonds with a tensile strength of .38 MPA and thermal resistivity as low as 22 mm^{2}K/W for 100KPa applied pressures [24]. This process demonstrated the feasibility of ready made CNT arrays that could be stored and bonded to surfaces as necessary.

The major goal of this study was to improve upon these results by achieving good strength and thermal performance at lower temperature, with a thinner bonding layer. CNT arrays were also grown and bonded with different metals. Bonds were created at various temperatures and tested for tensile strength. Samples were also created for thermal testing via the PA method.

CHAPTER 3

BACKGROUND AND LITERATURE REVIEW OF PHASE CHANGE THERMAL INTERFACES

3.1 Phase Change

Phase change (PC) describes the process of transition of a material from one state of matter to another. From a thermal engineering standpoint the beneficial transitions are melting from solid to liquid or evaporating from liquid to gas. The phase change process is ideal for thermal regulation due to its large amount of heat intake at constant temperature.

In nature, bees use the principle in hive design, filling in honey combs as needed to ensure that the hive temperature remains 35-36°C at all times [74]. The principle has also been applied to microelectronic cooling schemes in the form of heat pipes, such as Figure 32. Heat pipes employ evaporation, allowing a pool of liquid nearer the source to absorb heat and transform to gas, which can rapidly rise to the cooler interface, condense to liquid then be drawn back down via capillary action through a wick to repeat the cycle. Miniature heat pipes can transfer loads of 100-200W over a 50°C temperature range with an overall resistance of .1-.2 K/W, while maintaining some degree of flexibility that allows for easy package integration [75]. However, heat pipes are primarily used in the sink regions; TIM draw different advantages of the phase change process

Figure 32. LED die connected to radial heat sink through curved heat pipes.

3.2 Phase Change TIMs

While the phase change process can absorb a disproportionately large amount of heat compared to regular heating, its ability to regulate temperature is ultimately restricted by the amount of material, which can be controlled based on the pressure applied as Figure 33 shows. The low BLTs required for TIM preclude the use of much PCM and thus limit heat storage, beyond a short term buffer to handle surges in heat fluxes. However, PCM can still fulfill the purpose of matching the asperities on the surface, flowing into the contours in its melt state, leading to less contact resistance than solders, polymers or greases at lower pressures and thicknesses [38].

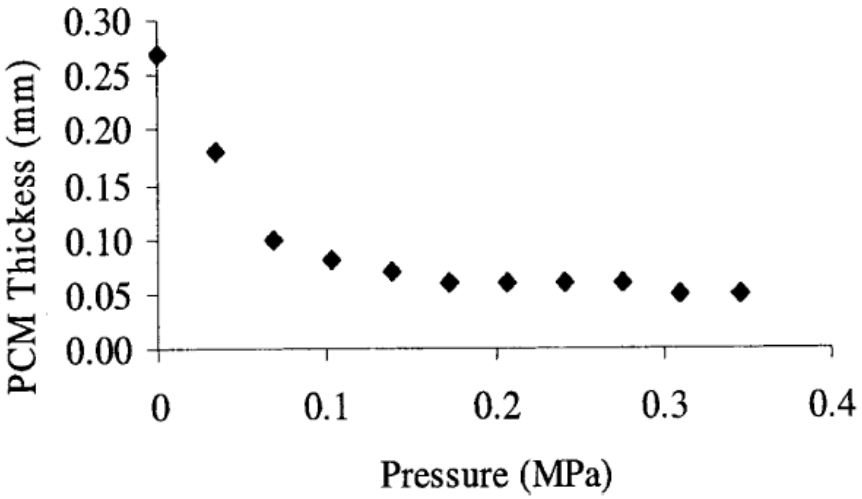

Figure 33. Graph of PCM BLT vs. pressure [38]

Surface chemistry plays a larger role in performance, with capillary force from surface tension in balance with the mechanical pressure and pressure from unfilled air pockets [2]. Increased conformability can be exploited by intentionally boosting surface roughness to increase contact area available for PCM.

PCM TIMs include various organics and polymers, such as polyesters and paraffins. The best exhibit resistances of 25-32 mm^2K/W [14, 76]. Compared to greases and solders this is still quite high due to the low internal conductivity, as can be seen

from Figure 34. While PCMs in liquid state can carry much higher heat fluxes, the resistance doesn't change due to higher temperature drops [77].

Interface Material	Thermal resistance ($cm^2 - °C/W$)	Pressure (kPa)
Chomerics T454 (PCM)	0.258	340
Eutectic Attach	0.04 – 0.17	---
Arctic Silver (Thermal Grease)	0.018	82

Figure 34. Resistances of a commercial PCM TIM compared to typical epoxy and solder.

PCMs are also subject to larger lifetime issues, such as pumpout and low mechanical stability in the liquid state. High temperature also degrades PCMs faster than purely solid polymers, increasing the junction resistance. While PCMs are chosen to have a liquidus temperature between ambient and the critical temperature of the device, even maintaining this temperature limits lifetime. An empirical equation along the structure of the Arrhenius gives lifetime resistance in terms of activation energy, E_a, time, t, the Boltzmann's constant, and temperature, T [2]:

$$R_{jc}(t) = R_{jc}(t_0) + \sqrt{t}\left(\frac{-E_a}{k_b T}\right) \tag{6}$$

One study found a 13% loss of organic material in the PCM by maintaining the temperature at $150^{\circ}C$ [77].

If the temperature is maintained low, a solid matrix can be used to solve mechanical issues. Fiberglass meshes have been used to provide mechanical rigidity against shock and vibration as well as offering a barrier against pumpout [6]. Like with greases, metallic filler such as zinc oxide(ZnO), alumina and carbon can be used to increase internal conductivity [78].

Both this filler and the matrixes can be replaced by CNT fibers or CNT arrays to improve overall performance.

3.3 CNT and phase change hybrid thermal interfaces

As with other TIMs, CNTs offer a high conductivity choice to add to PCMs, and offer similar benefits and drawbacks. The phase change nature adds complexity to the integration process, as MWNTs simply dispersed can separate and even delaminate the TIM when the PCM melts. Surface treatments and ultrasound modification of the CNT surface can be used to prevent separation. Ziegler-Natta polymerization can also be used to create the PCMs from monomer around the CNT filler [79].

The thermal conductivity also fluctuates with the phase change process. While both solid and liquid PCM conductivity see a proportional boost with CNT filler, the liquid showed a higher percentage improvement than the solid. This stems from the lower conductivity of the liquid phase, though the enhanced liquid still does not exceed that of unenhanced solid [80]. The thermal conductivity varies weakly with temperature above and below the transition temperature for the PCM – in the ranges below 45°C and 55°C for paraffin wax and below 50°C and above 63°C for palmitic acid [80, 81]. The CNTs actually affect the phase change temperature by physical and chemical disruption of the long range aligning forces that allow a polymer to shift from glass to crystalline phase. A 5% loading of SWNT increased the crystallization temperature of high density polyethylene, by 4°C [79]. A similar mechanism increases the latent heat capacity of the PCM, which can also provide tangential benefit to a TIM. By altering the van der Waals forces, a 1% loading of CNTs increased the heat of fusion by 13%. SWNTs increased this value more than MWNTs due to the greater molecular density and the larger surface area offered for the same volume [46].

Ultimately, CNT/PCM hybrids also suffer from the same issues as other composites, falling short of performance in both conductivity and heat storage expected through the law of mixtures. While homogeneity of the filler can be maintained, no alignment is possible in the composite state. Arrays are the only option.

3.3.1 CNT arrays incorporating PCMs

As highlighted earlier, while CNT array TIMs show high internal thermal conductivity and mechanical stability, the performance suffers from contact resistance, especially at low pressures. PCMs can remedy this both in solid and melt state by improving conformity.

Research in this area is limited, but the bulk has been performed by Fisher et al. One study employed a Honeywell PCM 45F pad, compressed to a 20um thick sheet, which was then placed over the exposed tips of a grown MWNT array as Figure 35 shows. This was then covered with a Cu plate, such that the total interface was Cu-PCM-CNT-Si. The resistance was measured with infrared thermography and reached a minimum of 5.2 mm^2K/W under a moderate 350KPa pressure and 40°C, similar to the lowest values in Table 1 above. However, the temperature of the experiment did not exceed the melt point of 45°C and a minimum 280KPa pressure was required just to have the PCM fill the voids in the array surface. The interface did outperform the Si-CNT-In-Cu tested at higher pressures in the same method, which had a resistance of 19.8 mm^2K/W [20, 62].

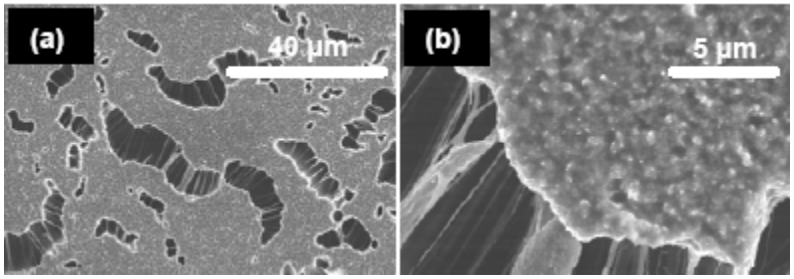

Figure 35. PCM coating surface of CNT array [29].

A later study by Fisher was able to create an improved interface. The PCM layer was again used to coat the exposed tips, but was deposited using a wicking process shown in Figure 36, in which the CNT array was inserted orthogonally into a pool of melted paraffin wax. Capillary forces allowed the wax to rise and form a <1um coat on top of the CNTs.

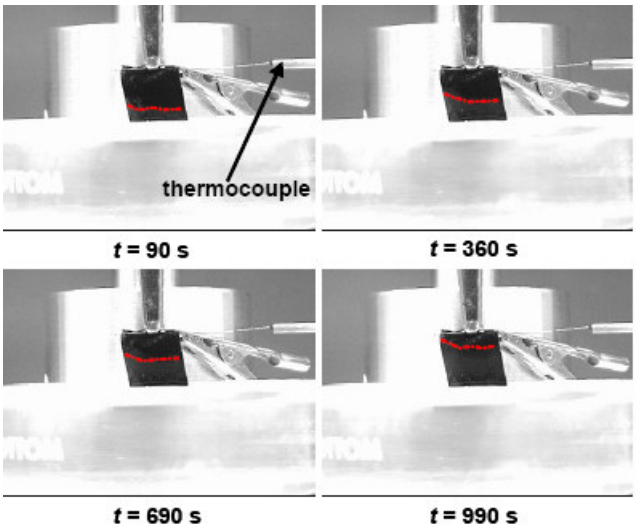

Figure 36. Wicking method of paraffin coating of CNTs showing advancing wax front[29].

When measured with PA testing under 207KPa pressure, this Si-CNT-PCM-Ag interface produced a resistance of 2 mm^2K/W for the low pressures shown in Figure 37, the lowest to date for CNT array TIMs. The tests were conducted at 60°C, above the melt temperature of paraffin wax at 50°C, allowing for the melted PCM to improve contact resistance without adding much thermal resistance. Partly this was explained by the good affinity the wax had with the Ag foil, where it was estimated to have a hydrophilic contact angle of 47°.

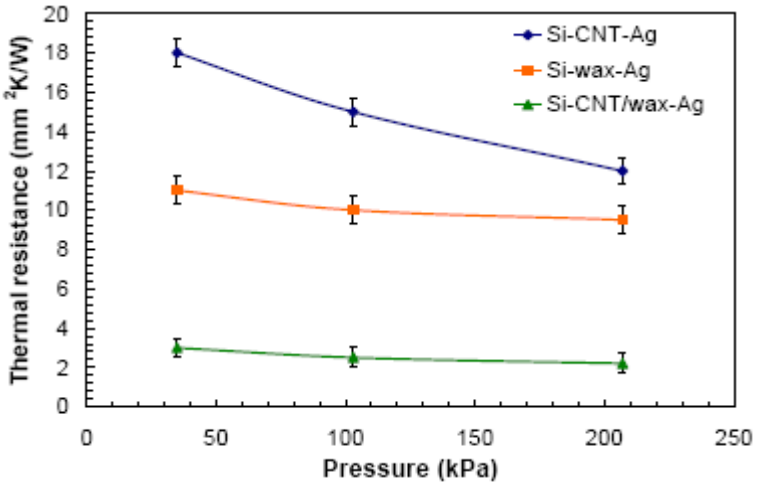

Figure 37. Resistance of Si-CNT-Wax-AG array compared to other TIMs [29].

Table 2. Performance of CNT TIMs which have PCM incorporated

Group	Interface Layer	R_{int} (mm^2K/W)	CNT Thickness (µm)	Applied Pressure(K Pa)	PCM	Ref.
Xu et. al.	Si-MWNT-PCM-Cu	5.2	10	340	Honeywell PCM 45F	[20]
Cola et. al.	Si-MWNT-PCM-Ag	2	45	0	Paraffin Wax	[29]

While these results are exciting, the process for creation of these interfaces is too complex to apply to manufacture. In addition, the interface, as set up, is vulnerable to pump out of the PCM in liquid state and eventual degradation. In this study we sought to create a more simple method for applying PCM to the CNT interface. We also explored different ways of containing the PCM using patterning of the array. Finally, thermal and mechanical testing was performed to analyze the benefits and drawbacks of these designs.

CHAPTER 4

INCREASING MANUFACTURABILITY OF CARBON NANOTUBE THERMAL INTERFACES

4.1 Introduction

The ideal thermal interface layer must be thermally conductive and mechanically strong. For a CNT layer, increasing conductivity through the layer consists of minimizing CNT internal resistance by growing dense, uniformly short, vertically aligned MWNTs and minimizing contact resistance by establishing a thermal bond between the interface layer and both the sink and source. Other groups have focused on lowering both these internal and contact resistances, however, not much exploration has been done on whether these resulting interfaces are mechanically stable. Obtaining high performance in both areas requires some tradeoffs. As the density of CNTs increase, their compliance decreases and may prevent the conformal mating with an interface during bonding. Thus, as the internal resistance decreases, the interface resistance may increase. Such issues may also arise with metallization thickness. Thicker metallization layers may also decrease the ability to conform to the bonding interface. Thus, we need to establish a methodology to understand the bonding of CNT based TIMs and how metallization affects the overall performance.

Prior work on CNT layers has established several procedures for creating bonding layers, such as thermal bonding using polymers or gold. This study focuses on examining the variables involved to improve these techniques and make them more amenable to current manufacturing and operating conditions. Carbon nanotubes arrays were grown via thermal CVD techniques and then transferred to various other substrates by coating the tips with a metal and bonding them using a thermocompression method. By altering the thickness and deposition rate of the metal layer, the grain size of the nanoparticles that made up this layer on the CNT surface was able to be controlled with good accuracy. This reduced grain size allowed for bonding to occur at temperatures of 150°C and even

below, ideal for processing steps of microelectronics that may incur damage and a reduction in durability or lifetime when bonded at higher temperatures [58]. The factor of cost in the production of the bond was also explored by comparing gold with the significantly less expensive copper for the bonding layer. The copper demanded a slightly longer processing time and had more limits in applicability, but successful bonding was accomplished.

Finally, a phase change material was implemented into the interface fabrication process. The phase change process had shown potential to improve thermal interfaces involving CNTs in prior work due to its ability to fill asperities and enhance lateral heat transport. The goal of this study was to examine both its ability to improve the metal bonded CNT array TIMs and its potential for containment within the array. For the former, the paraffin wax was implemented in a serial manner by coating the surface between the gold-gold diffusion bond, with the hopes of filling in any air gaps left behind in the bond. The ability of the CNT array to contain wax was also examined, by creating a parallel hybrid structure, with gaps in the array where the wax could flow in and fill. Two different void patterns – 4 small gaps and 1 large gap – were tested. While the size scales of these gaps were too large for use in an actual TIM layer, as they would create hotspots, the hope was this would clear the way for a finer honey-comb like dispersion of the wax in the future.

The wax addition steps were inserted into the gold bond fabrication process, with only a few additional microfabrication techniques necessary, and both interfaces were manufactured successfully. Some containment issues of the phase change materials were discussed.

4. 2 Experimental Procedure

4.2.1 CNT Array Growth

The process for the growth of CNT arrays has previously been established to sufficient detail and was replicated for this experiment. The CNT seed layer was created

in a Class 100 cleanroom environment. Silicon was used as the growth substrate, due to its high processing temperature limit. In all cases, a standard 550um thick Si wafer was coated with 200nm of SiO_2 as a passivating layer to prevent silicide formation. Atop this, a 5 nm Fe catalyst layer was deposited by E-beam evaporation. Past results studied the effect of variance of this catalyst layer thickness, but it was kept at the stable height for all growth in this study. Once deposited, the 10cm wafers were diced into a grid of $1cm^2$ squares using a dicing saw to create standard size CNT arrays for testing purposes. With proper blade selection and short cuts to minimize water exposure, oxidation and cracking could be avoided.

The CNTs were grown via thermal CVD using the First Nano Easy Tube furnace. The furnace utilized the thermal CVD process, first melting the catalyst into a liquid form in an inert environment of argon, creating mobile catalysts without allowing them to form into silicides. Then, process gases (methane, hydrogen, nitrogen) were introduced into the chamber for a short amount of time(<10min) before cooling it down, again in a nonreactive argon environment to prevent impurities. The process gasses employed for the growth stage were hydrogen, methane and acetylene, while nonreactive argon was used to keep the surfaces free of impurities for the heating and cooling stages. The flow rate of each gas was controlled by a mass flow controller. The rates and times to achieve growth of a certain height have been specified in literature but the particular variances in each machine necessitated us to spend some time examining the control of the height ourselves. A short water vapor flow step was also added at times to decrease the adhesion of the array to the silicon. The gaseous H_2O was introduce shortly after the growth phase, and operated by attacking the interface between the silicon and the CNT [82].

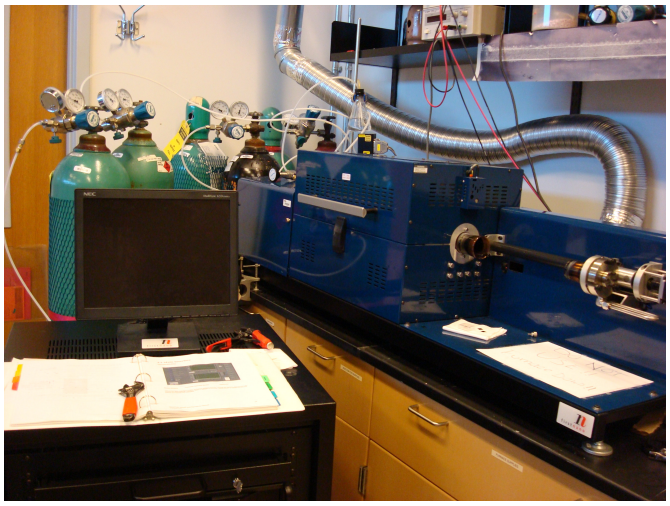

Figure 38. Thermal CVD used for CNT growth.

4.2.2 Metal Deposition, SEM Scanning and Bonding

The bonding procedure followed the overall protocol established in prior work.

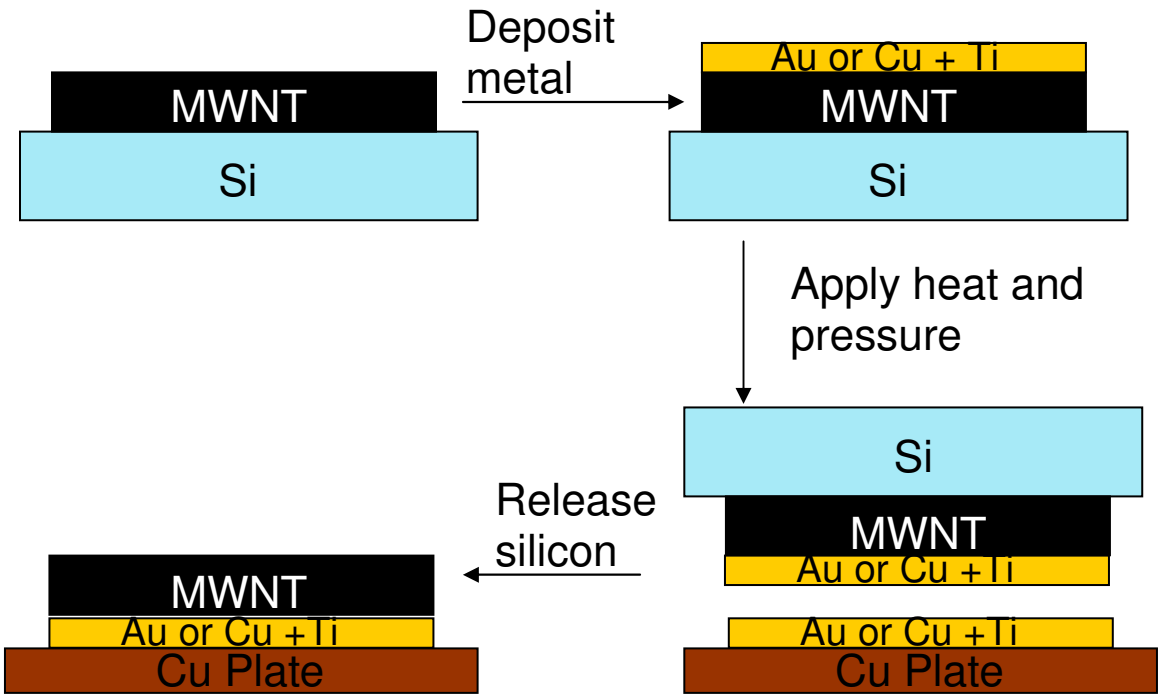

Figure 39. Basic thermocompression technique used in study (not to scale).

With the prerogative to obtain a stable bond at temperatures compatible with microelectronic devices that may utilize the thermal interface, the ideal choice was to

create a metal adhesion layer. Past work established that a 500 -1000 nm layer of Au deposited on top of the CNT array could be melted to form a bond between 150°C and 200°C and pressures of a few atmospheres. This still lies outside of the max processing temperature for many solid state devices. The main focus of improvement was to modify the bond layer to create a diffusion bond below temperatures that would damage such devices. The diffusion bond between metals can be modeled as series of triangular asperities in periodic contact with each other such as in Figure 40. An elementary equation relating the various bond and surface properties can be written as[83]:

$$t_{bond} \propto \frac{\ln(d_F / d_0)}{P^n} \tag{7}$$

Or as it relates to temperature by:

$$t_{bond} = \frac{T}{e^{(-Q/RT)}}\left(\frac{1}{P}\right)^n \tag{8}$$

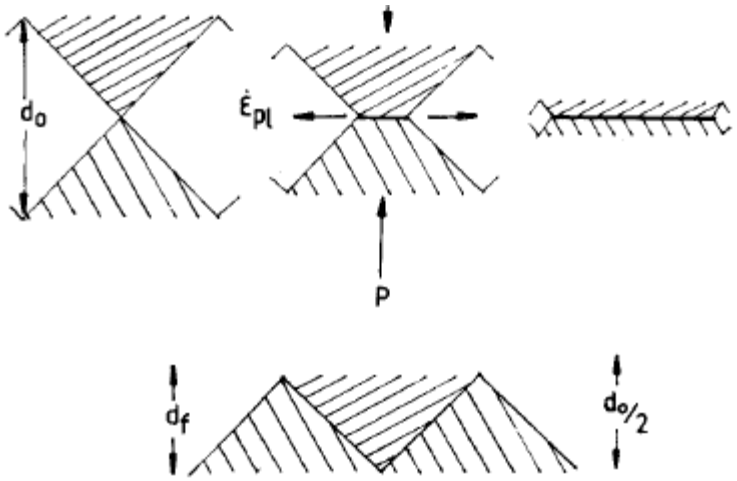

Figure 40. Diffusion bonding approximation proposed by Hamilton [83].

While these equations don't translate perfectly to the nanoscale regime of this study, the important points are that diffusion time should decrease as the asperity thickness decreases, and pressure and temperature increase. The diffusion temperature and speed were thus dependent on the particle size and thickness, with smaller aggregates of metal being more thermally excitable and susceptible to creep conformation with the opposing

surface. While large/macroscale 1mm thick samples of gold can be bonded at temperatures of just 100°C, the full process took 22h [84]. For the needs of microelectronic manufacturing the process time had to be much lower, so the bond time was held at a constant of a few minutes, and the temperature was explored, hopefully low given the thin bond.

The metal was deposited via CVC E-beam evaporator. Other than gold used in prior studies, this exploration also explored the viability of copper, as it possesses higher thermal conductivity and is already a staple in microelectronics. The choice for the metal layer as well its thickness and rate of deposition could be controlled here, allowing for the manipulation of the layer formation and hence the bond temperature. The metal was typically deposited on both the CNT tips and the bonding surface simultaneously to increase the number of bonding particles while ensuring the average size of the particles remained small. A thin 20 nm layer of titanium was first deposited as an adhesion layer, with the thicker 100, 200 or 500 nm gold or copper bonding layer evaporated immediately on top afterwards. After the bonding, the process was repeated with the free end of the CNT tubes and the second surface to which the CNTs were to be bonded. These were again bonded by applying pressure and heating.

The transfer and bonding processes were executed using a Carver press. The samples were loaded onto a platen outside the press, while the compression plates were heated to the appropriate temperature. When this was reached, the platen with the samples would be placed inside with another plate on top to ensure even bonding, and the press was compressed to just below 400KPa. This pressure was calculated by taking the weight load and dividing by the apparent area of the array. Thus the actual pressure on the CNT layer is much higher, however, the CNTs can handle much higher pressures without breaking. As it is the device to which they are bonded to which must survive the process and as the apparent area will be the same as the real area, 400KPa is accurate.

This pressure and temperature were held for a few minutes, then the press was opened and the samples were removed and cooled. If the process was a transfer, the substrate material was released with pressure applied along the edge. For any sort of characterization, the bond process was repeated on the exposed CNTs post-transfer, as will be discussed in the next chapter.

Figure 41. Carver thermal press loaded with sample for bonding.

All stages of the process were verified via SEM imaging. The Hitachi 3500H SEM allowed for rapid examination of properties like CNT height and growth density, however it's utility faltered beyond magnifications of a few thousand. The Zeiss SEM Ultra 60 allowed for extremely high magnification, allowing for clear views of features as small as a few nm, making it critical for examining the nanoparticle size. It also allowed for observation of the thickness of the gold layer. Both tools were generally non-destructive to the sample.

4.2.3 Phase Change Interface Fabrication

The PCM chosen for this study was Paraffin Wax(C_nH_{n+2} ,19<n<41), due to its low melting temperature below 60°C and its use in prior studies for comparison. This allowed for it to reach the liquid state by the normal operational temperature of LEDs and other common microelectronic devices. The particular brand used was Country Lane

General Candle Wax(#40500). The particular chemical and melting point data were not examined for this study, however this wax reached the melt state below 58°C, which can be used to estimate that n=34-38 in the chemical formula above.

Figure 42. Block of paraffin wax used in study.

The wax was applied and tested in two settings, a serial and parallel implementation. The aim of both processes was to find a simple way to contain the wax in a manner that it could assist in lowering the thermal interface resistance. The serial structure contained a <10um layer of wax sandwiched between the two top bonding layers of gold. This was less intended to help with lateral transport and more to fill in any air pockets not eliminated via the diffusion bond. The hope was that this wax would optimize conductivity, without being susceptible to pump-out as if it was wicked through the CNT layer, such as in prior studies.

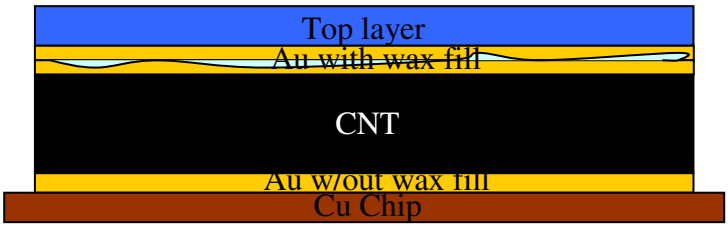

Figure 43. Serial phase change interface design.

The parallel implementation placed the wax within the CNT array itself. Two designs were tested, one with a single wax reservoir at the center of the array, and the other with four small pockets summing to an equivalent volume arranged in a grid near the center of

the CNT array. Since each region of wax took the place of high conductivity CNTs, however, the goal of this portion of the study was to examine the feasibility of implementing and filling this "honeycomb" pattern, rather than thermal testing. Further work would be needed to determine the optimal size and spacing of the wax pockets.

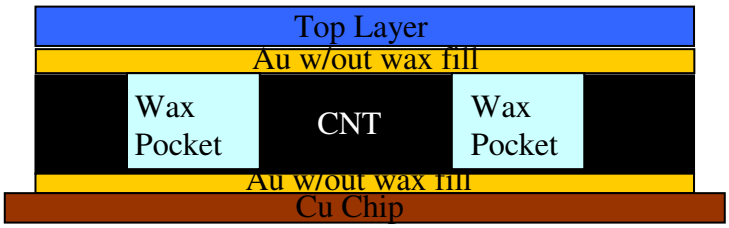

Figure 44. Parallel phase change design cross section with multiple small PCM reservoirs.

For both the serial and parallel structures, the fabrication techniques deviated only slightly from the previous fabrication method of CNT growth, coating and transfer. For the serial structure no difference would be noticed up to the final bond stage prior to mechanical or thermal characterization. The creation of the parallel structure required use of lithography techniques as in Figure 45. After growing the oxide layer on the Si substrate as usual, a 1um layer of negative resist NR7-1500P from Futurex inc was deposited across the top. The resist was then patterned using a darkfield mask under 365nm UV light for 40 seconds. After developing the resist, Fe could be deposited per normal using the e-beam evaporator. However, after deposition, the PR layer was stripped, leaving catalyst only in the desired pattern. This could be used to grow the patterned CNT array.

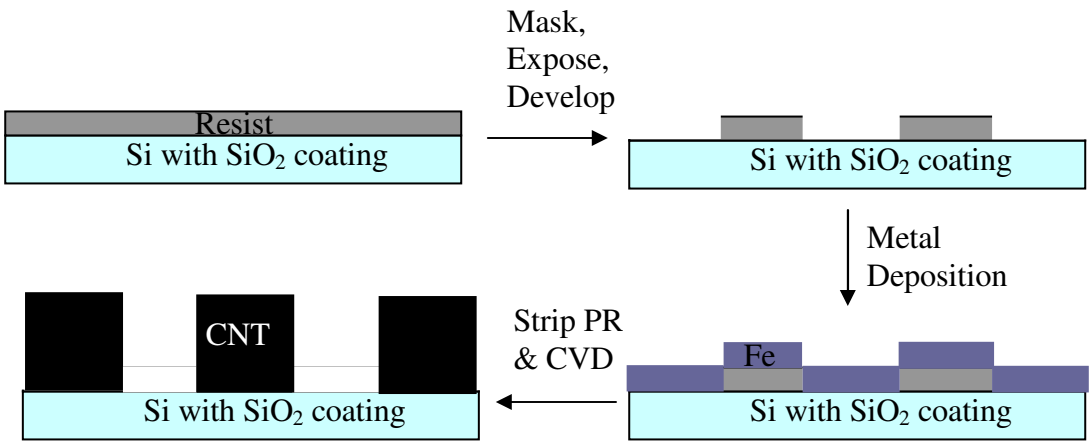

Figure 45. Microfabriation steps for patterned array with phase change.

The CNT array, patterned or not, was coated again with gold, and transferred to a copper plate. Here the array and plate were then coated again with the gold, before the wax was applied. This does create a 100nm layer of gold between the wax and silicon in the wax pockets for the parallel design, but given that the height of the array was 40um, the effect of this gold layer would be negligible on the results.

Prior work by Fisher[15] used a wicking process to create a 1um layer of wax on top of the CNT array, but this process would only coat the CNTs and leave nothing in the pockets that were intended to contain wax. Instead, scraps of solid paraffin were added directly on top of the gold surface or in the spaces left behind, after heating the copper square. The excess material was expunged in the thermal press, and could be scraped off the side of the square.

4.3 Results and Discussion

4.3.1 CNT array growth

The growth of the array went smoothly using recipes similar to prior work [24]. The CNTs grew at a rate of roughly 40 to 50 microns/min of growth phase. Previous use of the bare Fe catalyst indicated that the array reached a peak within the first five minutes of growth; however, we observed that it continued without signs of abatement well into 10 minutes from the start of the process, growing uniform arrays as high as 600 microns.

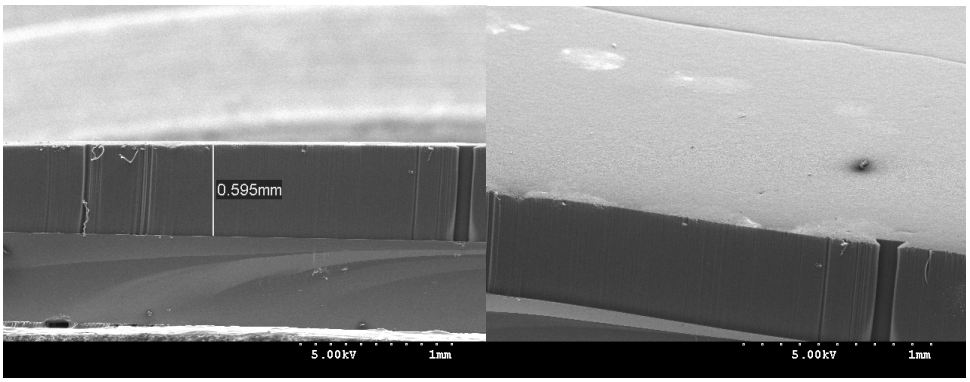

Figure 46. Long-term CNT growths.

Further examination under SEMs shows that the slow deposition rate of .2 angstroms/sec of Fe may form very small nanoparticles. These could prove more excitable and reactive than larger structures, leading to faster growth rates.

While the control of growth at this height could be interesting, the project required much shorter arrays to minimize interface resistance. The final recipe for the process is outlined in Table 3.

Table 3. Process data for growth of 40 micron CNTs via thermal CVD

Step Name	**Temperature**	**Time (min)**	**Ar (sccm)**	**H_2 (sccm)**	**CH_4 (sccm)**	**C_2H_2 (sccm)**
Ramp	25→800°C	12	500	0	0	0
Soak	800°C	10	500	0	0	0
Growth	800°C	1	0	75	150	16
Cool 1	800→25°C	20	200	0	0	0
Cool 2	800→25°C	180	100	0	0	0

The recipe consistently produced carbon nanotubes with a height of 40 microns with a variation of +/- 5 microns between samples.

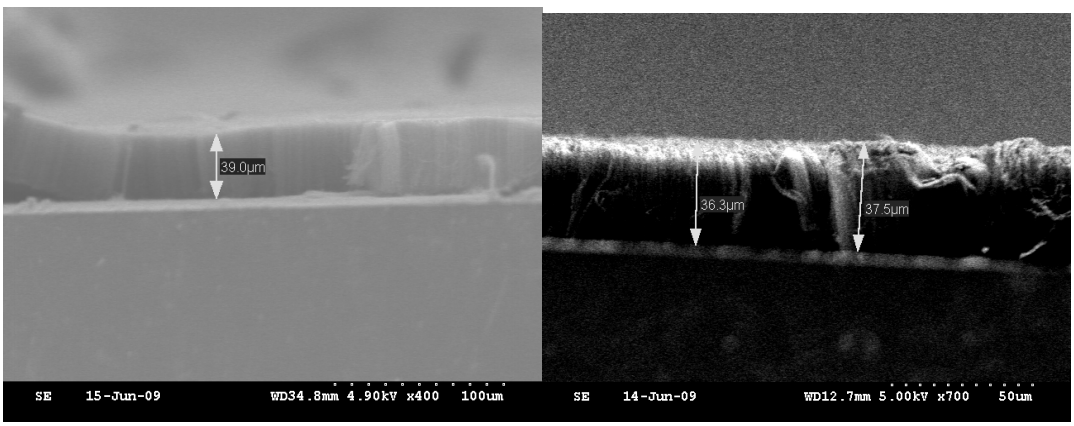

Figure 47. 40 micron CNT arrays used in study.

Similar fluctuations in height were visible near the edge of the same sample usually in the form of a shallow gradient. Other surface deformities such as bald spots and density variations also occurred especially if multiple die were grown at the same time. This was undoubtedly a result of the gas flow character shifting as it moved from the forward squares to the ones at the back. This could easily be resolved by providing sufficient distance between rows of CNT squares. Contamination issues also occasionally occurred from amorphous residue that had built inside the growth chamber. Even minor issues on the surface could have significant ramifications on metal coating or bonding steps. Cleaning the chamber ensured a level quality to the CNT array.

4.3.1 Transfer and Bonding Temperatures

For a given metal, the bonding temperature varied as a function of four variables outlined: the bonding pressure, the metal deposition rate, the metal layer thickness and the surface adhesion to the growth substrate. Of these, the bonding pressure was not examined in detail due to limitations on equipment precision, but simply maintained at below 400 KPa – sufficiently low for most commercial applications. The rest were studied via SEM imaging of several samples.

The metal deposition rate in the e-beam evaporator, as mentioned earlier, combined with the overall thickness controls the size of the nanoparticles formed on both the CNTs and the plate. Of the two factors, the thickness showed the larger definite effect. The nanoparticle size was examined at three thicknesses for gold – 100nm, 200nm, and 500nm, the last of which was the benchmark from the last study.

The average particle sizes were calculated by manual measurement of particle sizes across various samples for the same thickness. Most particles exhibited a roughly circular shape, and the diameter was used as the significant dimension. A two sample student's t-test samples was used to verify the correlation between the means:

$$t = \frac{\bar{X}_1 - \bar{X}_2}{S_{X_1X_2}\sqrt{\frac{2}{n}}} \tag{9}$$

The t is the standard error between the sample means X_1 and X_2, which can be calculated from these values plus the standard deviation S_{X1X2} and the sample and the size of the samples, n. Performing this test between samples verified that the means were statistically similar. The values for the particle sizes on the plate are shown in Figure 48.

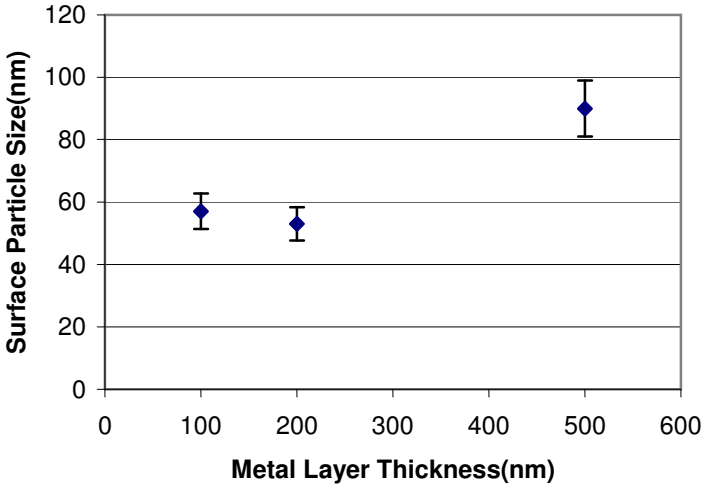

Figure 48. Average size of nanoparticles for a given thickness of metal deposition.

The average particle size dropped 50% from 90nm between 500nm and 200nm thickness. This is expected, since the larger thickness leads to a deposition of more gold on the surface. Surface tension from chemical forces would lead to the molecules aggregating in particles that were wider as they were taller. In addition, as the deposition rates were the same when studying the thickness, the 500nm case would have spent 150% more time in the high heat environment than the 200nm. This allows the particles more time in an energized state to move across the surface before grain boundaries formed.

There was only a marginal difference in particle size between the 200nm and 100nm samples. This statistic masks the stark difference in coverage between the two thicknesses. The 100nm did not display the dense, pebbled surface of the thicker samples,

but rather particles which dispersed randomly, sometimes in large clusters, but usually fairly isolated. The particle size also showed more variance, indicating that the issue was a combination of limited material and limited mobility.

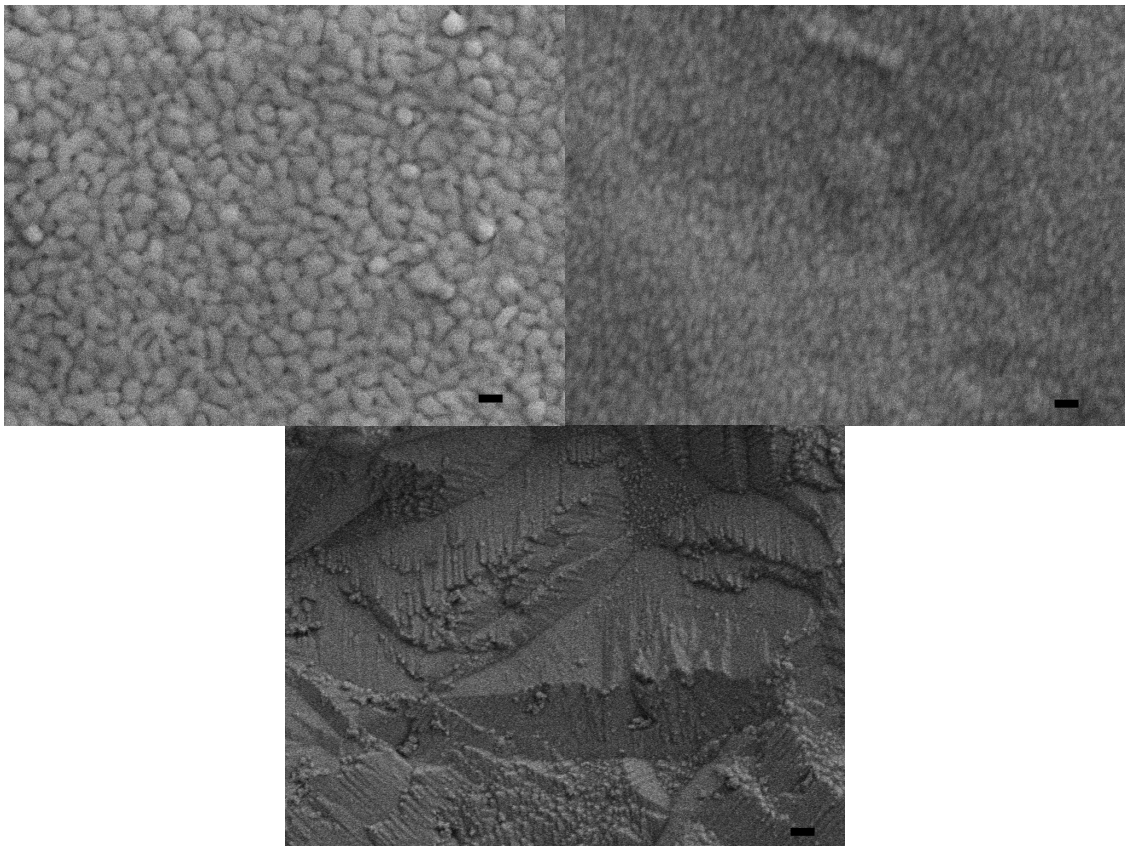

Figure 49. SEM images of plate with (Clockwise from top left) 500nm, 200nm and 100nm thick Au deposition (Black line is 100um).

Particle size on the CNT array surface posed a more difficult comparison between samples. The low thickness and noncontinuous nature of the CNT surface promotes the formation of discrete clusters rather than adjacent particles. This effect was visible even at 500nm though both top and isometric views as in Figure 50 reveal that all the CNTS were coated, but not uniformly.

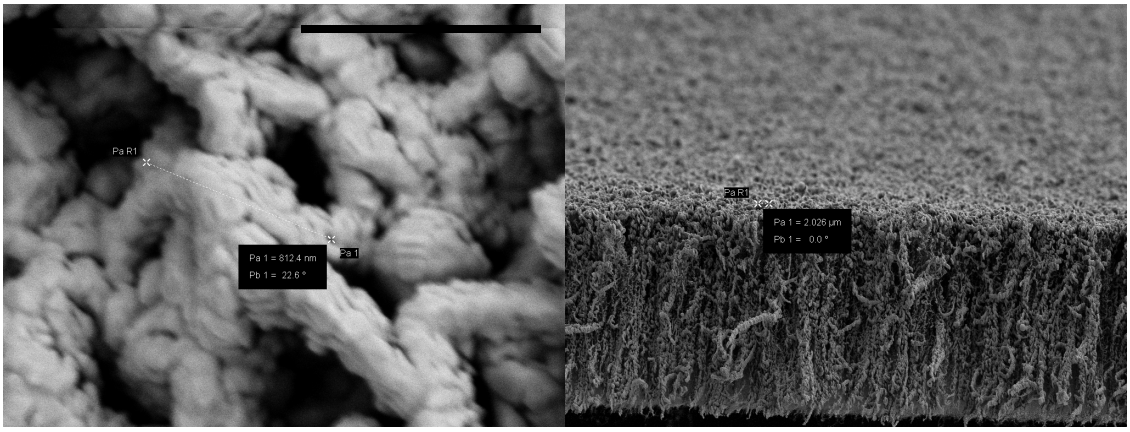

Figure 50. Thick coating of 500nm gold on CNT array surface (black line is 1um).

At 200nm and 100nm, the gold appeared only in clusters, measuring roughly 1-2um in width. Any trends in size were hard to identify.

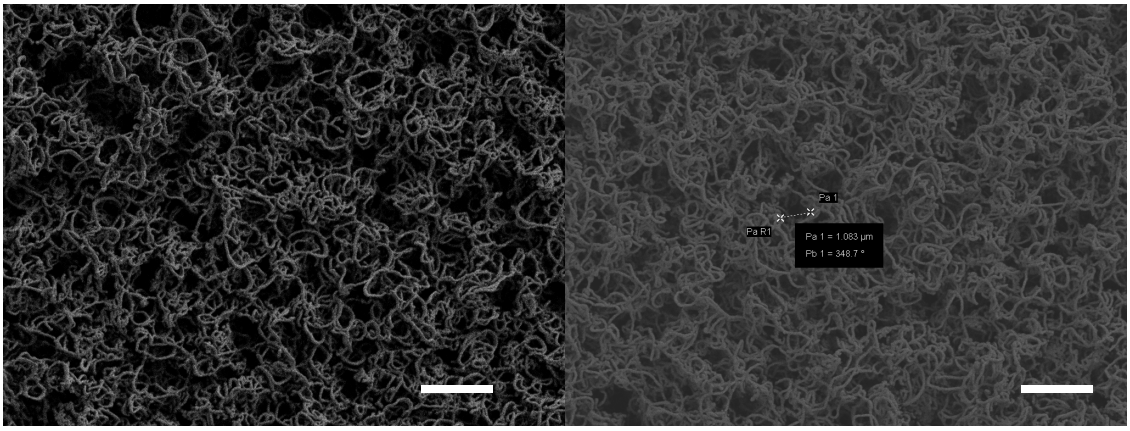

Figure 51. Less visible metal coverage of CNT array with 200nm Au(left) and 100nm Au(right) – white line is 1um.

The deposition rates proved less critical to controlling nanoparticle size on either plate or CNT surfaces. The 20nm titanium layer was deposited at a consistent rate of 2.0 Å/s, but the metal bonding layer was tested at rates of 1.0 and 2.0 Å/s with the 200nm and 100nm samples. In these samples, no clear pattern appeared correlating the rate and particle size, except for a small but statistically-insignificant particle size decrease with rate. Comparisons were also performed at rates of 3.0 and 1.5 Å/s for 500nm layers of gold. In this instance the particle size showed an increase from 90 ± 5nm to 94 ± 6nm as the rate was doubled. This small increase may indicate that the higher particle arrival rate

leads to the formation of larger islands than does the longer duration in melt state of the slower deposited sample.

The process following the metal deposition was the transfer, which was examined visually and through the SEM. Full transfer was considered when the full CNT array square appeared on the copper plate, without any gaps, holes or clear loss of tube density.

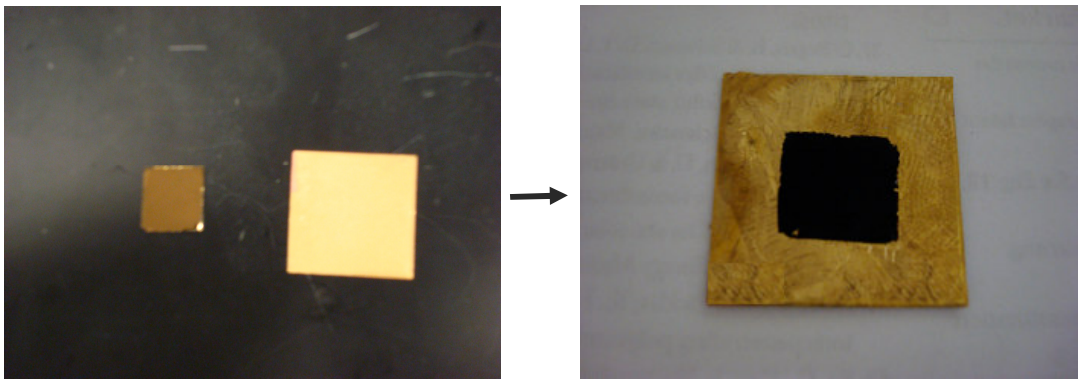

Figure 52. Near-ideal transfer of CNTs to copper square using gold bonding.

Bonding issues typically manifested as a result of either excessive adhesion to the growth substrate or insufficient bonding to the copper host. At most times, the regions that did not transfer properly were at the periphery of the CNT array, due to the presence of height variations in that region. However, more abnormal failures could occur, due to surface irregularities that appeared either in the growth or the metal deposition processes.

Bonding time also had an effect on the transfer process. The time in the thermal press was initial set to just 3 minutes per sample, but was shifted to 5 minutes after the latter proved to result in a better transfer yield rate. A short exploration of extreme bond times (30 mins+) found little further improvement at either 100nm or 200nm thickness indicating the diffusion process may have come to a finish by that time. A five minute time is ideal in that it is roughly similar to that of a process step for other TIMs in a high volume manufacturing process [2].

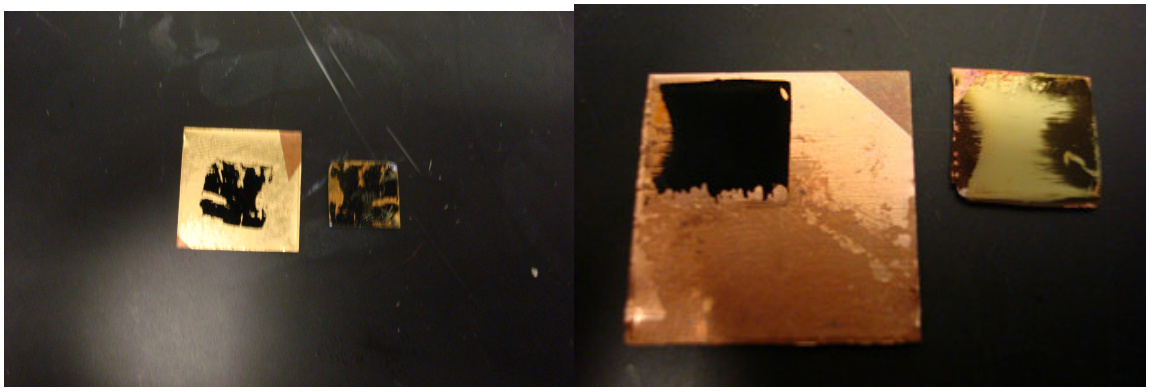

Figure 53. Transfer failures both severe (left) and at periphery(right).

Poor transfer at a given temperature could also be addressed by using a water vapor etch stage immediately after growth in the CVD to lower adhesion and remove some surface impurities. Past studies concluded an ideal etch rate of 80 ml/min for 5 minutes for releasing the CNT arrays, however, this study found a rate of 40 ml/min was sufficient for gold transfer processes. At higher rates, the flow proved excessive, causing surface defects by "washing" away tubes. Other than destroying the surface uniformity of the grown arrays, these drifting CNTs could linger in the CVD chamber and contaminate future growth processes. Excess loss of adhesion could cause CNT arrays to release from the substrate as a film either after growth or after experiencing some thermal stress in cooling down from the metal deposition process.

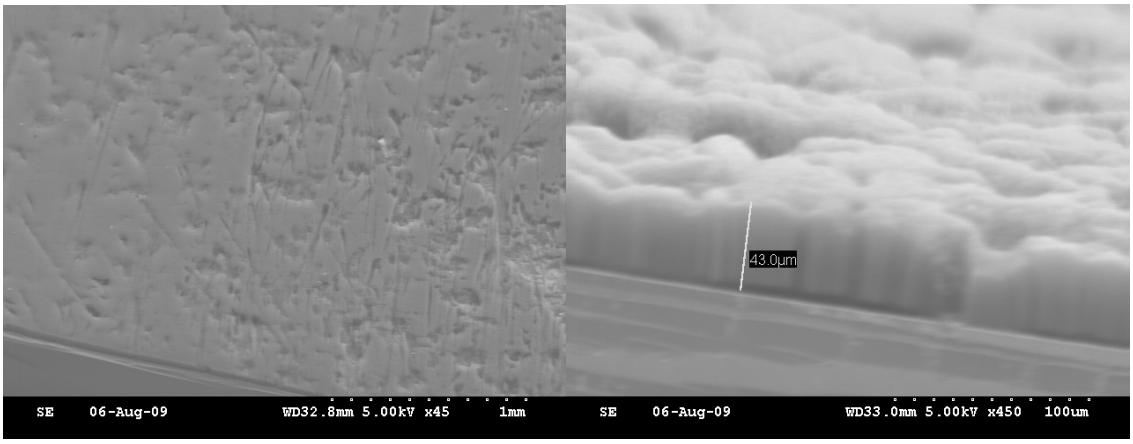

Figure 54. Damage to CNT array/washout of tubes from excessive water vapor etching.

The process was also vulnerable to minor scratching from human error, particularly during the release after the bonding. These factors limited a successful

transfer to a yield rate of 70%, but could be easily eliminated if the processes were automated.

Under SEM, it was possible to verify that macroscopically successful transfers did not contain microscale defects. With the Hitachi SEM, it could be observed that the CNTs maintained their vertical orientation and did not suffer permanent deformity or any significant surface damage from the pressures applied.

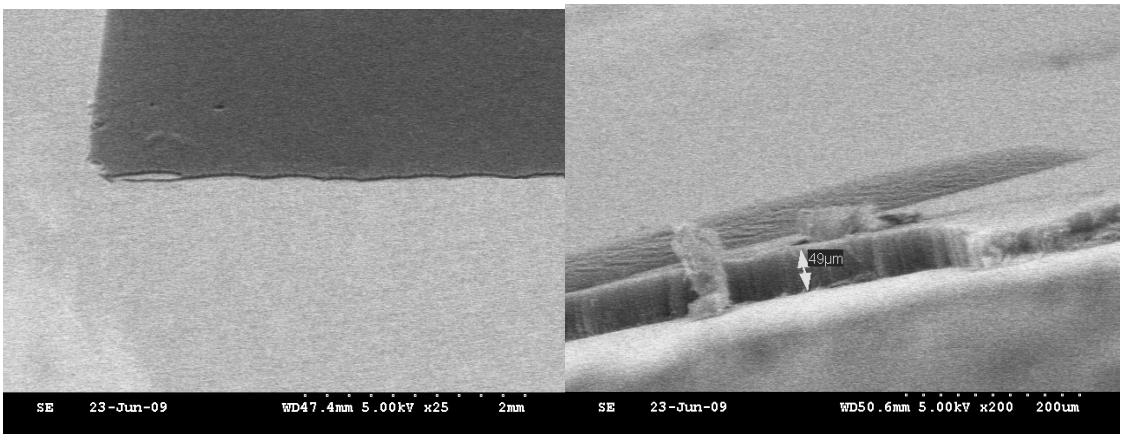

Figure 55. Retention of array geometry under SEM post-transfer.

Some amorphous carbon residue was left behind, but none made it through the transfer process or bonded to the copper square. This is an added benefit of the process, as it contacts tubes only of uniform height, while leaving behind carbon growths that could lower overall performance.

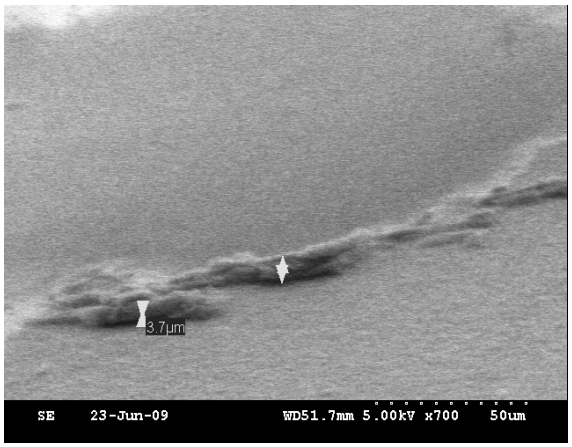

Figure 56. Amorphous carbon left behind on silicon wafer after transfer.

4.3.2 Gold Bonding Temperatures

The minimum bonding temperatures of these transfer and bonding processes were the primary focus in determining their applicability. Due to the time involved in producing samples, measurements were only taken at intervals of 5°C. Several samples were created in one batch and transfer was attempted at slightly greater and greater temperature until the full array transferred. This accounts for the uncertainty in the temperatures. Taking these into account, this study was still able to identify definite trends in that behavior as a function of the variance in the metal layer.

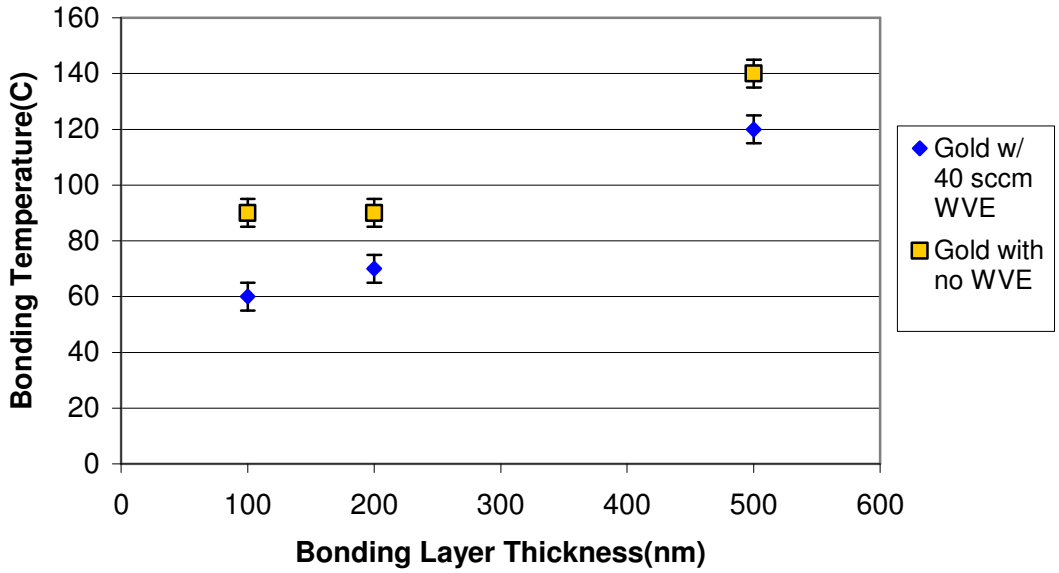

Figure 57. Minimum transfer temperature for various thickness gold coated arrays.

Lowering the thickness of the bonding layer had the largest effect on lowering the minimum process temperature, particularly between 500nm and 200nm. The 10°C drop from 200nm to 100nm was repeatably observed, but of less relative significance. These results mirror those observed relating thickness to nanoparticle size. A similar effect was observed with varying deposition rates for the 500nm thick layer, with the 1.5 Å/s exhibiting an average minimum bond temperature 5°C lower than the faster rate with higher nanoparticle size. As the tolerance for this measurement is itself 5°C though, these results only show a correlation between low particle size and low bond temperature. However, the diffusion bonding temperature and time have been shown to decrease with

both thickness and the size of the voids present when the surfaces are in contact. It follows that 200nm and 100nm samples bond at lower temperature due to the gold particles decreased thickness and area.

Water vapor etching also allowed for significant reduction in minimum process temperatures. A transfer/bond temperature as low as 60°C was repeatably obtained for the first time with a 100nm metal layer. This temperature may indicate that this process is now too low temperature for certain applications. If operation temperatures exceed that of the bond, the mechanical integrity may fail through fatigue. Thus, these minimum temperatures may actually be a lower bound for the process.

4.3.3 Cu vs. Au bonding comparison

Au was initially used due to its high thermal conductivity. However, copper presents both a higher conductivity and lower cost. Furthermore, a copper layer could form an ideal bond with copper sinks and not suffer from fatigue stress due to thermal lattice mismatch. It was thus selected as an alternative material to test the established transfer and bonding process.

The initial stage of metal deposition proceeded along similar lines to gold. The Cu was deposited in all cases at a rate of 2 Å/s. Though the transfer substrates were already copper squares, they were coated again in the evaporator to ensure the process mimicked that of gold in all ways. The matching lattice of the substrate and deposited metal did have a tendency to produce clusters of copper at higher thicknesses forming ridges and plateaus along the surface. For this reason only 100nm and 200nm cases were studied.

Under SEM, the surface coating followed the pattern of gold, with disperse Cu particles at 100nm, but a fully covered cobblestone pattern appearing at 200nm. In both cases, however, the average size of the Cu particles was roughly 50% greater than that of Au at a comparable thickness. The Cu particles at 100nm also appeared to be flatter, perhaps due to the surface forces due again to the lattice match. While again, the particle

sizes on the CNT surface was hard to identify and measure, there was no clear difference between this case and gold.

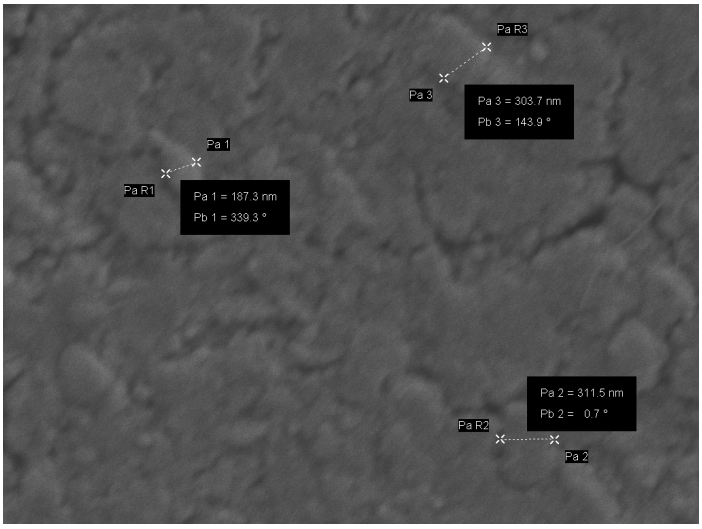

Figure 58. Wide Cu nanoparticle formation with 100nm deposition on Cu square.

Perhaps due to the larger particle size, transferring and bonding using Cu proved more challenging than gold. Since longterm thermocompression past the standard 5 mins was not tested with copper, it's also possible that a Cu-Cu diffusion rate slower than Au-Au was at fault. In any case, without water vapor etching no transfer was successful regardless of temperatures, and even with the 40ml/min etch rates employed in transferring gold at 60°C, much of the periphery of the square CNT array had too high adhesion. A 60 ml/min water vapor etch for five minutes was the bare minimum to bond at the temperatures targeted in this study.

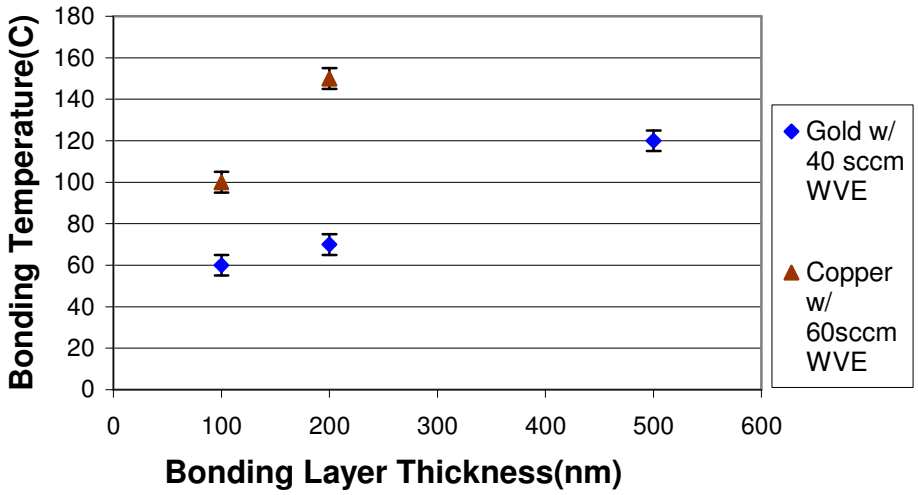

Figure 59. Comparison of minimum transfer temperatures for copper and gold.

This etch rate put a boundary on our exploration of minimum temperature in order to avoid damage caused by excess water etching. However, it was possible to bond copper as low as 100°C with a 100nm layer, which is sufficient for many applications in microelectronics. This sharp increase in minimum temperature, relative to the gold seems to correlate directly with an increase in nanoparticle size. Less simple to explain is the drop in bonding temperature between 200nm and 100nm Cu samples, and it can only be speculated that the nature of the Cu deposition on the Cu plate may be at work here.

4.3.4 PCM Interface Fabrication

The serial array posed no additional difficulty in fabrication up to the wax addition step. The parallel structure creation took longer, but posed no additional challenges in terms of CNT growth, coating or transfer. The relatively large size of the mask patterns used in this study, well above that of the wavelength of the light used, meant that the photolithography process could absorb any diffraction or scattering errors without damage on a scale that would have an effect on our results.

The mask contained a control along with the two patterns, each 2 cm^2 designed to accommodate the LED shape we were originally planning to test, however we switched

to a LED source close to the $1cm^2$ area of the diced squares. A diamond stylus was able to readily split the area in half prior to CNT growth.

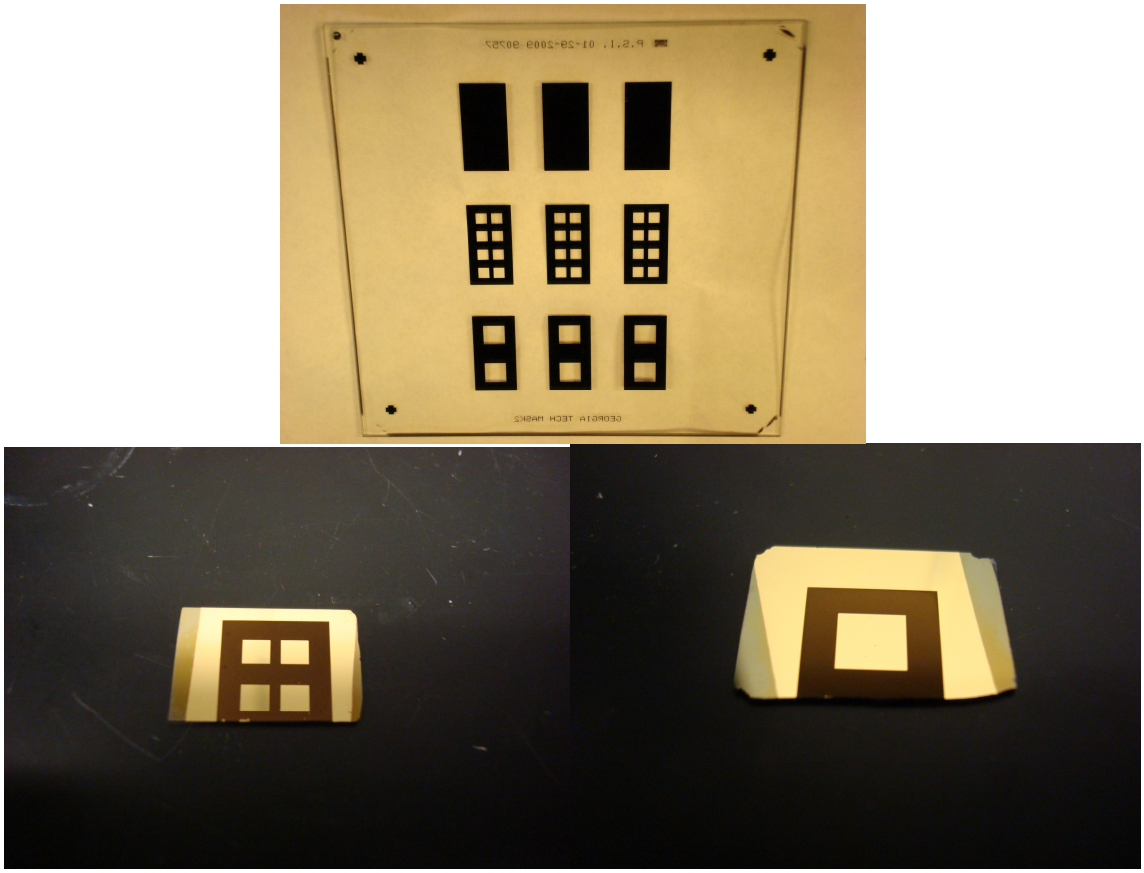

Figure 60. Mask and resulting patterning for parallel phase change incorporated arrays.

The extensive study of temperature, thickness and rate was not repeated for the phase change samples. No water vapor etch was ever used in the growth stage to avoid any undue damage on the exposed edges. The metal layers were all 100nm thick, deposited at 2 Å/s. Even at 150°C, though there were still some transfer issues in the parallel structures consisting of four smaller wax pockets, likely due to the finer features on the array. This varied from sample to sample however, and several transferred successfully, making them available for further processing. While the smaller reservoir sample did show successful transfer, as low as 130°C, the yield rate was too low. The "large" interface did not have any issues with the transfer process, as low as 100°C.

The wax application process was a challenging process. Though the pressure based molding/filling of wax was a basic procedure, only a very small volume of wax required to fill the gaps. The total volume of the gaps in both the large and small spaced parallel samples was the same and very small: (.5cm x .5cm)x 40e-4 cm = 1e-3 cm^3 or 1 mm^3. Even converting to mass using density and weighing out the right amount of wax took time to practice. Splitting them evenly for the parallel design with four spacings took even more time, and for the serial structure, with a minute amount of wax sandwiched between gold layers, the amount to be used could only be guessed at. Under thermal press, both serial and parallel structures leaked excess wax onto the exposed copper square, which had to be cleaned manually while still in the melt state.

At current CNT density, the wax could not simply be contained to the top of the gold layer or in pockets in the midst of the CNT array, for either size and spacing of the wax. The actual end result was the CNT array pattern coated in wax, with wax pocket(s) in their midst with a 2 micron layer of wax on top. This poses an issue in terms of portability of the design. While the previous Cu and Au samples could be transferred to tape and stored, the wax simply could not.

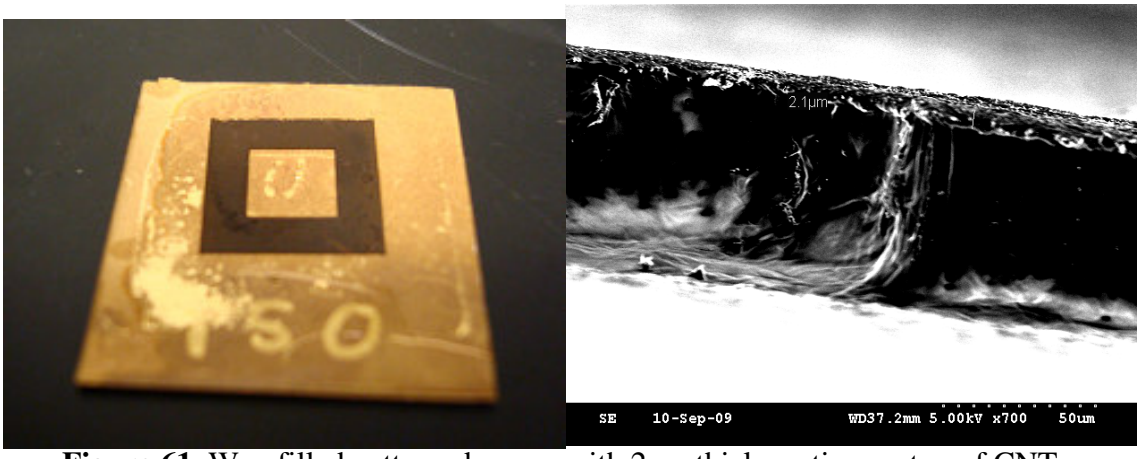

Figure 61. Wax filled patterned arrays with 2um thick coating on top of CNTs.

During these fabrication processes, the waxes underwent many melting and solidifying cycles, especially while trying to remove the remainder of the wax coating the gold coated copper. After this was accomplished, one sample of each of the three

implementations of wax was cycled above and below its melt temperature for 10 cycles to see any evolution or evacuation or the paraffin front. For all three cases, no change was visible at the macroscopic level. Under SEM, there did appear to be a very fine layer of wax that had come out of the CNT array and onto the copper square, by the 5th cycle. However, it stopped growing in breadth and thickness.

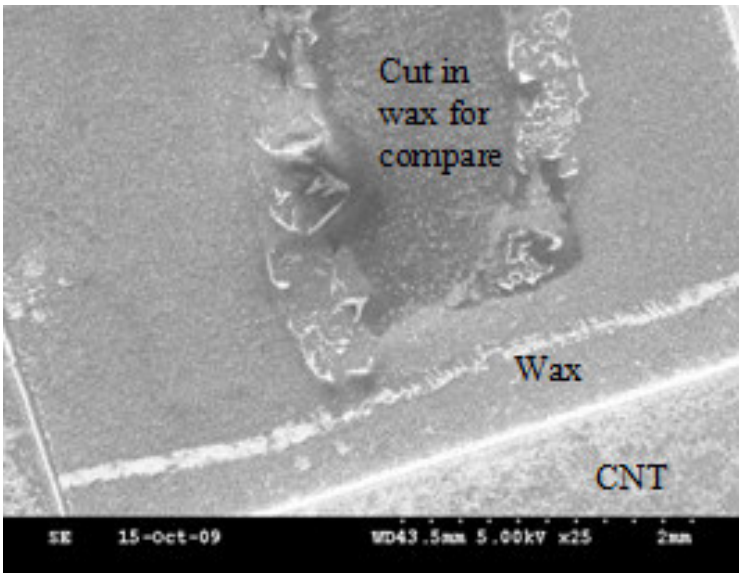

Figure 62. Wax layer in reservoir present but lower than height of CNT array.

More work must be done to determine if this leveling out effect indicates a level of stability or may cause long term problems.

4.4 Conclusion

The formation of carbon nanotube interfaces using the metal bonding method was examined and the range of its application. By controlling the growth of the CNT arrays and the deposition of a metal bonding layer, the temperature of the transfer process was controlled. This study established that it was possible to drastically lower the temperature for gold bonding with this process, demonstrating gold coated CNTs that transferred to copper squares at temperatures as low as 60°C. This opens the use of such a TIM to a range of new industrial applications that need low temperatures. The process was also adapted to use copper as a bonding layer at temperatures as low as 100°C, potentially lowering the cost of this interface. Patterned arrays were also transferred at temperatures

of 150°C and below and various implementation of phase change material into the process was examined for the first time. The metal bonding process for CNT array based TIMs was thus opened to a wide array of variables and utilities.

CHAPTER 5

THERMAL AND MECHANICAL CHARACTERIZATION

5.1 Introduction

While expanding the range of roles for a thermal interface material is important, the interface is ultimately only as useful as its performance. The various interfaces created in this study were prepared for characterization by bonding a second substrate to the top of the array. Whereas past studies focused solely on thermal performance, this study examined the mechanical capabilities of the bond more closely to understand the interface durability. A range of interfaces was subject to tensile testing, which revealed good results at lower bond temperatures than has been observed before. However, the results also demonstrated a trade-off in performance between the two features. The shear strength of a CNT thermal interface was also examined for the first time, and found to be particularly high.

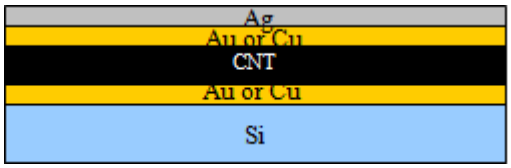

Figure 63. Sideview of bonded structure for PA thermal characterization.

The thermal interface resistivity of samples prepared as in Figure 63 was examined using PA testing. The performance matched that of industrial TIMs, and some of the best CNT based TIMs. The thermal data highlighted key trends that can be used to further refine the metal bond process, and in conjunction with mechanical data, establishes the larger framework necessary to implement CNT TIMs commercially.

5.2 Experimental Procedure

5.2.1 Preparation

For the standard gold and copper samples, preparation for testing simply involved another metal deposition and thermocompression stage after the transfer. The choice of

material for the top layer depended on the test. For mechanical tests, a bare silicon $1cm^2$ wafer was bonded to simulate a semiconducting chip.

This was a standard used in both the tensile and shear tests. For photoacoustic testing, the tool necessitated that we use a layer of silver foil(.025mm, annealed, 99.95% pure) for the laser to be effective. Again, both the foil or silicon were coated alongside the array in the e-beam, so that the bonding metal could diffuse into itself in the press. The settings for the e-beam evaporation and thermal press were kept identical to the transfer condition.

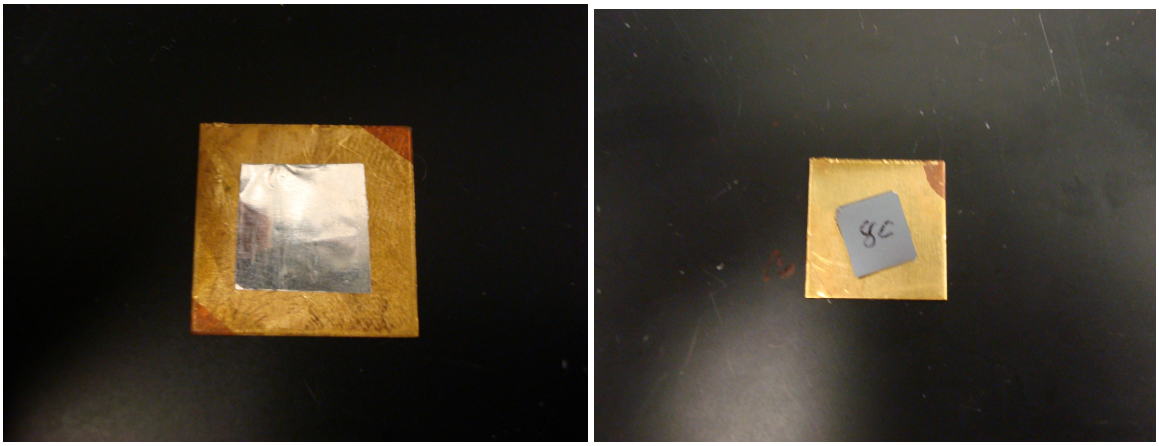

Figure 64. Samples prepared for PA testing (left) and tensile testing (right).

For PA sample preparation, the side of foil to be exposed to the laser also had to have 80nm of Ti deposited on it. The preparation for the phase change samples were identical, since the exposed array post transfer had metal coated on it prior to wax deposition. The serial interface was transferred and bonded at 100°C and the parallel samples were bonded at 150°C.

5.2.2 Tensile Testing

The tensile testing was carried out using the MTS Insight 2 tool in Dr. Ken Hall's research group. Either side of the chosen sample was fixed to a platen in the machine using a rapid drying glue. The machine was then programmed to pull the platen apart at a gradual rate of 1.6 mm/min, sampling the load at a rate of 10 Hz and using a 100N load cell to convert the mechanical force to a signal to pass to the computer. The peak in the

graph would account for the breaking force of the bond. As the CNT arrays used in this test were a standard 1cm x 1cm, this allowed for a simple conversion to the stress in KPa, and for direct comparison with other results. Again, as only the apparent CNT area was used in this calculation, the actual tensile strength was much higher than reported. However, as the density of the array was the same in all cases, comparison was possible.

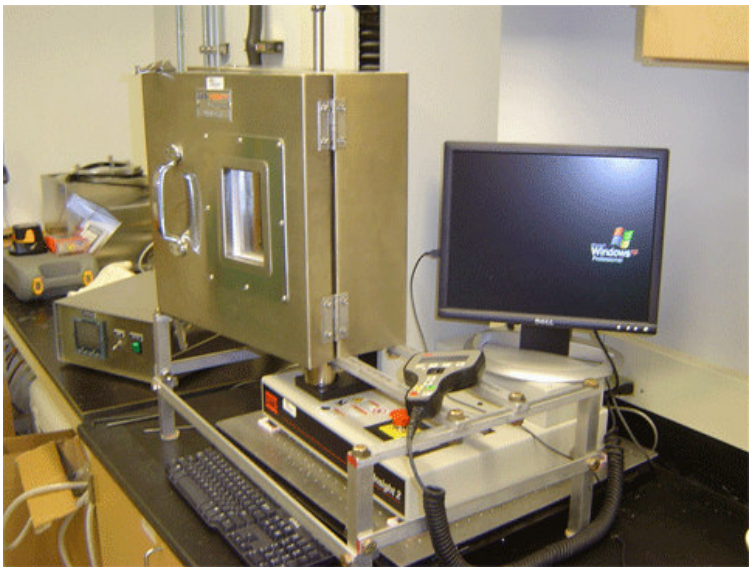

Figure 65. MTS Insight 2 tensile testing apparatus.

Shear tests were carried out using a standard die testing machine in the Packaging Research Center with the assistance of Nitesh Kumbhat. Samples were prepared as for tensile testing, but force was applied to the side of the sample until failure.

Figure 66. Die Shear Tester 580 by Royce Systems.

5.2.3 Thermal Testing

Thermal resistivity measurements were taken using the photoacoustical testing apparatus discussed earlier. After preparation, the samples were sent to the Xu research group at Purdue where Steve Hodsen ran the tests and relayed the results. The test employed a laser as a point source to heat the top layer at specified frequencies and then recorded the acoustic response in the air above the sample inside the enclosed containment chamber.

The PA measurements consist of any number of heating an N-layer material modeled in Figure 57 and base periodically using a laser with a frequency ω and intensity $1/2I_0\{1+\cos(\omega t)\}$. Absorption of the laser beam is permissible in any number of layers. As the thermal diffusion length in gas is much less than the chamber radius, the PA signal can be considered independent of the energy distribution of the laser.

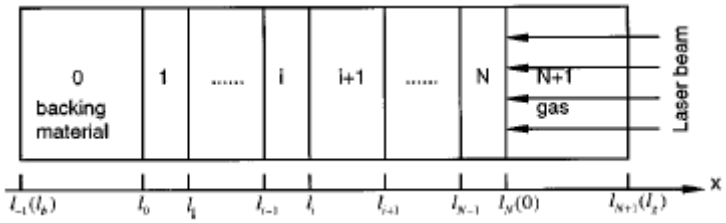

Figure 67. Model of an N-layer material used by PA testing[85].

Using this model, the temperature response of the interface can be taken as:

$$\theta_{N+1} = (1-\rho)\cdot B_{N+1} e^{-\sigma_{N+1}x} e^{j\omega t}, \tag{10}$$

Where the coeffecients are:

$$B_{N+1} = -\frac{[0\ 1]\sum_{m=0}^{N}\left(\prod_{i=0}^{m-1} U_i\right) V_m \begin{bmatrix} E_m \\ E_{m+1} \end{bmatrix}}{[0\ 1]\left(\prod_{i=0}^{N} U_i\right)\begin{bmatrix} 0 \\ 1 \end{bmatrix}}, \tag{11}$$

$$U_i = \frac{1}{2}\begin{bmatrix} u_{11,i} & u_{12,i} \\ u_{21,i} & u_{22,i} \end{bmatrix}, \quad V_i = \frac{1}{2}\begin{bmatrix} \nu_{11,i} & \nu_{12,i} \\ \nu_{21,i} & \nu_{22,i} \end{bmatrix}, \tag{12}$$

$$u_{1n,i} = (1 \pm k_{i+1}\sigma_{i+1}/k_i\sigma_i \mp k_{i+1} \times \sigma_{i+1}R_{i,i+1}) \times \exp(\mp\sigma_{i+1}l_{i+1}), \quad n = 1,2, \tag{13}$$

$$u_{2n,i} = (1 \mp k_{i+1}\sigma_{i+1}/k_i\sigma_i \mp k_{i+1} \times \sigma_{i+1}R_{i,i+1}) \times \exp(\mp\sigma_{i+1}l_{i+1}), \quad n = 1,2, \tag{14}$$

$$\nu_{n1,i} = 1 \pm \beta_i/\sigma_i, \quad n = 1,2, \tag{15}$$

$$\nu_{n2,i} = (-1 \mp k_{i+1}\beta_{i+1}/k_i\sigma_i + k_{i+1} \times \beta_{i+1}R_{i,i+1}) \times \exp(-\beta_{i+1}l_{i+1}), \quad n = 1,2, \tag{16}$$

$$E_m = \frac{G_m}{\beta_m^2 - \sigma_m^2}, \tag{17}$$

$$G_m = \begin{cases} \dfrac{\beta_m I_0}{2k_m} e^{-\Sigma_{i=m+1}^{N}\beta_i I_i} & \text{for } m < N \\ \dfrac{\beta_m I_0}{2k_m} & \text{for } m = N \\ 0 & \text{for } m = N+1. \end{cases} \tag{18}$$

In these equations, $\sigma_i=(1+j)a_i$ with $j=I$ and $a_i=(\pi f/a_i)^{1/2}$. The thermal diffusivity of layer i is a_i, the modulating frequency is f, the thermal conductivity is k_i the surface reflectivity is ρ, the optical absorption coefficient is β, and the thermal contact resistance between two adjacent layers is $R_{i,i+1}$. Using these equations the raw data measurements can be used to calculate resistivity accurately if the other properties are known [85]. As

any one point on the sample was assumed to represent the thermal resistivity at any point, this test assumed that the interface was isotropic.

Due to the inability of the wax to fill the CNT array, the parallel samples were not tested thermally. The serial structure retained the small amount of wax that was already placed inside, and was tested via the PA method.

5.3 Results and Discussion

5.3.1 Preparation

The bonding process to prepare the gold or copper samples exhibited the same behavior as the transfer. There were very few instances where transfer of an array to copper square succeeded at a particular temperature, but the foil or silicon wafer failed to bond to the other side of the array. The yield rate for sample preparation was thus limited mostly by the first transfer process at a given temperature.

The phase change samples had significantly less than 100% yield rate, based on the thickness of the wax layer on top of the gold coated CNT array. With any excess wax buildup past 1-2 microns, this layer sometimes prevented the bond from forming at all, particularly with the parallel structures which contained less bonding area.

5.3.2 Mechanical Strength

Prior testing by Cross found that a 500nm Au bond at 200°C possessed a tensile strength of 35 KPa, exceeding that of similar structures by other groups by a full order of magnitude. This study found that a similar 500nm Au bond had a tensile strength of 38 KPa at just 150°C. This value should not be taken as a definitive process value as only one sample was tested at this thickness. However, in light of our measurements at lower thicknesses, it is evident that our refinement of the metal transfer and bonding of CNTs could yield better quality than that displayed in a preliminary analysis.

The more extensive measurements were conducted with a deposited bonding layer of 100nm. This value was chosen instead of 200nm, as early testing found similar strength for samples bonded at the same temperature for both thicknesses for both gold

and copper bonds. This may seem odd due to the more thorough metal coverage observed on the plate side at 200nm. However, the diffusion process appears to be reagent limited by the disperse coating on the CNT surface. That is, there simply is not be enough nanoparticle clusters for all the particles on the 200nm plate to bond to anyway, thus the limited coverage offered by the 100nm coated samples suffices.

The gold and copper tested varied only in the amount of water vapor etching they experienced prior to transfer in preparation for the tensile test. The samples size for tests at each bonding temperature ranged from 3-5 samples, and thus the uncertainty in strength, as calculated via standard deviation, is fairly high.

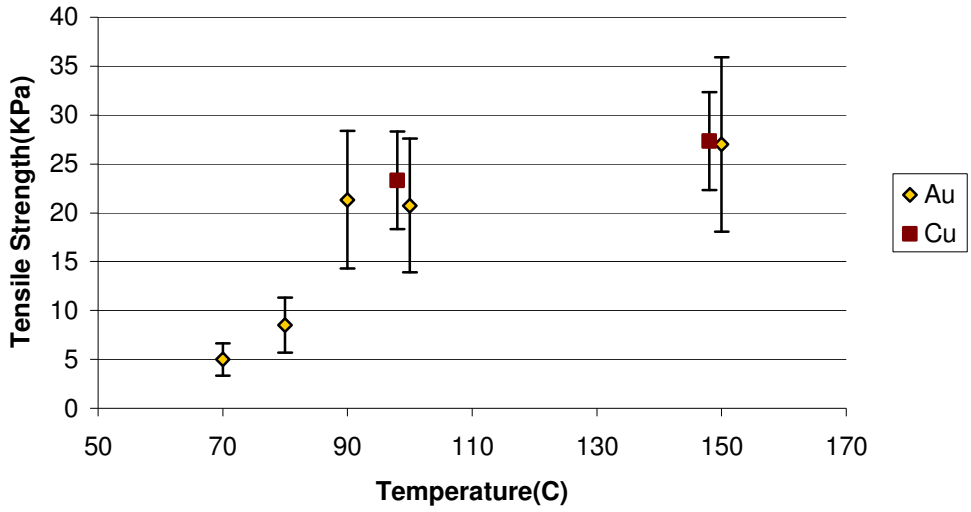

Figure 67. Tensile strength of Cu and Au samples bonded at various temperatures.

For both metals, the tensile strength follows the expected trend and clearly drops with temperature. The mathematical nature of the trend is hard to ascertain given the few data points, but after 90°C, all tests display a precipitous drop in mechanical integrity of the bond. Though it was established earlier that a bond was created at 60°C for gold, the tensile strength at this value was almost negligible with the bond breaking almost immediately in the machine. This is likely a limit in the diffusion bonding mechanism for the nanoparticle size used. However, this does not necessarily preclude the use of the

lower temperature bonds in mechanically insulated operating environments. Copper performed similar to gold at comparable temperatures, increasing its potential use as a replacement overall. For comparison, the tensile strength of an Indium based solder is 1.9MPa [86]. While the values in this study may fall well short in this measure, their properties may make them suited for applications where low mechanical stresses and environmental stability are imperative.

The failure mode of the bonds was also examined. If the bonding process was strong, one would expect the deformation point to be within the CNT array. Understanding whether this occurred was thus as important as the failure strength in determine routes for further improvement. SEM imaging reveals that for temperatures of 100°C and above the Au bonds broke within the array layer, through fracture of the CNTs themselves. However, lack of proper bonding can still manifest, again near the periphery. This is reflected by the delamination of the metal layer to one or either side. At 90°C and below, this failure mechanism becomes more prominent, with larger and larger regions CNT barren regions occurring more frequently, though there is still too much variance from sample to sample to quantify this change. Copper showed less regions of delamination than gold overall, only at the fringes of the array. The stronger bond may be a by product of depositing copper on copper and could prove useful in applications involving copper heat sinks. The failure modes are shown in the following series of pictures.

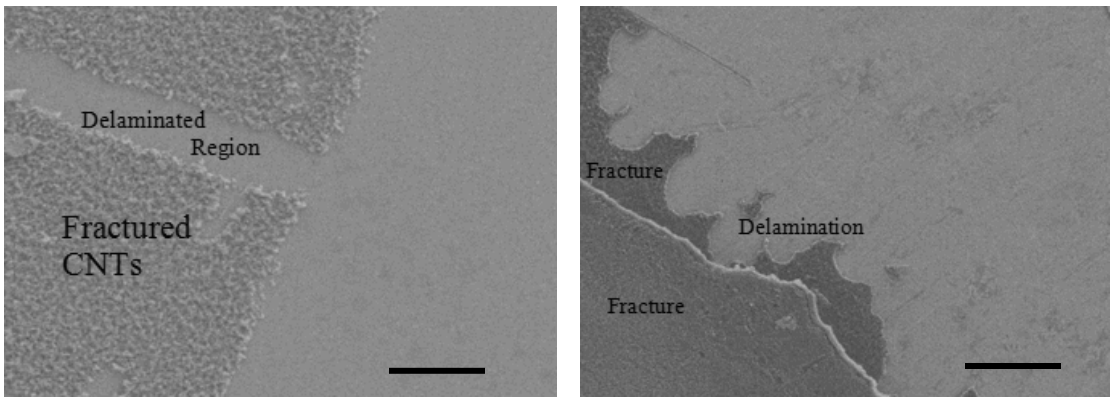

Figure 68. Post tensile testing pictures on silicon wafer side(left) and copper square(right) showing modes of failure (black bar is 200um).

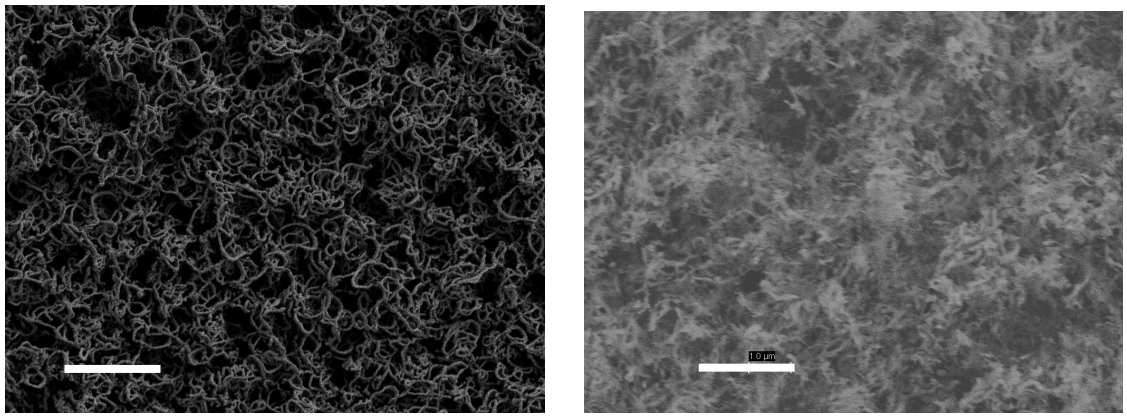

Figure 69. Closeup of CNTs prior(left) and post(right) tensile test(white lines are 2um).

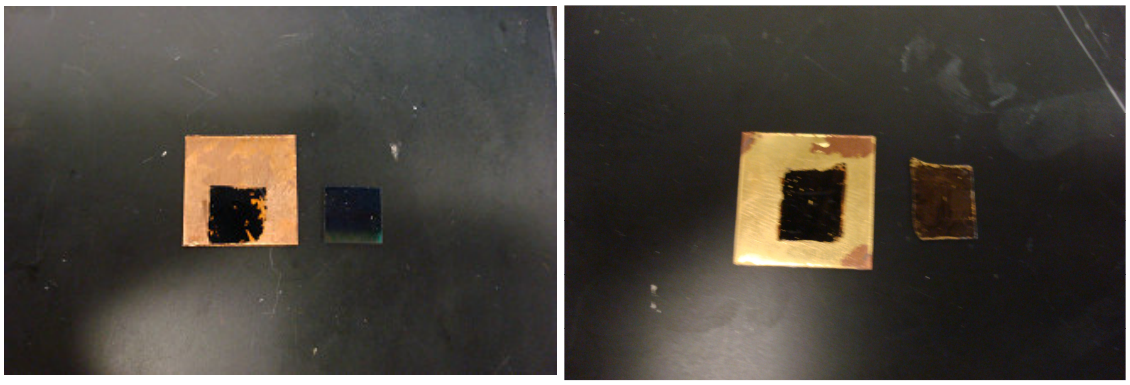

Figure 70. Failure with some delamination (left) and through mostly CNT fracture(right)

While extensive fatigue testing was not conducted, two of the higher temperature/stability bonds (100°C and 150°C) were run through five cycle heating-cooling process up to the bonding temperatures. The tensile strength of these samples fell within the values of other samples in the data range, at least showing no immediate weakness of the bonding mechanism.

For phase change samples, tensile testing proceeded in the same manner as with prior samples. Again, three cases were tested: the serial implementation and the two parallel ones. The sample sizes employed for all three sets were just n=3 due to difficulty of proper transfer and bonding for the test, thus, the error is again, fairly significant.

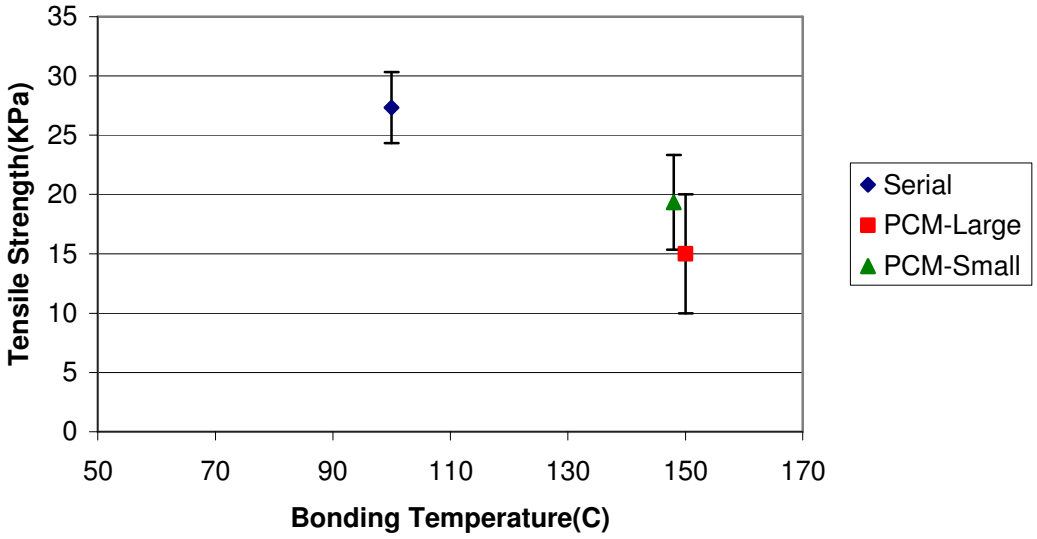

Figure 71. Tensile strength for sample incorporating phase change designs.

The strength for the serial samples was very similar to those of the 100°C gold sample without any phase change material. This should be expected as the same amount of area is covered with CNTs for bonding. The only doubt was whether the wax would cause severe disruption in the gold-gold diffusion process, and it appears to have not done so in the serial structure, at least for the samples that successfully bonded. As noted, the bonding process even for the serial case was a fickle one.

Both parallel implementation based samples exhibited lower tensile strength. Again, this should be no surprise as it is the CNTs bonding that afford the interface its strength. Removing them to create space for the paraffin reservoirs should reduce the strength. The 25% reduction of area roughly matches the drop in strength for the parallel implementation with one large wax gap, though the sampling size are too low to confirm the relationship is exactly linear. The interface with smaller pockets showed an even greater drop in strength, due to the transfer issues involving its finer features. Based on similar issues in bonding with the LEDs for thermal testing, it is also possible that in this case, the excess wax on the CNTs may have a more prominent interference effect.

The shear strength of the transfer process was only examined for a couple samples, to get a base point. A 100°C, a non PCM containing – 100nm Au bonded sample withstood a force of up to 1.2 kg, translating to a shear strength of 11.8Kpa which is to our knowledge the highest measurement for a CNT TIM. For comparison, a series of lead-free Sn based solder had shear strengths of .49-1.88 Mpa and an In based solder had an initial shear strength of 6Mpa [11, 87]. Again, there is much room for improvement, particularly as shear strength is a more important value for chip stability than tensile strength. Macroscopically, the failure mode in shear appeared to be through fracture of CNT and not delamination of the metal bond.

5.3.3 Thermal Testing

Photacoustic tests were conducted on 4 samples. Two were on gold bonded samples at 80°C and 90°C to examine the performance of some of the lowest temperature bonds created in this study. The mechanical tests indicated a sharp drop off in bond quality at this point and the resistivity measurements sought to confirm the trend. A copper bonded sample at 150°C was tested. Even though it was the higher bound for our test, it still fell short of the 220°C temperature that higher thickness gold samples were bonded at in previous studies. Finally, the serial phase change sample created at 100°C was tested under an operational condition of 60°C to induce the melt state. All interface tested were created using just 100nm metal bonding layers. Deviations in the measured value stem from fluctuations in PA measurement. Due to the time involved in a single test, each data point reflects only a single sample test.

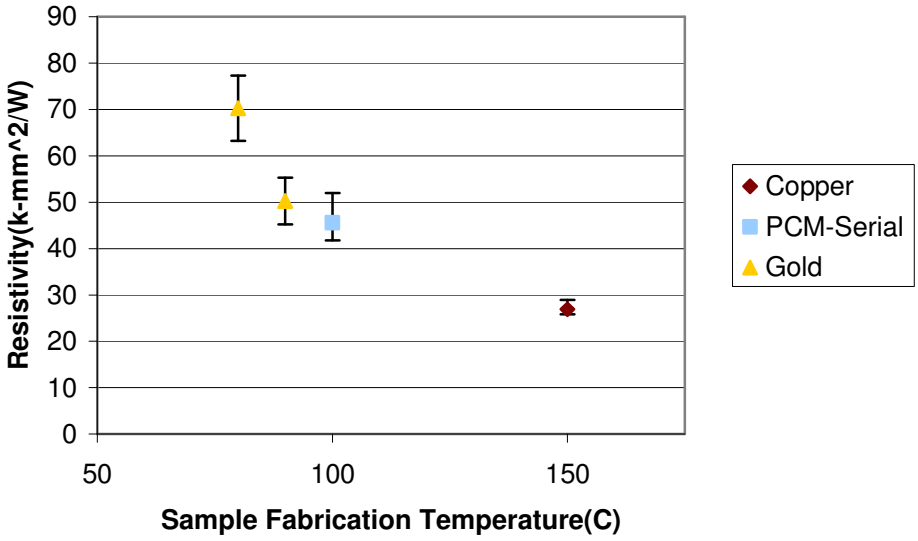

Figure 72. Thermal resistivity measurements via PA testing.

The resistivity values obtained were significantly higher than those obtained by prior use of this method, but there are several reasons for this. One, all the samples tested were done so at atmospheric pressures with no additional loading. Prior tests were tested at a range of loads from 50Kpa to 350Kpa, which enhances contact of the foil with the CNTs beyond what the bond can accomplish. The lowest resistivities of 10 mm^2K/W (not pictured) were obtained somewhere between these pressure values. Second, the bonds were created at much lower temperatures and thickness than the 500nm, 220°C bonded samples. As mechanical tests showed, there was some loss of performance as the values dropped below these levels. In comparing these results with the larger set of CNT TIM data for all interface fabrication schemes, the bonding pressures and amount of metal used are significantly less than with other methods.

The performance was still quite good overall. The copper samples showed a resistivity of just 25 mm^2 K/W, and lies close to the 21.5mm^2K/W value obtained for the higher temperature gold bond at the same testing pressure. This firmly establishes the viability of copper as a substitute for gold in the transfer and bond process, at least at high temperatures.

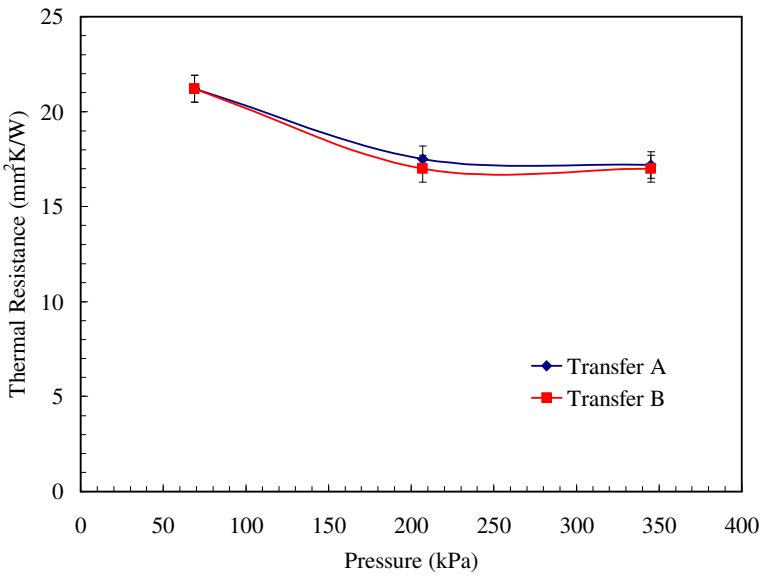

Figure 73. Thermal resistance of transferred Au-bonded interfaces from previous studies[24].

The serial phase change sample came in at roughly double the value at 44.6 mm^2 K/W. This may be from the decrease in temperature alone as it follows the temperature-resistivity trend. However, it does add to the body of evidence that the paraffin may be interfering with the bond in some manner. Further exploration of the phase change and comparison with gold bonding will be necessary to explore this.

The very low temperature gold bonded samples performed relatively poorly, but still managed to come in at under the upper bound of 75 mm^2 K/W resistivity of commercial TIMs. The drop in performance at these temperatures matches that found in the tensile strength, as was suspected. Yet, the 90°C sample is not much more resistive than the 100°C phase change. To compete against epoxies that can be applied at room temperature and provide lower resistivity, though, the bonding process at low temperatures needs to be improved.

5.4 Conclusion

The interfaces created in Chapter 4 were mechanically and thermally characterized. The mechanical results showed performance comparable to bonds formed

at higher temperatures in prior research. They also showed a severe but expected drop off in bond quality with bonding temperature, particularly for bonds lower than 90°C, where failure occurred through delamination of the metal bond rather than CNT fracture. The shear strength of a few gold interfaces were also examined for the first time in literature and found to exhibit relatively high values. The thermal results also reflected this tradeoff in performance for gold, though the resistivity values still fell in a range that was comparable to some poorer commercial TIMs. The thermal tests also further established the utility of copper as a viable alternative for gold. The phase change sample tested did not show any clear benefit, however, further testing may be needed to verify this. In general, this work opens up several areas of further exploration for future thermal and mechanical testing particularly in low temperature interface fabrication and bonding with alternative metals.

CHAPTER 6

FUTURE WORK

This study built upon the results of various metal based CNT array TIM creation techniques, particularly the transfer and bonding process utilizing gold. While past work focused exclusively on the thermal performance of these interfaces, this study examined other properties of the process, creating solid paths to make the technique commercially viable. The bonding temperature necessary for application of the interface was drastically lowered, as the variables controlling the bond were studied. The process was also replicated with copper as the bonding layer, allowing for cheaper fabrication cost than the gold or palladium used in prior metal bond studies. The mechanical strength of the interfaces was also fully characterized for the full range of interfaces created, establishing a baseline to test future interfaces against. Phase change elements were also incorporated into the interface, though the problems observed in containment indicate that new strategies need to be attempted. Finally, thermal characterization of the interfaces allowed for a full picture of how the bonding temperature, strength and resistivity all related to one another.

Now that a full range of bonding has been developed and characterized for this process, further work should focus on improving performance at the various bond temperatures, with a focus on thermal performance. The development of a physical model to describe transfer through the metal diffusion bond to the CNT array would be useful in identifying variables to target. Even a model to describe a CNT TIM without transfer would be useful as one has not yet appeared in literature [1]. Based on imaging and results in this study, the loss of thermal performance is due to the thin metal layers necessary to achieve a low temperature bond. Particularly on the CNT array side, this low coating limits coverage to the point that many nanotubes simply aren't coated, limiting the avenues for heat transfer given the poor lateral thermal conductivity between tubes. An immediate step forward would be to mix the best of both worlds and employ a thin

200nm metal layer on the plate, but a thicker 300nm-500nm layer on the CNT array. This might allow for full contact with the carbon nanotubes while retaining a low enough particle size to allow for <100°C bonds. However, it would be best to start by optimizing the 100°C and 150°C cases, where the performance is already near that of existing thermal interface materials.

The pressure aspect also needs to be examined in future tests. Other work has shown that high temperatures and pressures are not necessary at least for a gold-gold diffusion bond with the application of ultrasonic pulses to increase bond strength at relatively low temperatures shown in Figure 74[88]. This technique may be worth exploring.

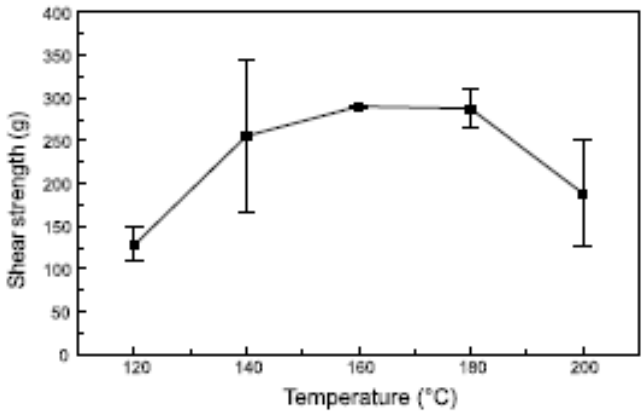

Figure 74. Strength of gold-gold diffusion bonds formed at various temperatures with sonication [88].

This additional bonding will undoubtedly help the tensile and shear strength of the interface by bringing more CNTs into play. Due to the fracture mode of bond failure, adding more CNTs may be the easiest way to increase the mechanical properties of the bond. For an even greater increase, it would be worth exploring higher density arrays such as those created by PECVD shown in Figure 75. CNT arrays grown in this manner exhibit an order of magnitude more density than that of thermal CVD. Another method to increase tube density would be controlling the size of the particles in the Fe seed layer. Many groups have seen success in controlling CNT size via this mechanism[34].

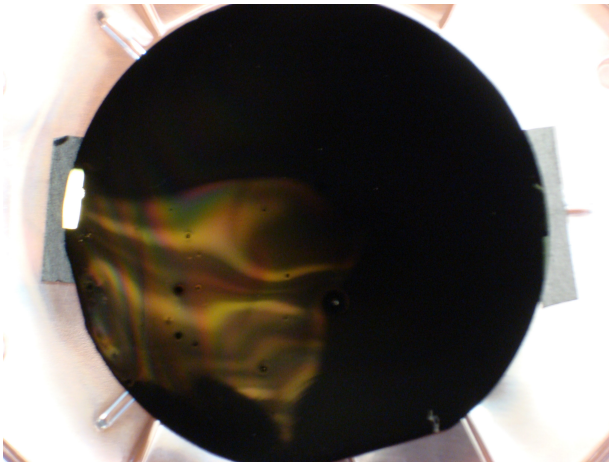

Figure 75. CNTs grown via "Black magic" PECVD – so dense they are reflective.

While this study identified some potential benefit in resistance reduction, it mainly discovered difficulties in trying to store the wax in a contained manner. There is certainly strong doubt as to the long term durability of any CNT/PCM hybrid interface. Higher density arrays may also prove more effective in containing the liquid form of PCMs via capillary forces. At the same time, this needs to be balanced with the capability to fill the arrays with PCM, as that posed another challenge. Ideally, one would want a more disperse arrangement of CNT and wax such as that in 76, even more than the small reservoir design examined in this paper. A beehive structure would be a biological parallel, which for a rectangular CNT array would translate to a checkerboard pattern. This sort of structure could limit the area of CNTs lost.

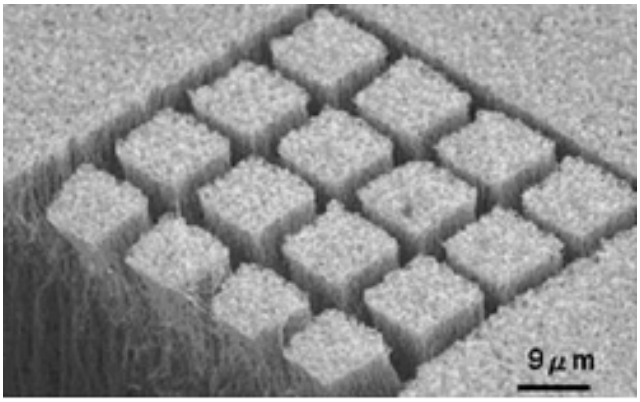

Figure 76. Grid CNT array configuration for containing PCM.

Longterm testing is also necessary for all the samples presented above. Thermal fatigue and associated shear stresses are a significant source of failure in interfaces. While the arrays developed via the bonding process did show exemplary shear strength, and have shown promise of reducing thermal stress and related degradation in the past, this must be fully studied.

In terms of commercial application, more work needs to be present on standardization of the processes. Differences in the array growth process from user to user must be analyzed and eliminated in order to ensure a repeatable height for the CNT arrays. The full transfer and storing process should also be explored. Prior work has already demonstrated that CNTs can be transferred and stored on tape. One can envision expanding the process such that the CNTs are grown on substrate, coated with metal, then transferred to polyimide tape by simple stiction to create a stored array like Figure 77. The exposed ends could be coated once more and then the tape could be sold in sheets as a thermal interface that could be applied to a surface with some pressure and temperature. While this increases the accessibility of the CNT interface, thermal greases and even solder still emerge on top in ease of application. The mechanical and thermal properties must remain the top priority.

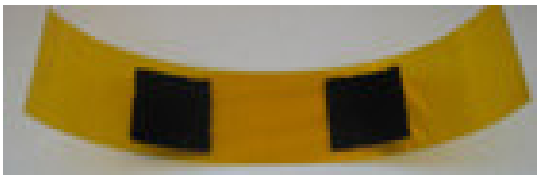

Figure 77. CNT arrays bonded to tape for easy storage and use.

Larger scale arrays should also be tested to see the scalability of the interface properties to apply to various size chips. The diffusion bonding process must be explored across species, as in commercial application, it may not be possible to have the same metal on the bonding surface. The most probable exception to this is when the bonding metal is copper, but even in this area, the nanoparticle Cu – bulk Cu bond process should

be explored in detail. Finally, the pressure also needs to be examined in conjunction with the bonding temperature.

In short, alternatives to current TIMs are desperately need to handle high flux and high lifetime devices. The work presented in this study expands the versatility of the CNT array as a novel high-performance thermal interface material and cements the viability of the metal bond process in the creation of such CNT TIMs. By controlling the bonding layer, the diffusion based interface was established at extremely low temperatures. While mechanical and thermal characterization of these bonds showed a definite tradeoff in performance for the lower temperatures, it also established the utility of different metals and the potential for incorporation of various interface designs. New directions and lines of research were opened for improving both the performance and commercial viability of the metal bond process.

REFERENCES

1. Howe, T.A., C.K. Leong, and D.D.L. Chung, *Comparative evaluation of thermal interface materials for improving the thermal contact between an operating computer microprocessor and its heat sink.* Journal of Electronic Materials, 2006. **35**(8): p. 1628-1635.
2. Prasher, R., *Thermal interface materials: Historical perspective, status, and future directions.* Proceedings of the Ieee, 2006. **94**(8): p. 1571-1586.
3. Wang, P. and A. Bar-Cohen, *On-chip hot spot cooling using silicon thermoelectric microcoolers.* Journal of Applied Physics, 2007. **102**(3): p. -.
4. Gordon, K., *Solid State Lighting Research and Development: Manufacturing Roadmap*, D.o. Energy, Editor. 2008: Washington, D.C.
5. Pastukhov, V.G., et al., *Miniature loop heat pipes for electronics cooling.* Applied Thermal Engineering, 2003. **23**(9): p. 1125-1135.
6. Viswanath, R., et al., *Thermal Performance Challenges from Silicon to Systems.* Intel Technology Journal, 2000. **Q3**.
7. Wei, J., *Challenges in cooling design of CPU packages for high-performance servers.* Heat Transfer Engineering, 2008. **29**(2): p. 178-187.
8. *Thermal Interface Comparison: Thermal Pads vs Thermal Grease.* AMD Publication. **26951**.
9. De Mey, G., et al., *Influence of interface materials on the thermal impedance of electronic packages.* International Communications in Heat and Mass Transfer, 2009. **36**(3): p. 210-212.
10. Grujicic, M., C.L. Zhao, and E.C. Dusel, *The effect of thermal contact resistance on heat management in the electronic packaging.* Applied Surface Science, 2005. **246**(1-3): p. 290-302.
11. *Indium Alloy Properties sorted by Temperature.* Indium Corp., 2009.
12. Chung, D.D.L., *Materials for thermal conduction.* Applied Thermal Engineering, 2001. **21**(16): p. 1593-1605.
13. Chiu, C.P., J.G. Maveety, and Q.A. Tran, *Characterization of solder interfaces using laser flash metrology.* Microelectronics Reliability, 2002. **42**(1): p. 93-100.
14. Gwinn, J. and R. Webb, *Performance and testing of thermal interface materials.* Microelectronics journal, 2003. **34**(215).
15. Yi, W., et al., *Linear specific heat of carbon nanotubes.* Physical Review B, 1999. **59**(14): p. R9015-R9018.
16. Tong, T., et al., *Dense, vertically aligned multiwalled carbon nanotube arrays as thermal interface materials.* Ieee Transactions on Components and Packaging Technologies, 2007. **30**(1): p. 92-100.
17. Wang, X.W., et al., *Structure and thermophysical properties of single-wall Si nanotubes.* Physica B-Condensed Matter, 2008. **403**(12): p. 2021-2028.
18. Lai, Y., et al., *Liquid cooling of bright LEDs for automotive applications.* Applied Thermal Engineering, 2009. **29**(5-6): p. 1239-1244.
19. Ngo, Q., et al., *Thermal interface properties of Cu-filled vertically aligned carbon nanofiber arrays.* Nano Letters, 2004. **4**(12): p. 2403-2407.

20. Xu, J. and T.S. Fisher, *Enhancement of thermal interface materials with carbon nanotube arrays.* International Journal of Heat and Mass Transfer, 2006. **49**(9-10): p. 1658-1666.
21. Xu, Y., et al., *Thermal properties of carbon nanotube array used for integrated circuit cooling (vol 100, art no 074302, 2006).* Journal of Applied Physics, 2006. **100**(12): p. -.
22. Cola, B.A., X.F. Xu, and T.S. Fisher, *Increased real contact in thermal interfaces: A carbon nanotube/foil material.* Applied Physics Letters, 2007. **90**(9): p. -.
23. Xu, J. and T.S. Fisher, *Enhanced thermal contact conductance using carbon nanotube array interfaces.* Ieee Transactions on Components and Packaging Technologies, 2006. **29**(2): p. 261-267.
24. Cross, R., *Processing Vertically Aligned Carbon Nanotubes for Heat Transfer*, in *Mechanical Engineering*. 2008, Georgia Tech: Atlanta.
25. Johnson, R.D., et al., *Thermocompression bonding of vertically aligned carbon nanotube turfs to metalized substrates.* Nanotechnology, 2009. **20**(6): p. -.
26. Humpston, G. and S.J. Baker, *Diffusion bonding of gold.* Gold Bulletin, 1998. **31**(4): p. 131-132.
27. Prasher, R.S., *Rheology based modeling and design of particle laden polymeric thermal interface materials.* Ieee Transactions on Components and Packaging Technologies, 2005. **28**(2): p. 230-237.
28. Sinha, S., et al., *Off-axis thermal properties of carbon nanotube films.* Journal of Nanoparticle Research, 2005. **7**(6): p. 651-657.
29. Cola, B.A., et al., *Carbon nanotube array thermal interfaces enhanced with paraffin wax. Proceedings of ASME Summer Heat Conference* 2008.
30. Pop, E., S. Sinha, and K.E. Goodson, *Heat generation and transport in nanometer-scale transistors.* Proceedings of the Ieee, 2006. **94**(8): p. 1587-1601.
31. Conway, A.M., et al., *Accurate thermal analysis of GaNHFETs.* Solid-State Electronics, 2008. **52**(5): p. 637-643.
32. Gurrum, S.P., et al., *Thermal issues in next-generation integrated circuits.* Ieee Transactions on Device and Materials Reliability, 2004. **4**(4): p. 709-714.
33. Buso, S., et al., *Performance degradation of high-brightness light emitting diodes under DC and pulsed bias.* Ieee Transactions on Device and Materials Reliability, 2008. **8**(2): p. 312-322.
34. Wang, Z.M., et al., *Microfluidic cooling of semiconductor light emission diodes.* Microelectronic Engineering, 2007. **84**(5-8): p. 1223-1226.
35. Christensen, A. and S. Graham, *Thermal effects in packaging high power light emitting diode arrays.* Applied Thermal Engineering, 2009. **29**(2-3): p. 364-371.
36. Horng, R.H., et al., *Thermal Management Design from Chip to Package for High Power InGaN/Sapphire LED Applications.* Electrochemical and Solid State Letters, 2009. **12**(6): p. H222-H225.
37. Weng, C.J., *Advanced thermal enhancement and management of LED packages.* International Communications in Heat and Mass Transfer, 2009. **36**(3): p. 245-248.

38. Maguire, L., M. Behnia, and G. Morrison, *Systematic evaluation of thermal interface materials - a case study in high power amplifier design.* Microelectronics Reliability, 2005. **45**(3-4): p. 711-725.
39. Mahajan, R., C.P. Chiu, and G. Chrysler, *Cooling a microprocessor chip.* Proceedings of the Ieee, 2006. **94**(8): p. 1476-1486.
40. Abadi, P.P.S.S., C.K. Leong, and D.D.L. Chung, *Factors That Govern the Performance of Thermal Interface Materials.* Journal of Electronic Materials, 2009. **38**(1): p. 175-192.
41. Deppisch, C., et al., *The material optimization and reliability characterization of an indium-solder thermal interface material for CPU packaging.* Jom, 2006. **58**(6): p. 67-74.
42. Macris, C., et al., *Performance, Reliability, and Approaches Using a Low Melt Alloy as a Thermal Interface Material.* Proceedings IMAPS, 2004.
43. Gowda, A., et al., *Voids in thermal interface material layers and their effect on thermal performance.* Electronics Packaging Technology Conference, 2004. **6**.
44. Abtew, M. and G. Selvaduray, *Lead-free solders in microelectronics.* Materials Science & Engineering R-Reports, 2000. **27**(5-6): p. 95-141.
45. Leong, C.K. and D.D.L. Chung, *Carbon black dispersions as thermal pastes that surpass solder in providing high thermal contact conductance.* Carbon, 2003. **41**(13): p. 2459-2469.
46. Shaikh, S., K. Lafdi, and K. Hallinan, *Carbon nanoadditives to enhance latent energy storage of phase change materials.* Journal of Applied Physics, 2008. **103**(9): p. -.
47. Tasis, D., et al., *Chemistry of carbon nanotubes.* Chemical Reviews, 2006. **106**(3): p. 1105-1136.
48. Pipes, R.B., et al., *Self-consistent properties of carbon nanotubes and hexagonal arrays as composite reinforcements.* Composites Science and Technology, 2003. **63**(10): p. 1349-1358.
49. Zheng, L.X., et al., *Ultralong single-wall carbon nanotubes.* Nature Materials, 2004. **3**(10): p. 673-676.
50. Choi, T.Y., et al., *Measurement of the thermal conductivity of individual carbon nanotubes by the four-point three-omega method.* Nano Letters, 2006. **6**(8): p. 1589-1593.
51. Pop, E., et al., *Thermal conductance of an individual single-wall carbon nanotube above room temperature.* Nano Letters, 2006. **6**(1): p. 96-100.
52. Shakouri, A., *Nanoscale thermal transport and microrefrigerators on a chip.* Proceedings of the Ieee, 2006. **94**(8): p. 1613-1638.
53. Melechko, A.V., et al., *Vertically aligned carbon nanofibers and related structures: Controlled synthesis and directed assembly.* Journal of Applied Physics, 2005. **97**(4): p. -.
54. Gaillard, J., M. Skove, and A.M. Rao, *Mechanical properties of chemical vapor deposition-grown multiwalled carbon nanotubes.* Applied Physics Letters, 2005. **86**(23): p. -.
55. Belluci, S., *Carbon nanotubes: physics and applications. Phys. Stat. Sol.*, 2005. **2**: p. 34-47.

56. Du, J.H., J. Bai, and H.M. Cheng, *The present status and key problems of carbon nanotube based polymer composites.* Express Polymer Letters, 2007. **1**(5): p. 253-273.
57. Huang, H., et al., *Aligned carbon nanotube composite films for thermal management.* Advanced Materials, 2005. **17**(13): p. 1652-+.
58. Yuen, S.M., et al., *Preparation and thermal, electrical, and morphological properties of multiwalled carbon nanotube and epoxy composites.* Journal of Applied Polymer Science, 2007. **103**(2): p. 1272-1278.
59. Satyanarayana, N., et al., *Carbon nanotube reinforced polyimide thin-film for high wear durability.* Tribology Letters, 2007. **27**(2): p. 181-188.
60. Huang, L.M., *Oriented growth of single-walled carbon nanotube arrays.* Abstracts of Papers of the American Chemical Society, 2003. **226**: p. U690-U690.
61. Franklin, N.R., et al., *Patterned growth of single-walled carbon nanotubes on full 4-inch wafers.* Applied Physics Letters, 2001. **79**(27): p. 4571-4573.
62. Cola, B.A., et al., *Photoacoustic characterization of carbon nanotube array thermal interfaces.* Journal of Applied Physics, 2007. **101**(5): p. -.
63. Amama, P.B., et al., *Dendrimer-assisted controlled growth of carbon nanotubes for enhanced thermal interface conductance.* Nanotechnology, 2007. **18**(38): p. -.
64. Musso, S., et al., *Fluid dynamic analysis of gas flow in a thermal-CVD system designed for growth of carbon nanotubes.* Journal of Crystal Growth, 2008. **310**(2): p. 477-483.
65. Miao, H.Y., et al., *Growth of carbon nanotubes on transition metal alloys by microwave-enhanced hot-filament deposition.* Thin Solid Films, 2005. **484**(1-2): p. 58-63.
66. Cola, B.A., et al., *Carbon nanotube array thermal interfaces for high-temperature silicon carbide devices.* Nanoscale and Microscale Thermophysical Engineering, 2008. **12**(3): p. 228-237.
67. Liu, X., et al., *Implications of catalyst control for carbon nanotube based thermal interface materials.* Journal of Applied Physics, 2008. **104**(8): p. -.
68. Pipes, R. and P. Hubbert, *Scale effects in carbon nanostructures- Self-similar analysis.* Nano Letters, 2003. **3**: p. 239-243.
69. Cola, B.A., J. Xu, and T.S. Fisher, *Contact mechanics and thermal conductance of carbon nanotube array interfaces.* International Journal of Heat and Mass Transfer, 2009. **52**(15-16): p. 3490-3503.
70. Panzer, M.A., et al., *Thermal properties of metal-coated vertically aligned single-wall nanotube arrays.* Journal of Heat Transfer-Transactions of the Asme, 2008. **130**(5): p. -.
71. Son, Y., et al., *Thermal resistance of the native interface between vertically aligned multiwalled carbon nanotube arrays and their SiO2/Si substrate.* Journal of Applied Physics, 2008. **103**(2): p. -.
72. Zhang, K., et al., *Carbon nanotube thermal interface material for high-brightness light-emitting-diode cooling.* Nanotechnology, 2008. **19**(21): p. -.
73. Qu, L. and L. Dai, *Gecko-foot-mimetic aligned single-walled carbon nanotube dry adhesives with unique electrical and thermal properties.* Advanced Materials, 2007. **19**(22): p. 3844-+.

74. Bujok, B., et al., *Hot spots in the bee hive.* Naturwissenschaften, 2002. **89**(7): p. 299-301.
75. Maydanik, Y.F., et al., *Miniature loop heat pipes - A promising means for cooling electronics.* Ieee Transactions on Components and Packaging Technologies, 2005. **28**(2): p. 290-296.
76. Prasher, R.S. and J.C. Matayabas, *Thermal contact resistance of cured gel polymeric thermal interface material.* Ieee Transactions on Components and Packaging Technologies, 2004. **27**(4): p. 702-709.
77. Nurmawati, M.H., K.S. Siow, and I.J. Rasiah, *Analysis of phase change material for use as thermal interface material.* International Journal of Polymer Analysis and Characterization, 2004. **9**(4): p. 213-228.
78. Aoyagi, Y., C.K. Leong, and D.D.L. Chung, *Polyol-based phase-change thermal interface materials.* Journal of Electronic Materials, 2006. **35**(3): p. 416-424.
79. Trujillo, M., et al., *Thermal and morphological characterization of nanocomposites prepared by in-situ polymerization of high-density polyethylene on carbon nanotubes.* Macromolecules, 2007. **40**(17): p. 6268-6276.
80. Wang, J.F., H.Q. Xie, and Z. Xin, *Thermal properties of heat storage composites containing multiwalled carbon nanotubes.* Journal of Applied Physics, 2008. **104**(11): p. -.
81. Wang, J.F., H.Q. Xie, and Z. Xin, *Thermal properties of paraffin based composites containing multi-walled carbon nanotubes.* Thermochimica Acta, 2009. **488**(1-2): p. 39-42.
82. Zhu, L.B., et al., *Aligned carbon nanotube stacks by water-assisted selective etching.* Nano Letters, 2005. **5**(12): p. 2641-2645.
83. Pilling, J., *The Kinetics of Isostatic Diffusion Bonding in Superplastic Materials.* Materials Science and Engineering, 1988. **100**: p. 137-144.
84. Ornellas, D.L. and E. Catalano, *Diffusion Bonding of Gold to Gold.* Review of Scientific Instruments, 1974. **45**(7): p. 955-955.
85. Hu, H.P., X.W. Wang, and X.F. Xu, *Generalized theory of the photoacoustic effect in a multilayer material.* Journal of Applied Physics, 1999. **86**(7): p. 3953-3958.
86. *Indium Thermal Interface Materials*. 2008.
87. Zhong, Z.W., et al., *Characterization of SnAgCu and SnPb solder joints on low-temperature co-fired ceramic substrate.* Soldering & Surface Mount Technology, 2007. **19**(4): p. 18-24.
88. Luk, C.F., Y.C. Chan, and K.C. Hung, *Development of gold to gold interconnection flip chip bonding for chip on suspension assemblies.* Microelectronics Reliability, 2002. **42**(3): p. 381-389.